Forschungszentrum Karlsruhe
in der Helmholtz-Gemeinschaft

Wissenschaftliche Berichte
FZKA 7264

Quasi-Optical Mode Converter for a Coaxial Cavity Gyrotron

J. Jin

Institut für Hochleistungsimpuls- und Mikrowellentechnik
Programm Kernfusion
Association EURATOM-FZK

März 2007

Forschungszentrum Karlsruhe

in der Helmholtz-Gemeinschaft

Wissenschaftliche Berichte

FZKA 7264

Quasi-Optical Mode Converter for a Coaxial Cavity Gyrotron

Jianbo Jin

Institut für Hochleistungsimpuls- und Mikrowellentechnik

Programm Kernfusion

Association EURATOM-FZK

Dissertation an der Southwest Jiaotong University, Sichuan, P. R. China

Forschungszentrum Karlsruhe GmbH, Karlsruhe

2007

Forschungszentrum Karlsruhe GmbH
Postfach 3640, 76021 Karlsruhe

Mitglied der Hermann von Helmholtz-Gemeinschaft
Deutscher Forschungszentren (HGF)

ISSN 0947-8620

urn:nbn:de:0005-072642

Quasi-Optische Modenkonverter für Gyrotrons mit koaxialem Resonator

Zusammenfassung

Megawatt Gyrotrons werden in volumetrischen Moden hoher Ordnung betrieben. Also ist es notwendig, quasi-optische Modenwandler zur Transformation der Resonatormode in einen fundamentalen Gauß'schen Strahl für die Transmission zur Anwendung einzusetzen. Die vorliegende Arbeit beschäftigt sich mit der Synthese von quasi-optischen Modenwandlern für das 170GHz, $TE_{34,19}$-Mode, 2MW, CW Gyrotron mit koaxialem Resonator, das am Forschungszentrum Karlsruhe (FZK) entwickelt wird. Diese Forschungsarbeit ist Teil des EFDA-Projekts (TW5-THHE-CCGDS2) für den Internationalen Thermonuklearen Experimentalen Reaktor (ITER).

Ein quasi-optischer Modenwandler ist die Kombination aus einer offenen Hohlleiterantenne (Launcher) und einem Spiegelsystem. Die Verbesserung der generellen Methode für das Design des Launchers mit Wandstörung zur Wandlung in die fundamentale Gauß'sche Mode wird beschrieben. Durch die verbesserte Methode können kürzere Launcher mit angepassten Amplituden der Störung ausgelegt werden. Diese Methode wird mit dem Design eines Launchers für die $TE_{22,6}$-Mode bei 118 GHz verifiziert.

Da bei der $TE_{34,19}$-Mode das Verhältnis von Kaustikradius zu Resonatorradius 0.323 beträgt, erhält man bei Darstellung der Mode in geometrischer Optik kein geschlossenes oder fast geschlossenes Polygon im Querschnitt des Hohlleiters. In diesem Fall liefert die generelle Methode zur Auslegung von Launchern keinen reinen fundamentalen Gauß'schen Strahl. Die Synthese von quasi-optischen Modenwandlern für Gyrotrons wird hierbei sehr schwierig und es ist eine große Herausforderung einen Launcher mit einem reinen Gauß'schen Strahl, hoher Effektivität der Konvertierung und geringen Verlusten auszulegen. Es wird eine Phasenregel als Qualitätskriterium bei der Optimierung und die Wahl der Parameter bei quasi-optischen Modenwandlern vorgeschlagen.

Für dieses Gyrotron werden Störungen höherer Ordnung in der Wand des Launchers vorgeschlagen. Der Launcher wird numerisch optimiert, die Felder an den Kanten werden unterdrückt. Die Felder im Launcher werden gut durch die Repräsentation der Moden wiedergegeben, das abgestrahlte Feld wird mittels des skalaren Beugungsintergrals berechnet. Es bietet einen einfachen Weg für die Simulation der Feldverteilung in einer Hohlleiterantenne mit offenem Ende und für die Berechnung

des abgestrahlten Feldes einer Hohlleiterantenne mit offenem Ende und geringen Feldern an den Kanten.

Die Prozedur für die numerische Optimierung des Spiegelsystems ist verbessert worden, die Toleranzbedingung von phasenkorrigierenden Spiegeln wurde untersucht. Eine Effektivität der Konversion von 95,8% in die fundamentale Gauß'sche Mode mit 20 mm Strahltaille und einer Leistungstransmission von 90% wurden mit dem optimierten quasi-optischen Modenkonverter in der Ebene des Fensters erreicht. Die Methoden zur Verbesserung der Anfangsbedingungen von phasenkorrigierenden Spiegeln werden erforscht. Basierend auf den verbesserten Anfangsbedingungen wurde das Spiegelsystem verbessert. Es wird erwartet, dass damit die Leistungstransmission mehr als 95% in der Fensterebene ist.

Abstract

Megawatt gyrotrons operate in high-order volume cavity modes. Thus it is necessary to use a quasi-optical mode converter to transform the operating mode into a fundamental Gaussian beam for transmission and application of the generated high-power millimeter waves. This work concentrates on the synthesis of the quasi-optical mode converter for the 170GHz, $TE_{34,19}$-mode, 2MW, CW coaxial-cavity gyrotron at Forchungszentrum Karlsruhe (FZK). The investigations are part of an EFDA project (TW5-THHE-CCGDS2) for the International Thermonuclear Experimental Reactor (ITER).

A quasi-optical mode converter is the combination of an open waveguide antenna (launcher) and a mirror system. The improvement of the general method for the design of so-call dimpled-wall launcher to provide a good Gaussian mode content is described. By means of the improved method, very shorter perturbation lengths can be obtained with matched perturbation amplitudes. This method is verified through the design of a launcher operating in the $TE_{22,6}$ mode at 118 GHz.

For coaxial-cavity gyrotrons operating in very high-order cavity modes such as the $TE_{34,19}$ mode, due to the ratio of caustic to cavity radius of 0.323, the ray-representation of the $TE_{34,19}$ mode cannot form a closed or even almost closed polygon in the cross-section of the launcher. In this case, the general method fails to provide a dimpled-wall launcher to transform the high-order cavity mode into a nearly Gaussian distribution. The synthesis of the quasi-optical mode converter for this gyrotron becomes very difficult and is a great challenge to obtain a high quality RF beam with high conversion efficiency and low power losses. The setting of parameters used in the quasi-optical mode converter for this gyrotron is very critical. A phase rule is proposed as a quality criterion for monitoring the optimization and the choices of parameters of the quasi-optical mode converter.

High-order harmonics introduced to the launcher wall deformations are proposed for this gyrotron. The launcher is numerically optimized, the fields on the cut edges are suppressed. The fields in the launcher are well approximated by the waveguide modes, the radiated fields are calculated using the scalar diffraction integral. It provides a simple way for the simulation of the field distribution in an opened-end waveguide antenna and for the calculation of the radiated field from the opened-end waveguide antenna with low fields on the opened-end edges.

The procedure for the numerical optimization of the mirror system is improved, the tolerance conditions of the phase correcting mirrors are investigated. A conversion efficiency of 95.8% to the circular fundamental Gaussian distribution with 20mm

beam waist and power transmission of 90% are achieved in the window plane using the optimized quasi-optical mode converter. The methods to ameliorate the initial conditions of the phase correcting mirrors are explored. Based on the ameliorated initial conditions, the mirror system can be improved and is anticipated to enhance the power transmission to more than 95% in the window plane.

Index Terms: Gyrotron, quasi-optical (QO) mode converter, phase-correction, mode conversion.

Contents

Chapter 1 Introduction

In the electromagnetic spectrum, millimeter waves in the 30~300 GHz frequency band occupy a somewhat unique position since there are very few types of sources which can operate at high power. High power millimeter wave sources are conventionally realized with vacuum electronics tubes and lasers. Lasers are generally not capable of efficient operation beyond mid-infrared wavelengths, and conventional RF sources also face serious handicaps due to the inverse frequency scaling of their components. For klystrons, Traveling Wave Tubes (TWTs), Backward Wave Oscillators (BWOs), and other slow-wave devices, since the sizes of their interaction structures are in the order of the operating wavelength, it becomes more and more difficult to manufacture and align the fragile components as the operating wavelength decreases. At millimeter wavelengths these tubes produce only a small output power due to the small interaction circuit volume. More importantly, their small size results in the inability to handle high power levels or current densities because ohmic heating and/or arcing result in the failure of the device. As a result, such slow-wave sources are limited to frequencies of less than 100 GHz. Solid-state devices can generate power at microwave and millimeter-wave region; however, the power of these devices is several orders of magnitude lower than that of vacuum tubes. A comparison of the available output power from vacuum tubes with the output power available from solid-state devices is shown in Fig.1.1 [1]. Contrary to these tubes the resonance condition of the gyrotron is defined by a magnetic field which allows a free choice of the resonator diameter. Therefore gyrotrons can operate with low-loss higher-order volume modes. Gyrotrons can produce electromagnetic radiation in the part of the electromagnetic spectrum known as millimeter-submillimeter waves, near-millimeter waves or far-infrared, and have the advantage that the output power is very high as shown in Fig.1.1. Gyrotrons, or electron cyclotron masers, are able to produce continuous millimeter waves in the MW-range and bridge the power gap between slow-wave devices and lasers. They are capable of producing very high output power with theoretical efficiencies of forty percent, thus being important sources for the millimeter wave regime [2, 3].

1.1 Gyrotron

The cyclotron resonance masers (CRM) (the gyrotron family including the high harmonic gyrotron, the gyroklystron, the gyroTWT, and the gyroBWO; the CARM and the magnicon) were introduced in 1964 [4]. In CRMs the relativistic dependence of the cyclotron frequency of electrons on their energy leads to coherent radiation of

fast waves by the electrons gyrating in the external homogeneous magnetic field. This effect (under certain conditions) may be very important even for subrelativistic beams with 20-100 keV energy electrons. The gyrotron is the most practically attractive variety of CRM. In 1967, the gyrotron was invented at IAP Nizhny Novgorod by A.V. Gaponov-Grekhov, A.L. Goldenberg, V.A. Flyagin, and B.K. Yulpatov, which delivered low output power of 6W [5].

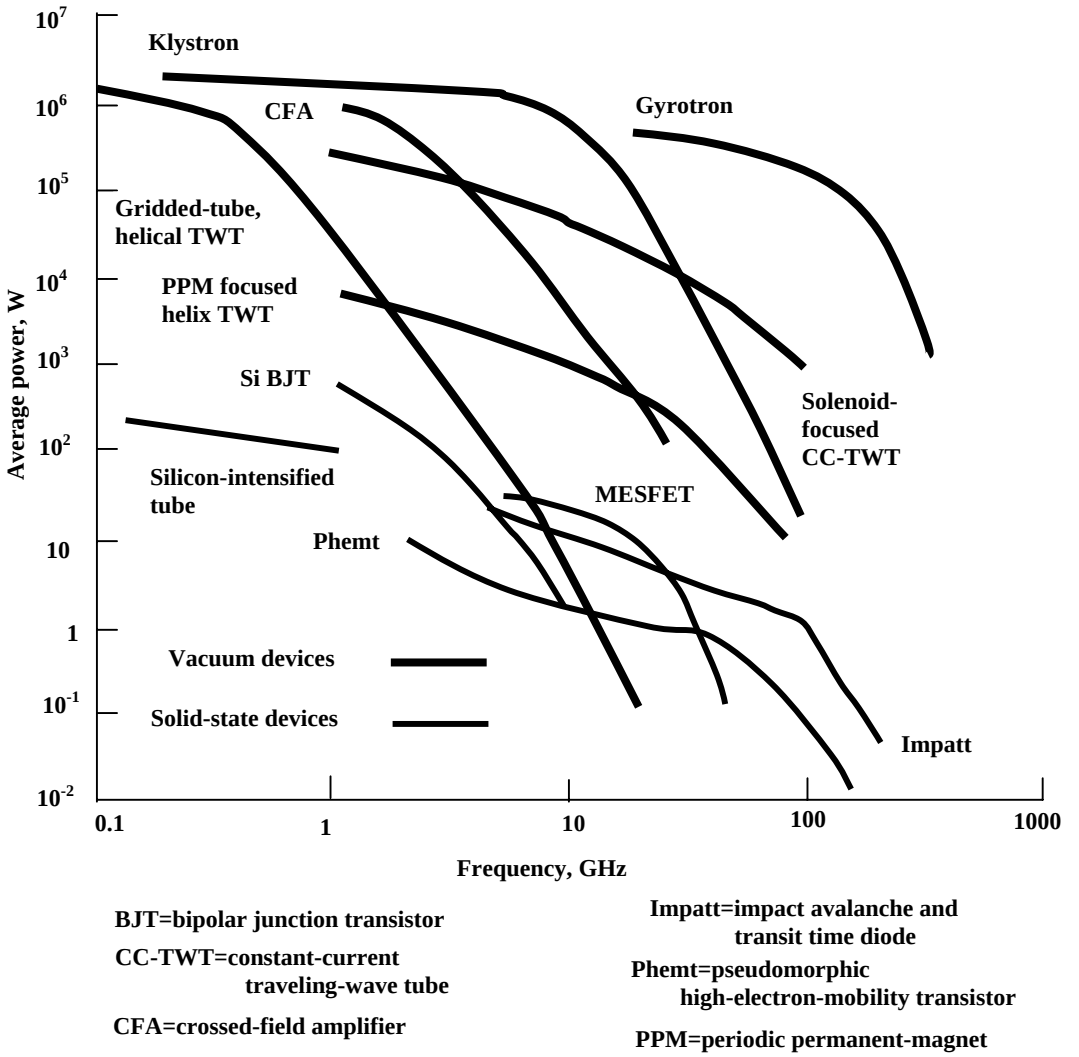

Figure 1.1: Continues power handling capacity from many solid state and tube devices as a function of frequency [1].

Actually, the gyrotron is a CRM-monotron with specific electron-optical and electrodynamic systems (see Fig.1.2). Since early 1970s, the output powers of gyrotrons have been improved by Russian scientists by means of employing magnetron injection guns and tapered, open-ended waveguide cavities that

maximize the efficiency by tailoring the electric field distribution in the resonator [5-13]. A magnetron-type electron gun which forms an annular electron beam was suggested as the basic element of the electron-optical system. In such a system electrons are emitted from the cathode under the action of the electric field produced by the voltage applied between the cathode and the anode and move in the gradually increasing magnetic field towards the interaction space. In this motion the electron beam is adiabatically compressed. Part of the energy of the electron motion along the lines of magnetic force is transformed into gyration energy which grows according to the adiabatic invariant $p_{gyro}^2 \big/ B = const$ (p_{gyro} is the orbital momentum of particles), while the spread in transverse energies is minimized. As a result, a substantial part of the kinetic energy of the electron beam at the input to the interaction space placed in the region of a nearly homogeneous magnetic field is related to the gyration of the particles and under appropriate conditions can be consumed by the RF field. The intense magnetic field oriented along the beam axis in the interaction cavity field causes the electrons to gyrate in small orbits around their original path, producing a net helical trajectory (see Fig.1.3).

As a result of this helical motion, the electrons emit radiation. If the magnetic field and the cavity are properly matched to the beam parameters, this radiation will couple into a resonant cavity TE mode which is amplified. With sufficiently good coupling and proper design, large amounts of monochromatic radiation can then be extracted. The transmission quality of an electron beam in the beam-wave interaction was investigated in [14-16], a method to enhance the efficiency of gyrotrons by tapering the magnetic field was proposed in [16]. Since for such a fast-wave device there is no requirement to couple into the fundamental waveguide mode, the interaction cavity can be significantly larger than the wavelength of the output radiation, thus avoiding the frequency-scaling problem associated with slow-wave devices. The electrons leaving the interaction space can be collected for energy recovery by a depressed collector.

For the first time the gyrotron was used to create plasmas in 1973, in Nizhny Novgorod [17]. Historically, gyrotron research has been driven by a need for electron cyclotron resonance heating (ECRH) of fusion plasmas. The use of high wave heating power requires strong microwave tubes in the MW-range. Practically every year, gyrotron developers showed higher and higher gyrotron operating modes. Ten years ago the $TE_{15,2}$ mode (fifteen azimuth and four radial variations) seemed to be a very high gyrotron mode [18]. Several years ago the $TE_{22,6}$ mode was a favorite mode for gyrotron developers [19]. In the last years extremely high-order modes like $TE_{31,17}$ were successfully used in gyrotrons [20]. Currently, the development of gyrotrons is proceeding in two directions. One is the development of high power, millimeter wavelength gyrotrons as power sources for ECRH of plasma, electron-cyclotron current drive (ECCD), stability control and diagnostics of

magnetically confined plasmas for generation of energy by controlled thermonuclear fusion in tokamaks and stellarators as well as for industrial technologies such as sintering of advanced ceramics. The second direction is the development of high-frequency, medium-power gyrotrons used, for example, as millimeter-to-submillimeter wavelength sources for plasma scattering diagnostics measurements and electron spin resonance (ESR) experiments [21].

Nuclear fusion represents a most promising option for an independent, sustainable, inherently safe and clean source for future global energy supply. ECRH and ECCD have proven to be well-established heating and current drive methods for both tokamaks [22-28] and stellarators [28-37]. Long pulse and continuous wave (CW) gyrotron oscillators delivering output powers of 100-960 kW at frequencies between 28 and 170 GHz have been used very successfully in the thermonuclear fusion research for plasma ionization and startup, ECRH and local current density profile control by non-inductive ECCD at system power levels up to 4.5 MW [38].

Gyrotrons are widely used as microwave sources for ECRH in stellarators, such as in Wendelstein 7-AS and Wendelstein 7-X (Germany), NCSX and HSX (USA), LHD (Japan), H-1 (Australia), etc. ECRH and ECCD are important tools for plasma devices especially for stellarators, as they provide both net current free plasma start up from the neutral filling gas and efficient heating of the plasma to the high temperatures required for thermonuclear fusion [39,40]. The development of ECRH is closely linked to the development of stellarators, and one of the key issues for stellarators is the development and demonstration of high-power gyrotrons with CW capability. A $TE_{28,8}$ mode, 140 GHz gyrotron with 1 MW output power for continuous-wave operation (30min) has been developed at FZK for the stellarator Wendelstein 7-X at IPP Greifswald [41].

Fast-frequency tunable gyrotrons are of interest for controlling instabilities in magnetically confined plasmas in large fusion reactors. The confining magnetic field depends on the radial position in tokamaks and stellarators. Hence, the electron cyclotron resonance interaction between the RF wave and the plasma electrons occurs only in a small plasma layer where the resonance condition is approximately fulfilled. Other plasma flux surfaces can be reached by a change of the gyrotron frequency or by mechanically steerable mirrors in the plasma vessel making use of the Doppler shift. Since it is difficult to find a mounting for such mirrors that can withstand the torque during a plasma disruption and since a reduction of the number of movable parts (flexible cooling pipes) inside the plasma vessel is desired, the first solution is more advantageous [42]. A step-tunable 105-140 GHz, 1 MW, 10s gyrotron is under development at IAP Nizhny Novgorod/Gycon with collaboration of FZK for the ASDEX-Upgrade tokamak at IPP Greifswald [43].

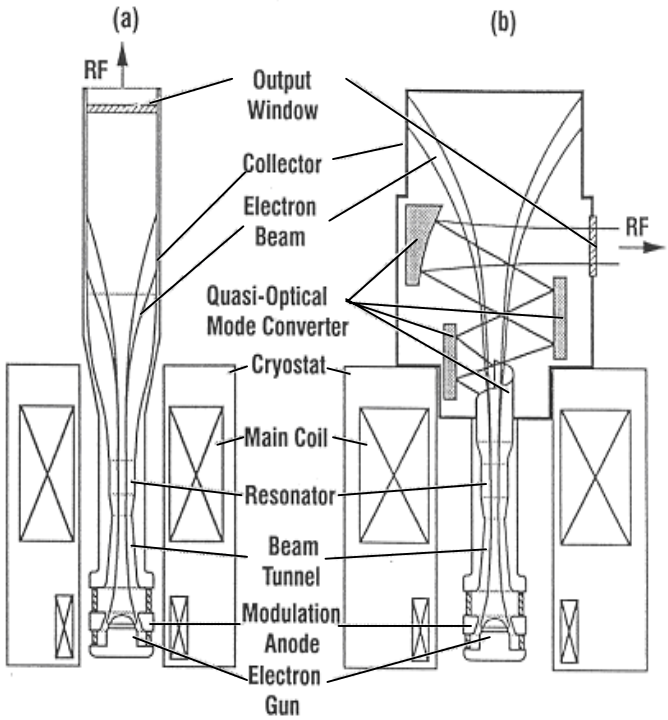

Fig.1.2 Schematic drawing of gyrotron with different output coupling system.

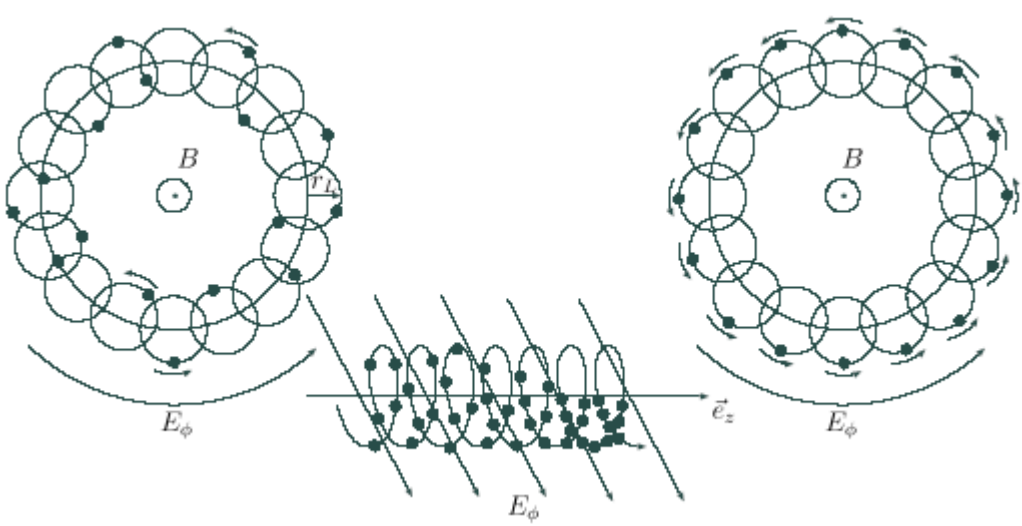

Fig.1.3 Principle of the field-electron interaction in the resonator of gyrotron.

Table 1.1 Present experimental development status of short pulse (3 μs - 15 μs) coaxial-cavity gyrotron oscillators.

Institution	Frequency [GHz]	Mode cavity	Mode output	Power [MW]	Efficiency [%]	Corrug.Cavity inner	Corrug.Cavity outer
FZK Karlsruhe	137.78	$TE_{27,16}$	$TE_{27,16}$	1.03	24.3	yes	no
Pulse length ≤ 100 ms	139.96	$TE_{28,16}$	$TE_{28,16}$	1.17	27.2	yes	no
			TEM_{00}	0.95	20	yes	no
				0.95	29(SDC)		
				(dual beam output)			
	142.02	$TE_{29,16}$	$TE_{29,16}$	1.04	24.4	yes	no
	138.70	$TE_{27,14}$	TEM_{00}	1.14	26.1	yes	no
	146.70	$TE_{28,15}$	TEM_{00}	1.13	25.6	yes	no
	156.90	$TE_{30,16}$	TEM_{00}	1.24	25.4	yes	no
	164.98	$TE_{31,17}$	$TE_{31,17}$	1.17	26.7	yes	no
			TEM_{00}	2.2	28	yes	no
				(single-beam output)			
				1.5	30	yes	no
				1.5	48(SDC)	yes	no
	167.14	$TE_{32,17}$	TEM_{00}	1.22	25.6	yes	no
	170	$TE_{34,19}$	TEM_{00}	1.2	20	yes	no
IAP, Nizhny Novgorod	45	$TE_{15,1}$	$TE_{15,1}$	1.25	43	no	no
Pulse length ≤ 0.1 ms	100	$TE_{21,18}$	$TE_{21,18}$	1.0	35	yes	no
				0.5	20	no	no
	100	$TE_{25,13}$	$TE_{25,13}$	2.1	30	no	no
				1.6	38	no	no
	103	$TE_{22,13}$	$TE_{22,13}$	1.0	40	yes	
				0.7	30	yes	
				0.3	14	no	
	110	$TE_{17,1}$	$TE_{17,1}$	0.7	25	no	
	110	$TE_{20,13}$	$TE_{20,13}$	1.15	35	yes	
	110	$TE_{21,13}$	$TE_{21,13}$	1.0	35	yes	
	140	$TE_{28,16}$	$TE_{28,16}$	1.5	33.5	yes	
				1.15	50(SDC)	yes	
			$TE_{76,2}$	1.17	35.2	yes	
			TEM_{00}	1.1	30	yes	
				(dual-beam output)			
	224 ($2\Omega_c$)	$TE_{33,8}$	$TE_{33,8}$	0.1	11	yes	no
IAP, FZK Karlsruhe	133	$TE_{27,15}$	$TE_{27,15}$	1.3	29	no	no
Pulse length 30 μs	140	$TE_{28,16}$	$TE_{28,16}$	1.0	23	no	no
MIT, Cambridge	137	$TE_{25,11}$	TEM_{00}	0.5	7.5	no	no
Pulse length 3 μs	139.6	$TE_{26,11}$	TEM_{00}	0.9	13	no	no
	142.2	$TE_{27,11}$	TEM_{00}	1.0	14.5	no	no
	140	$TE_{21,13}$	TEM_{00}	0.5	7.5	no	no

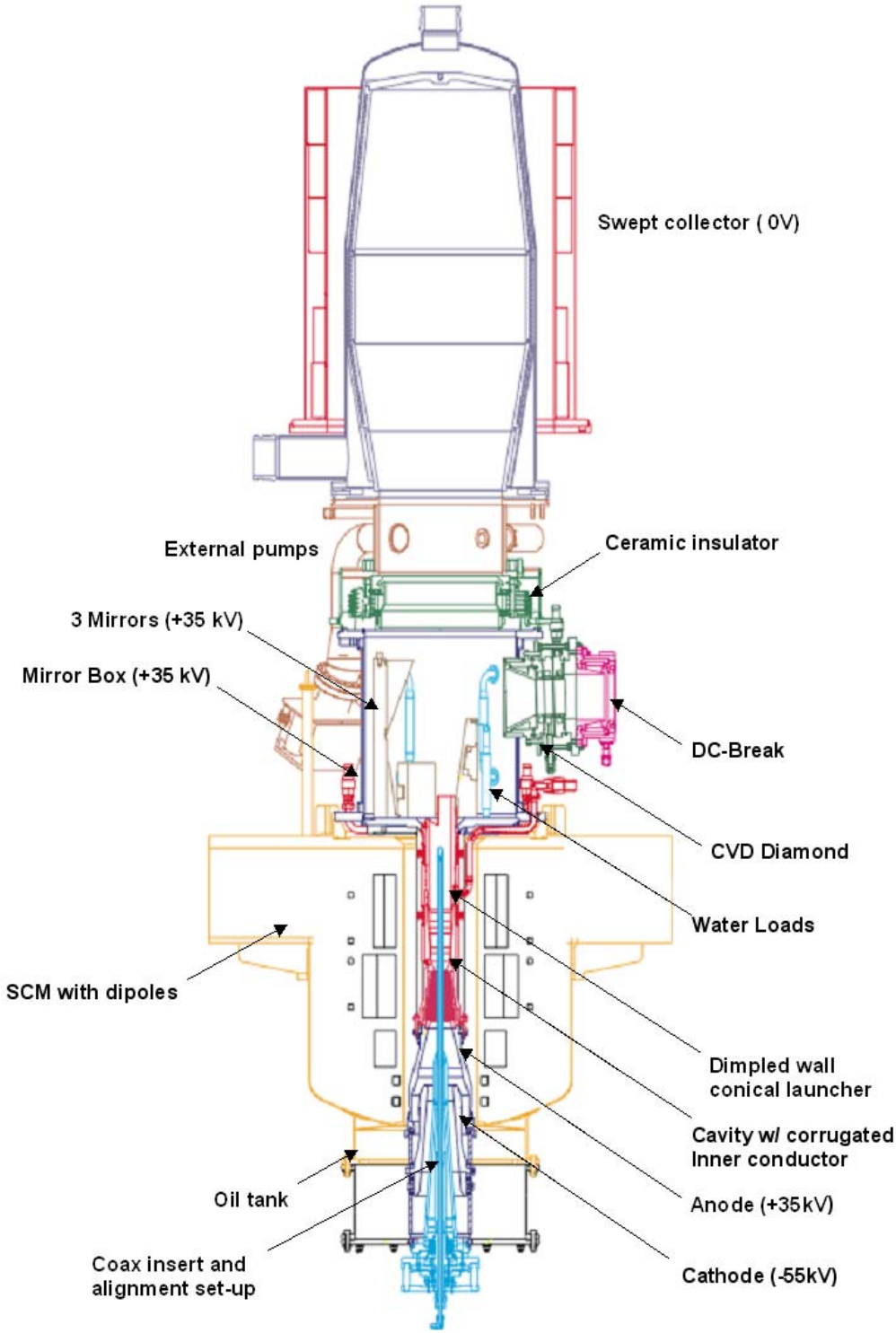

Fig.1.4 Schematic of the European 170 GHz, 2 MW, CW coaxial-cavity gyrotron with SC magnet.

The tokamak experiment International Thermonuclear Experimental Reactor (ITER) is the next step towards a fusion reactor. Reactor-relevant plasmas require microwave systems in a frequency range of 100-170 GHz with 25-50 MW total output power for heating, current drive and magnetohydrodynamic (MHD) control. It is foreseen to inject 20 MW-CW at 170 GHz using gyrotrons as electromagnetic wave sources. Obviously, a higher unit power (~ 2 MW/gyrotron) is highly desirable since such a tube would strongly reduce the total cost and result in a simpler system, the output power per gyrotron should be as high as possible in stationary operation. Gyrotrons, with coaxial cavities are able to generate power in the 2MW level [20].

At FZK the development work on coaxial-cavity gyrotrons started in 1992, the principal feasibility and the basic operating problems of coaxial gyrotrons were investigated, theoretical design tools have been developed, and later specific problems related to the coaxial arrangement have been studied in detail [20, 44-48]. Coaxial-cavity gyrotrons have the potential to generate a microwave power in the multi-megawatt range in continuous wave (CW) operation at frequencies around 170 GHz since very high-order volume modes can be utilized. The use of very high-order volume modes is possible because the presence of the coaxial insert practically eliminates the restrictions of voltage depression and limiting current and in addition, the problem of mode competition is reduced by a selective influence of the diffractive quality factor of the competing modes [49,50]. The increase of the RF output power per unit would result in a reduction of the installation costs of the electron cyclotron wave (ECW) system at ITER and it would allow, if necessary, to enhance the amount of microwave power injected in total into the plasma. As a result, the feasibility of manufacturing a 2 MW, CW coaxial gyrotron operating at 170 GHz has been demonstrated and all information necessary for a technical design and industrial manufacturing has been obtained. The present experimental development status of short-pulse coaxial-cavity gyrotron oscillators is shown in Table 1.1 [see Ref. 36 and the references therein]. Based on these results, a 2MW, 170GHz, $TE_{34,19}$ coaxial-cavity gyrotron is under development in cooperation between European Research institutes (FZK Karlsruhe, CRPP Lausanne, HUT Helsinki) and European tube industry (TED, Velizy, France), which is foreseen to be used for electron cyclotron resonance heating (ECRH) and stability control of magnetically confined plasmas in the ITER [51]. The structure of the coaxial-cavity gyrotron is shown in Fig.1.4.

A short summary of the experimental results of a short-pulse pre-prototype at FZK are given here [52]:

- The performance of the electron gun is according to the design. A stable electron beam up to a current of 80 A without any instabilities has been obtained. No limitations in high voltage operation due to built-up of a Penning discharge have been observed. Parasitic low frequency oscillations have been successfully suppressed.

- The $TE_{34,19}$ mode, which is the nominal mode of the 2 MW, CW prototype, has been excited at 170 GHz over a reasonably wide parameter range. At a magnetic field of 6.716 T, limited by the available SC-magnet at FZK, a maximum RF output power of about 1.15 MW has been measured. The oscillation range of the nominal mode, however, is somewhat reduced by a more severe mode competition compared to theoretical predictions. As a consequence, a denser mode spectrum has been excited in the experiment than expected from simulations. The reason for that is under investigation.

- The q.o. system has been tested both at low power ("cold") and in the gyrotron ("hot"). Both, the results from the "cold" and "hot" measurements show significant disagreement in comparison with the design calculations. In very recent simulations it has been found that a wrong field pattern radiated from the launcher has been taken for designing the mirrors. With the correct field pattern of the launcher a good agreement is obtained between measurements and simulation. This confirms the confidence into the numerical design tools. Measurements of the stray radiation losses have been performed. An internal load has been found to be an efficient absorber for the stray radiation.

Table 1.2 Design parameters of the 170 GHz, 2 MW, CW coaxial-cavity gyrotron.

operating cavity mode	$TE_{34,19}$
frequency, GHz	170 GHz
RF output power, P_{out}	2 MW
generated RF power (~10% internal losses)	2.2 MW
Beam current, I_b	75 A
accelerating beam voltage, U_c	90 kV
retarding collector voltage, U_{coll}	$\cong$ - 34 kV
output efficiency, η_{out}	$\geq$ 45 %
cavity magnetic field, B_{cav}	6.87 T
velocity ratio, α	1.3
Beam radius in the cavity, R_b	10.0 mm
Beam width (guiding centers), ΔR_b	0.25 mm

In the experiment, the stray radiation losses inside the tube are about 8 %, which does not satisfy the requirement of more than 95% power transmission inside the gyrotron. The stray radiation is too large for stable operation and leads to heating the structure of the gyrotron, so the q.o. mode converter should be improved. This work concentrates on improving the q.o. mode converter to achieve a high conversion efficiency, to obtain a nearly Gaussian wave beam with a Gaussain content of more

than 95%, and to suppress the stray radiation losses to less than 5% in the 170GHz, $TE_{34,19}$-mode, coaxial-cavity gyrotron.

1.2 Quasi-Optical Mode Converter

High power gyrotrons operate in low-loss volume modes with a high-order mode index. These gyrotron cavity modes are not suitable for power transmission in free space due to their strong diffraction and polarization losses. For long-pulse high-power gyrotrons the implementation of an output coupler is required that separates the spent electron beam from the outgoing RF power in order to increase the electron beam interception area of the collector. It is the short-wavelength, high output power and rotating asymmetric high-order cavity mode of such tubes which have led to the need for novel mode conversion concepts. The preferred output mode of the gyrotron is the fundamental Gaussian beam TEM_{00}. The down-conversion of these high-order cavity modes with complicated field structure by using conventional waveguide mode transducers with highly oversized waveguide diameter is practically impossible due to the extreme waveguide mode competition involved. Therefore, a mode conversion from the cavity mode to the eigenwave of the transmission line is required. The adaptation can be made inside the gyrotron with a special quasi-optical (q.o.) mode converter.

The higher the operating mode is, the more it is appropriate to employ an asymptotic procedure for its description, namely the method of geometrical optics (g.o.) (see e.g. [53,54]). In the frame of this method the initial mode is represented as a system of rays successively reflected from the waveguide walls (Brillouin-Keller concept). To directly convert the complicated field structure of rotating high-order asymmetric gyrotron cavity modes into a linearly polarized Gaussian beam, i.e. to modify the configuration of rays, one can use q.o. devices, a proper combination of a specific mode converting waveguide slot radiator (launcher) together with a few curved mirrors [55,56], often called Vlasov converter.

The q.o. mode converter is a part of the internal electrodynamic system of the gyrotron like the cavity and the uptaper (see Fig.1.2) which reduces the ohmic loss of the resonant gyrotron mode and allows a low loss transport of the microwave radiation out of the resonator. Radial output coupling of the RF power into the fundamental Gaussian ($TEM_{0,0}$) free-space mode has three significant advantages for high-power operation:

- Firstly, the linearly polarized $TEM_{0,0}$ mode is directly usable for low-loss transmission as well as for effective antenna feeding and no further mode converters are needed. Therefore, q.o. mode converters are also used for

relatively modestly overmoded systems when a very compact mode converter to the $TEM_{0,0}$ mode is required [57,58].

- Secondly, the converter separates the electron beam from the RF-wave path (Fig.1.2b), so that the electron collector is no longer part of the output waveguide as in the case of a tube with an axial output (Fig.1.2a). Hence, the collector can be designed especially for handling the high electron-beam power. In addition, energy recovery with a depressed collector becomes possible.

- Thirdly, the harmful effects of RF power reflected from the output window are expected to be significantly reduced especially if the window disk is slightly tilted.

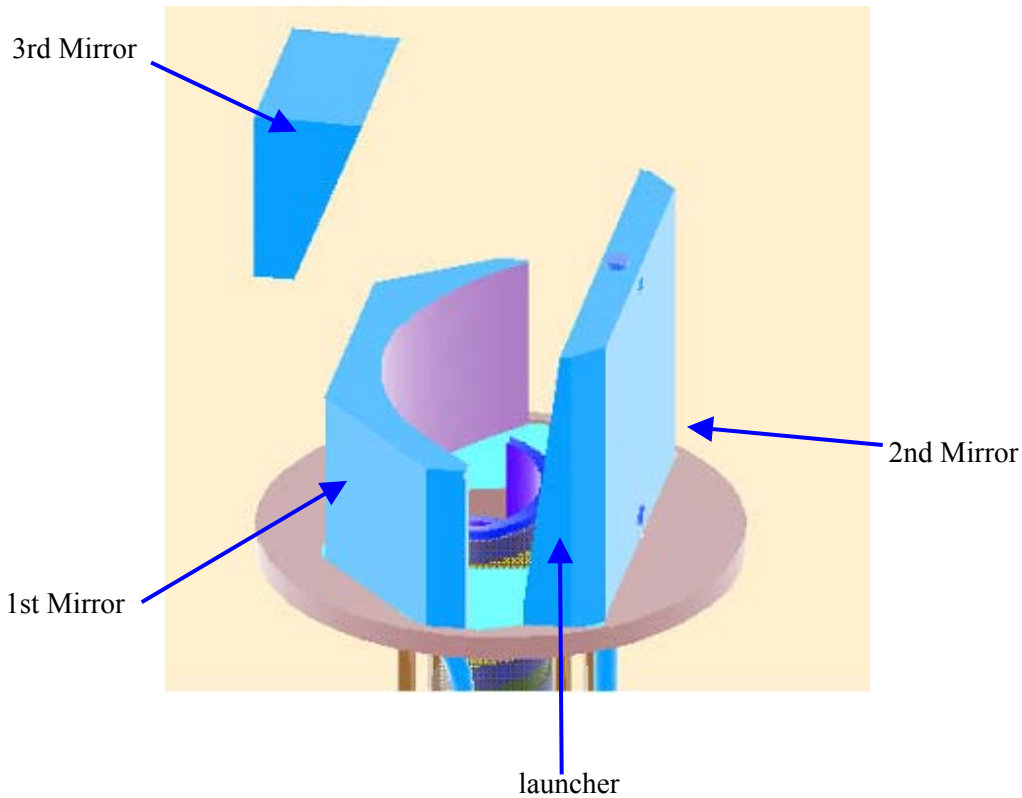

Fig.1.4 Schematic of quasi-optical mode converter.

Currently, all long-pulse high-power gyrotrons for nuclear plasma fusion applications employ a q.o. mode converter to transform the rotating high-order cavity modes into a linearly polarized fundamental Gaussian beam [59-63]. A q.o. mode converter transforms a high-order operating mode into a paraxial wave beam with linear polarization and separates the electron and wave beams. The electron

beam goes to the collector and the wave beam usually comes out of the tube in the direction perpendicular to the magnet axis. This separation gives the possibility to solve collector and window problems practically independently. The mode converter consists of a special irregular cut ending waveguide up-taper from the cavity, quasi-parabolic or quasi-elliptical reflector and one or two specially shaped mirrors. Sometimes more mirrors are applied to transmit the wave beam inside the gyrotron magnet bore hole cylinder. The converter forms an optimal spatial field structure over the window surface: the flattened distribution for long pulse gyrotrons with ceramics (BN) windows, where thermal conductivity of window material is relatively low, or Gaussian distribution (optimal for wave beam transmission) for diamond windows. Fig.1.4 shows the q.o. mode converter used in the $TE_{34,19}$ mode coaxial cavity gyrotron at FZK, where the first mirror is a quasi-elliptical mirror.

This dissertation is organized in the following manner. Analysis and synthesis methods for the launcher are presented in Chapter 2. Chapter 3 describes the synthesis of mirror systems. Chapter 4 focuses on the design and experimental investigation of the pre-prototype of the q.o. mode converter for the $TE_{34,19}$-mode coaxial-cavity gyrotron. Chapter 5 presents the improvement of the q.o. mode converter for the $TE_{34,19}$-mode coaxial-cavity gyrotron, the tolerance conditions of the converter and the quality of the corrected beam wave are discussed. Finally, Chapter 6 contains the summary as well as some concluding remarks.

Chapter 2 Cylindrical Waveguide Antenna

An internal q.o. mode converter is actually a kind of open mirror line, which consists of a launcher and a few curved mirrors (see Fig.1.4), so it will produce diffraction losses inside the gyrotron. In megawatt gyrotrons the acceptable level of stray radiation losses in the tube is less than 5% for stable operation and to avoid heating the structure of the gyrotron. The cylindrical waveguide antenna of the q.o. mode converter is an opened-end launcher where fields on the edges of cuts would produce diffraction losses. In order to achieve low diffraction losses from the launcher cuts, the wave beam in a launcher should be pre-shaped to reach low fields on the edges of the cuts and to provide high Gaussian contents in the radiated fields. For a high quality outgoing wave beam, a simple mirror system consisting of quasi-optical reflector and toroidal mirrors can be used to couple the wave beam out of the tube [63]. In this chapter, the method to deform the launcher wall in order to achieve low fields on the cuts is introduced and the method for the analysis of the fields in the launcher is presented.

2.1 Geometric Optical Description

In high order mode gyrotrons, the diameter of the cylindrical launcher is usually 15 times larger than the free-space wavelength, so that the wave beam in the launcher can be described in terms of geometric optics. For a TE_{mn}-mode gyrotron, the field $u(r,\phi,z)$ in the cylindrical launcher can be given as (in a cylindrical coordinate system shown in Fig.2.1):

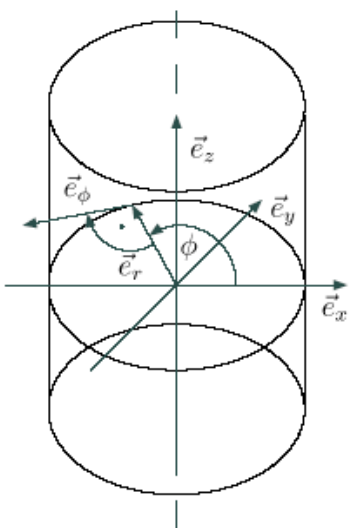

Fig.2.1 Cylindrical coordinate system.

$$u(r,\phi,z) = A_0 J_m(k_r r) e^{\pm jm\phi} e^{\pm jk_z z} \tag{2.1}$$

$$k_r = \frac{X_{mn}}{a}$$

$$J_m'(X_{mn}) = 0 \tag{2.2}$$

$$k_z = \sqrt{k_0^2 - k_r^2}$$

where A_0 is a constant which represents the amplitude of the field, z and r are the longitudinal and radial position, ϕ is

azimuthal angle, J_m and $J_m^{'}$ represent the m-order Bessel function and its derivative, X_{mn} is the n-th zero of the m-order Bessel function (or derivative), a is the radius of the launcher, k_r and k_z are the radial and longitudinal wave numbers, k_0 is the free-space wave number. In equation (2.1), the field distribution in the radial direction (in Fig.2.1, direction $\vec{e}_r$) is actually a standing wave. A standing wave can be decomposed into two traveling waves: the incoming and outgoing traveling wave. Bessel function can be described as the sum of the first kind of Hankel function $H_m^{(1)}(z)$ and the second kind of Hankel function $H_m^{(2)}(z)$.

$$J_m(k_r r) = \frac{H_m^{(1)}(k_r r) + H_m^{(2)}(k_r r)}{2} \tag{2.3}$$

$$u(r,\phi,z) = A_0 J_m(k_r r) e^{\pm jm\phi} e^{\pm jk_z z} = \frac{A_0}{2}\left(H_m^{(1)}(k_r r) + H_m^{(2)}(k_r r)\right) e^{\pm jm\phi} e^{\pm jk_z z} \tag{2.4}$$

with the incoming traveling wave:

$$u^{in}(r,\phi,z) = \frac{A_0}{2} H_m^{(1)}(k_r r) e^{\pm jm\phi} e^{\pm jk_z z} \tag{2.5}$$

and the outgoing traveling wave:

$$u^{out}(r,\phi,z) = \frac{A_0}{2} H_m^{(2)}(k_r r) e^{\pm jm\phi} e^{\pm jk_z z} \tag{2.6}$$

$H_m^{(1)}(z)$ and $H_m^{(2)}(z)$ are conjugate complexes

$$H_m^{(1)}(z) = \left(H_m^{(2)}(z)\right)^* \tag{2.7}$$

The superscript "*" represents the complex conjugate. In the case of $z>m$, $H_m^{(2)}(x)$ can be approximated as

$$H_m^{(2)}(z) \approx \sqrt{\frac{2}{\pi\sqrt{z^2 - m^2}}} e^{j\left(-\sqrt{z^2-m^2} + m\arccos\frac{m}{z} + \frac{\pi}{4}\right)} \tag{2.8}$$

The phase of the outgoing traveling wave is

$$\arg\left(u^{out}(r,\phi,z)\right) \approx -\sqrt{k_r^2 r^2 - m^2} + m\arccos\frac{m}{k_r r} + \frac{\pi}{4} - m\phi - k_z z \tag{2.9}$$

The wavefront with a constant phase c satisfies

$$c - \arg(u^{out}) = 0 \tag{2.10}$$

In the geometric optics (g.o.) limit, plane wavefronts can be represented by rays [64, 65], so that a rotating wave of a circular waveguide is a continuous flow of rays. The direction of the ray is along the gradient of the wavefront

$$\vec{N}(r,\phi,z) = \nabla\left(c - \arg\left(u^{out}(r,\phi,z)\right)\right) \tag{2.11}$$

$$\approx k_r\sqrt{1-\frac{m^2}{k_r^2 r^2}}\vec{e}_r + \frac{1}{r}m\vec{e}_\phi + k_z\vec{e}_z \tag{2.12}$$

Accordingly, the direction of the ray representation of the incoming traveling wave can be obtained

$$\vec{N}_{in} = -k_r\sqrt{1-\frac{m^2}{k_r^2 r^2}}\vec{e}_r + \frac{1}{r}m\vec{e}_\phi + k_z\vec{e}_z \tag{2.13}$$

For a rotating mode only one outgoing and one incoming traveling waves contribute to the field structure in the observation point as shown in Fig.2.2 (a). The incoming traveling wave can be regarded as the reflected ray of the outgoing traveling wave on the waveguide wall surface in the frame of g.o. shown in Fig.2.2(b).

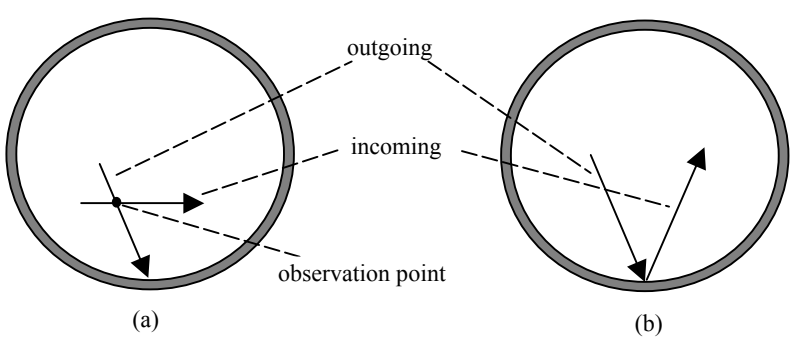

Fig.2.2 Ray representations of the outgoing and incoming traveling waves in a circular waveguide: (a) at an observation point, (b) reflection on the waveguide wall.

Such ray representations describe with sufficient accuracy the fields of higher-order modes (n>>1) over the entire cross section of the waveguide except for the domain near the caustic. On the launcher wall, the outgoing direction becomes

$$\vec{N}(a,\phi,z) \approx \frac{\sqrt{X_{mn}^2 - m^2}}{a}\vec{e}_r + \frac{1}{a}m\vec{e}_\phi + k_z\vec{e}_z \tag{2.14}$$

The ray propagates at the Brillouin angle ψ relative to the waveguide axis

$$\cos\psi = \frac{\vec{N}\cdot\vec{e}_z}{\left|\vec{N}\right|\left|\vec{e}_z\right|} = \frac{k_z}{\sqrt{k_r^2 + k_z^2}} = \frac{k_z}{k_0}, \qquad \sin\psi = \frac{k_r}{k_0} \tag{2.15}$$

In the transverse plane, the projection of the ray is in the direction $\vec{N}_t$

$$\vec{N}_t = \frac{\sqrt{X_{mn}^2 - m^2}}{a}\vec{e}_r + \frac{1}{a}m\vec{e}_\phi \tag{2.16}$$

The angle between the vector $\vec{N}_t$ and the vector $\vec{e}_\phi$ can be calculated as

$$\cos\theta = \frac{\vec{N}_t\cdot\vec{e}_\phi}{\left|\vec{N}_t\right|\left|\vec{e}_\phi\right|} = \frac{m}{X_{mn}} \tag{2.17}$$

If the point of interest is located at the waveguide wall the ray has the distance R_c from the waveguide axis

$$\cos\theta = \frac{R_c}{a} \Rightarrow R_c = a\cos\theta = a\frac{m}{X_{mn}} \tag{2.18}$$

Hence if all plane waves are presented by g.o. rays they form a caustic at the radius R_c (see Fig.2.3). All the rays move tangentially to the caustic position. In the g.o. the field is assumed to disappear inside of the caustic radius which is not true for the real waveguide mode. In an unperturbed circular waveguide the density of the rays along the caustic is uniform [54].

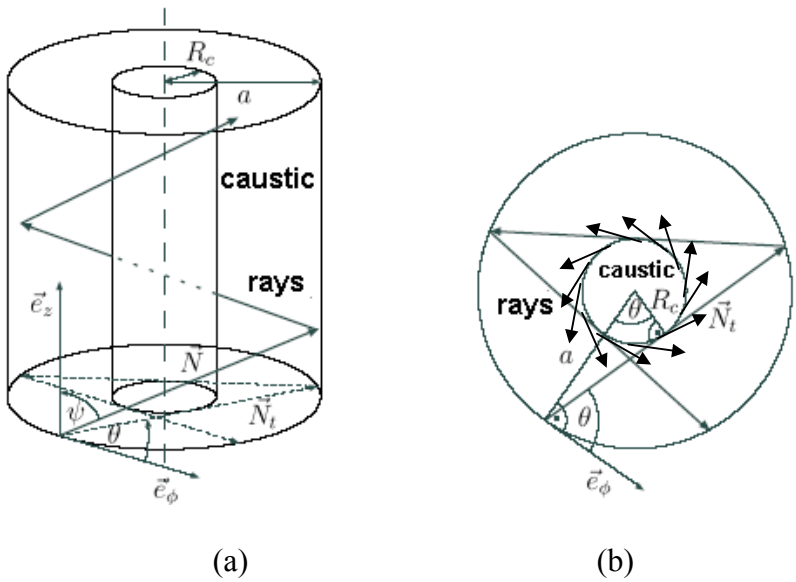

(a) (b)

Fig.2.3 Geometric optical description of a wave beam in a cylindrical waveguide: (a) side view; (b) top view

2.2 Vlasov launcher

For many applications it is preferable to propagate millimeter- and submillimeter-wave radiation in the form of a quasi-optical wave beam with a linear polarization of the electric field and a Gaussian radial profile of the intensity. For transformation of whispering gallery modes into such wave beams q.o. mode converters were first suggested in [55,56].

The principle schemes of the q.o. mode converter for (a) rotating asymmetric modes and (b) for circular symmetric modes are shown in Fig. 2.4. As already shown, TE- and TM-modes in a circular waveguide can be decomposed into a series of plane waves that can be represented as a set of rays that fill the region between the waveguide wall and the caustic. The requirement of a zero azimuthal electric field at the waveguide wall defines their relative phases. The transverse locations of the rays are defined by the requirement that at a particular point of interest the ray direction must coincide with the Poynting vector direction of the original TE- or TM-mode field distribution. In Fig.2.4, a whispering gallery mode propagates and radiates through the open end of a launcher. The rays leaving the open end of the launcher can be considered as a set of rays parallel in the axial direction and spherically diverging in the transverse direction. Then, as shown in Fig.2.4, reflected by a quasi-parabolic reflector, these radially diverging rays can be transformed into a plane wave beam with linear polarization. Weakly relativistic gyrotrons always operate in TE modes.

The distance that a ray has propagated in the axial direction between two subsequent reflections from the waveguide wall is:

$$L_B = 2a\left[1-\left(\frac{m}{X_{mn}}\right)^2\right]^{\frac{1}{2}}\cot\psi \tag{2.19}$$

In the transverse direction a section of angle:

$$\Delta\varphi = 2\theta = 2\arccos\left(\frac{m}{X_{mn}}\right) \tag{2.20}$$

reflects all rays exactly once (see Fig.2.3).

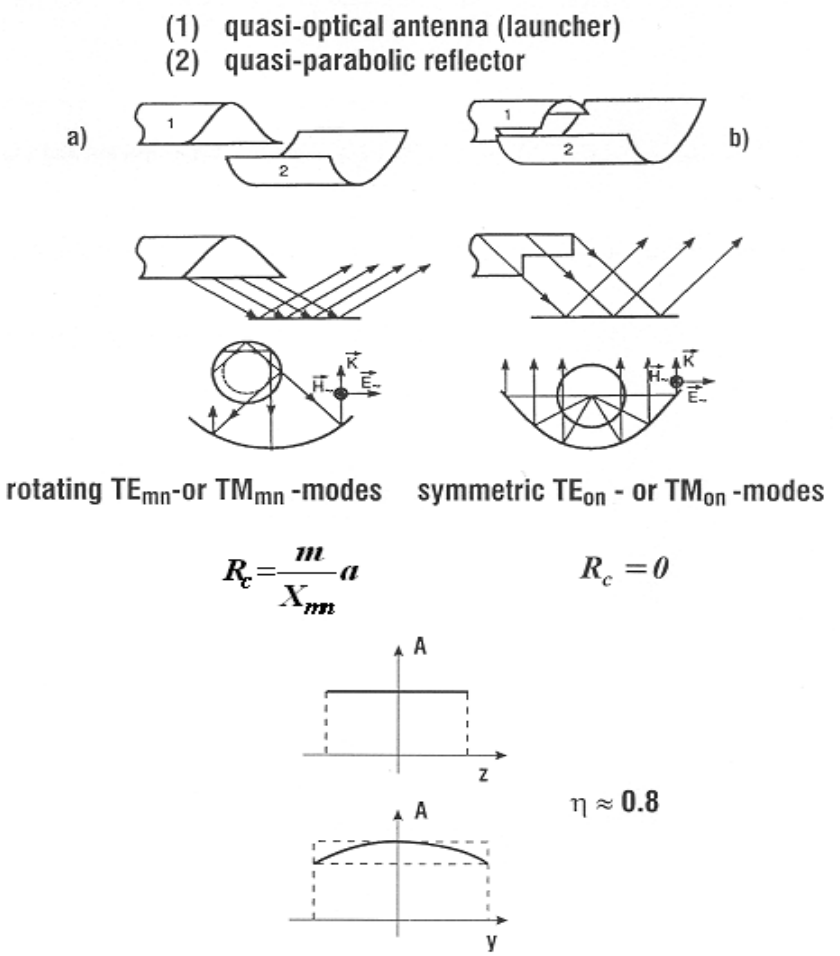

Fig. 2.4 Principle schemes of quasi-optical mode converters and amplitude distribution at the launcher.

2.2.1 Helical Cut

For modes with m≠0 the reflection points of each of the rays are placed on the waveguide surface in a helical line with the angle of inclination

$$\tau = \arctan\left(\frac{\theta \tan\psi}{\sin\theta}\right) \tag{2.21}$$

The distance (pitch) that a ray has propagated in the axial direction when it has completed a full turn is

$$L = 2\pi a \cot\tau = 2\pi a^2 \frac{k_z}{X_{mn}} \sqrt{1-\left(\frac{m}{X_{mn}}\right)^2} \left(\arccos\left(\frac{m}{X_{mn}}\right)\right)^{-1} \tag{2.22}$$

The Brillouin region is defined as a waveguide wall section with the length L and the transverse width defined by Δφa which reflects each ray once. This can be found from the unfolded launcher with the helical line shown in Fig.2.5.

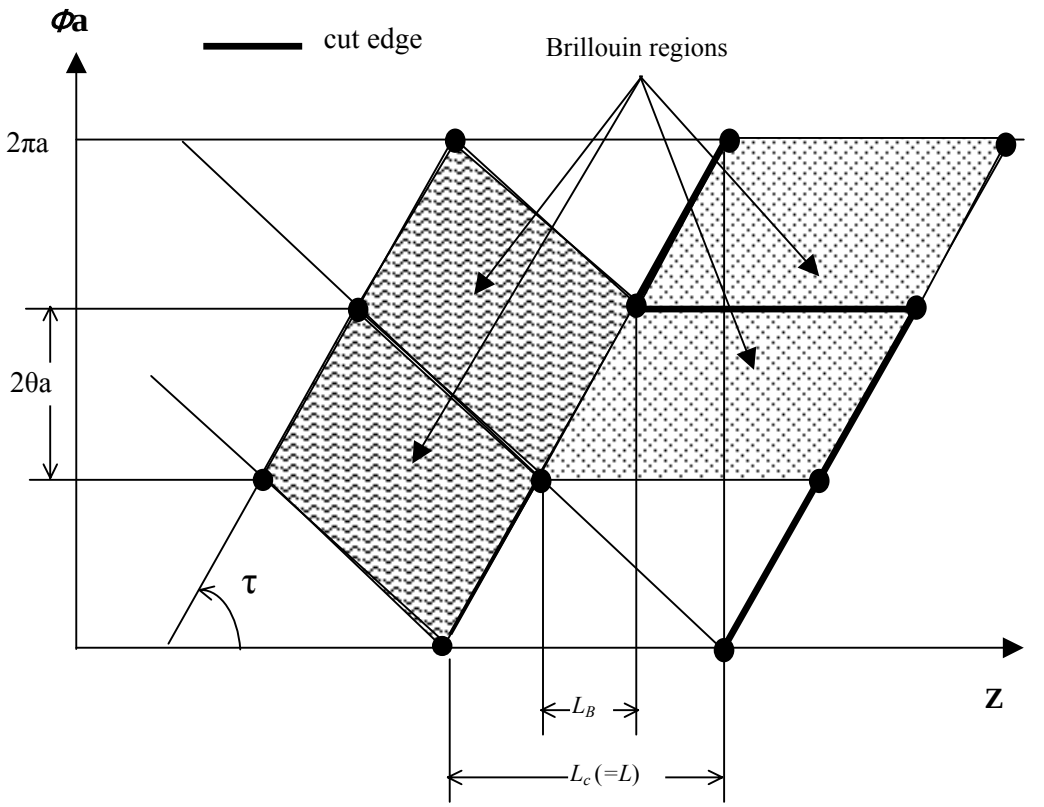

Fig.2.5 Unfolded surface of a cylindrical waveguide. The edges of launcher cuts are indicated.

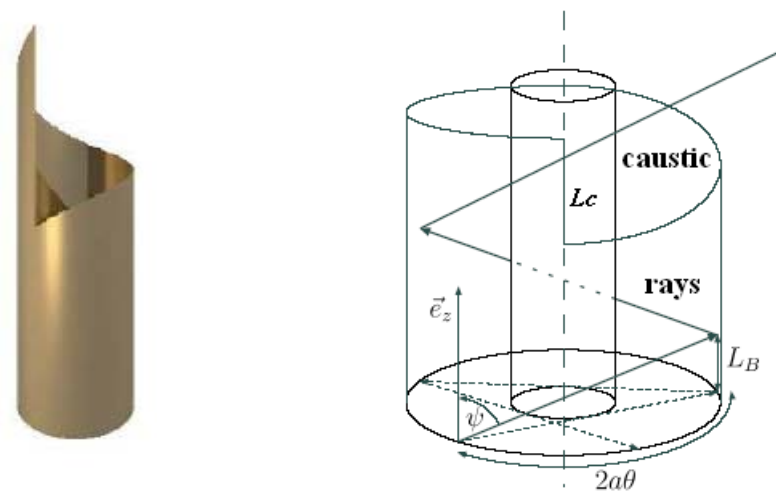

(a) (b)

Fig.2.6 Cylindrical launcher with helical cut:
(a) schematic drawing; (b) ray representation in launcher.

A Vlasov-type launcher with a helical cut is shown in Fig.2.6(a) and the g.o. description of the beam wave in the launcher is shown in Fig.2.6(b). The aperture area of the launcher is obviously equal to the area of Brillouin region, the cut length L_c=L.

2.2.2 Rectangular Cut

In a cylindrical launcher, the electron beam is divergent due to the decrease of the longitudinal magnetic field of the gyrotron magnet (see Fig.1.2(b)). The transverse size of electron beam becomes large so that the launcher wall could be hit by the electrons. Moreover, the wave beam reflected by the quasi-optical reflector may strike a launcher with a large cut length. So the launcher cut should be shortened as much as possible. According to the value of 2π%2θ, here % is a modulo operator (the rest of division), the launcher cut can be shortened in the following ways [66].
In the case of 2π%2θ> θ, the azimuthal angle of the cut is ξ=2θ, and the cut length can be shortened to Lc=L-ΔL, where Lc represents the cut length and L is given in equation (2.22)

$$\Delta L = a\frac{2\pi\%2\theta}{\tan\alpha} \tag{2.23}$$

The field distributions on the unfolded launcher wall are shown in Fig.2.7, the cut length is shortened by ΔL.

In the case of $2\pi\%2\theta < \theta$, the azimuthal angle of the cut is $\xi=2\theta+2\pi\%2\theta$ and the cut length can be shortened as

$$L_c = L - \Delta L - L_B \tag{2.24}$$

The field distributions on the unfolded launcher wall are shown in Fig.2.8, the cut length is shortened by $\Delta L+L_B$. From Fig.2.8 we can see that the azimuthal angle of the aperture is enlarged by $2\pi\%2\theta$, so the quasi-optical reflector has to be increased in the azimuthal direction. This could be a problem since such a large reflector is difficult to be integrated into the gyrotron.

When $2\pi\%2\theta=0$, the azimuthal angle of the cut can be set as $\xi=2\theta$, $\Delta L=0$, and the cut length becomes

$$L_c = L - L_B \tag{2.25}$$

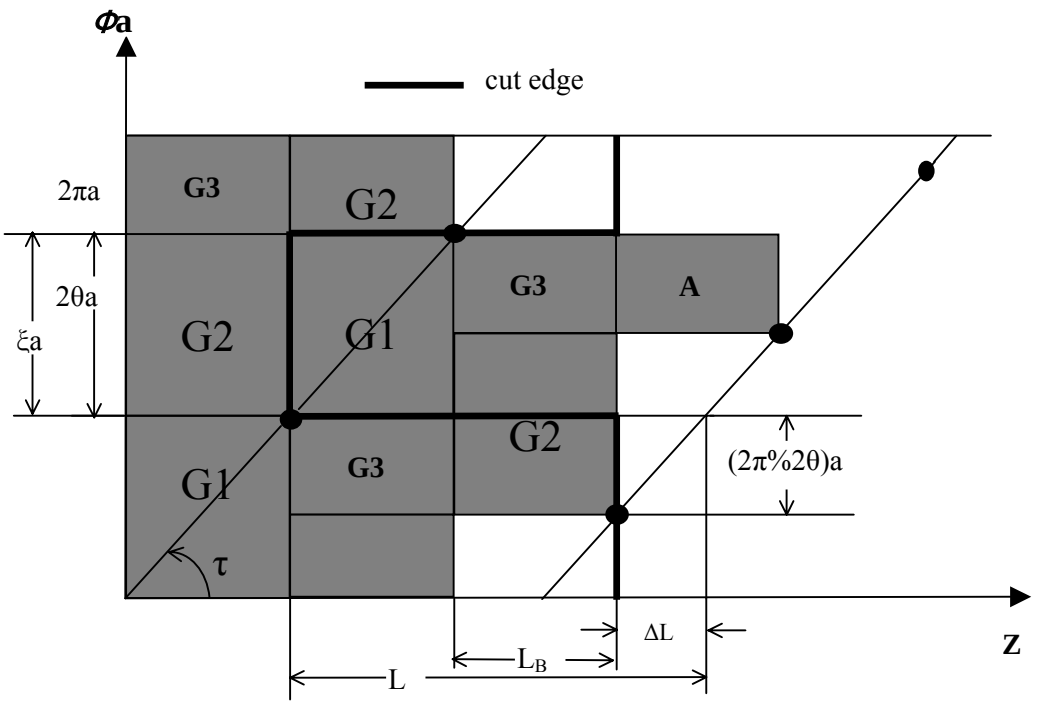

Fig.2.7 Field distributions (dark sections) on the unfolded wall of a Vlasov launcher, where $2\pi\%2\theta > \theta$.The edges of the launcher cuts are indicated.

The field distributions on the aperture and the unfolded launcher wall can be found from Fig.2.9. A Vlasov-type launcher with rectangular cut is shown in Fig.2.10(a), the ray representation in the launcher is shown in Fig.2.10(b).

In a Vlasov-type launcher, the power densities on the wall are uniform in the dark sections as shown in Figs. 2.7-9 and the fields on the edges of cuts are relatively strong. Such strong fields on the cut edges produce diffraction and reflection from the cuts. The wave beam radiated from a waveguide cut and reflected from a quasi-optical reflector has a spatial structure different from a Gaussian wave beam. The Gaussian component amounts to about 80%, while the remaining 20% of the radiation propagate at relatively large angles to the beam direction, because of the scattering at the edge of the cut, and are usually lost in open transmission lines. However, large stray radiation is unacceptable for megawatt gyrotrons.

Back scattering effects due to diffraction of the incident high-order mode by the helical and straight edges of the launcher have been estimated by using the method of equivalent currents [67]. For ψ <70° the total reflected power is lower than –30 dB.

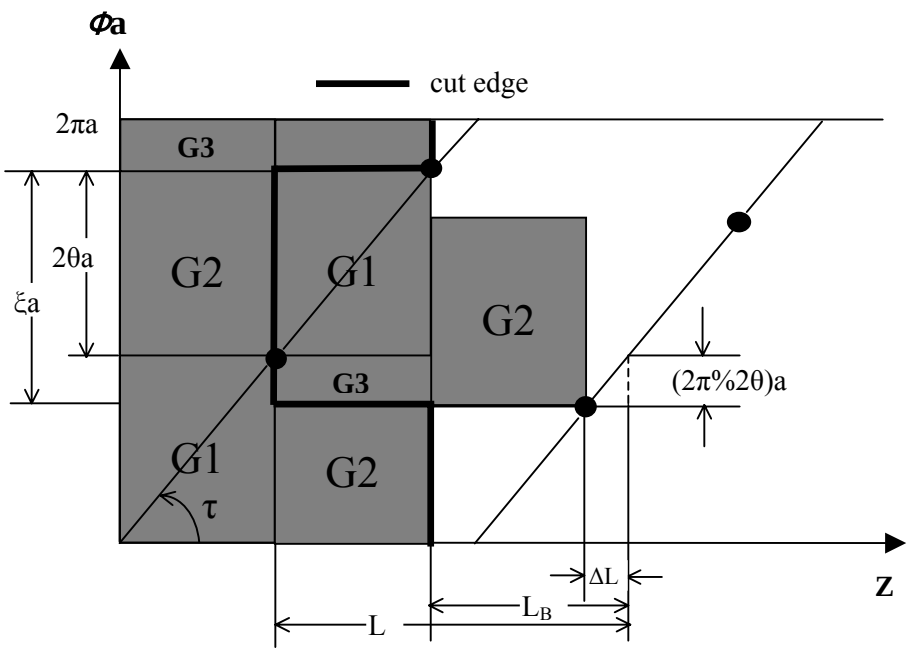

Fig.2.8 Field distributions (dark sections) on the unfolded wall of a Vlasov launcher, where $2\pi\%2\theta < \theta$. The edges of the launcher cuts are indicated.

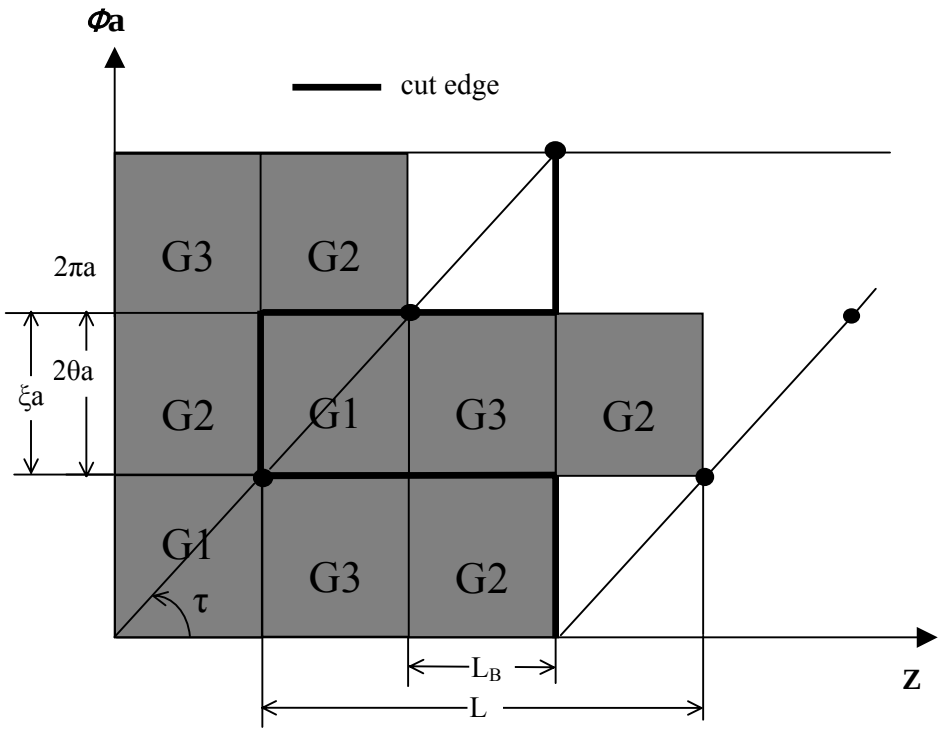

Fig.2.9 Field distributions (dark sections) on the unfolded wall of a Vlasov launcher, where 2π%2θ=0. The edges of the launcher cuts are indicated.

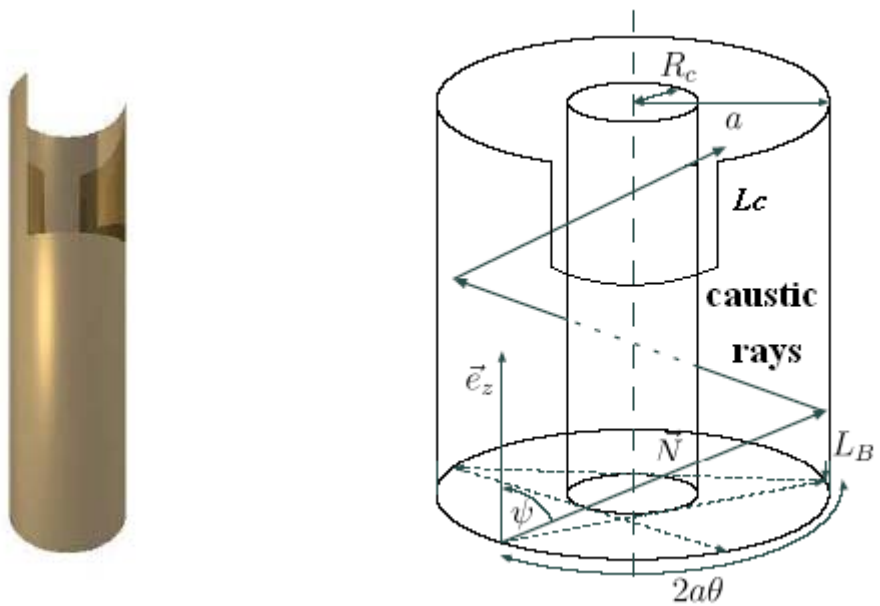

(a) (b)

Fig.2.10 Cylindrical launcher with rectangular cut:
(a) schematic drawing; (b) ray representation in launcher.

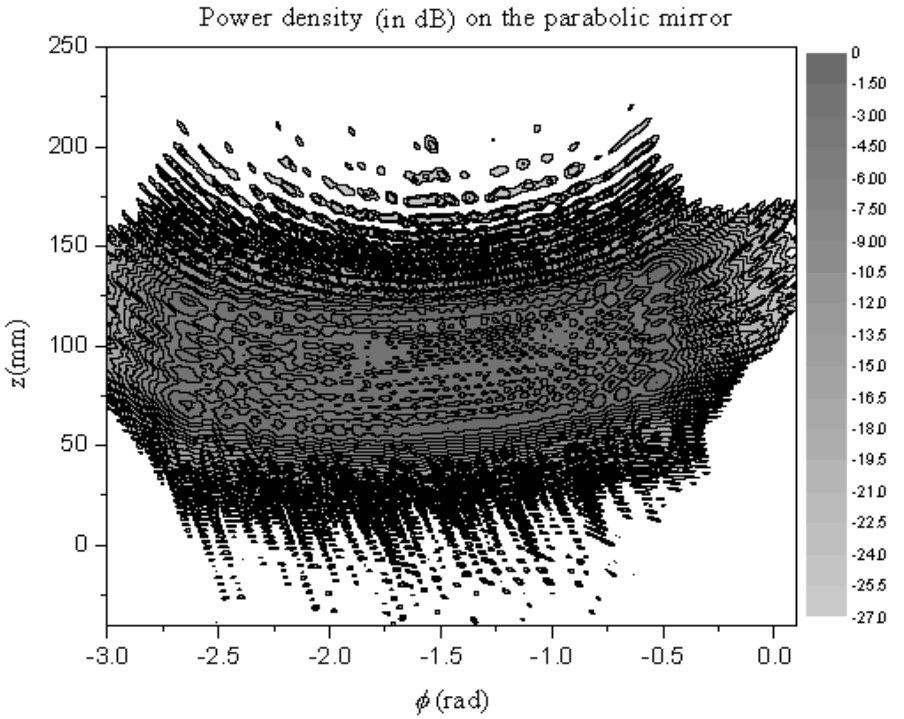

Fig.2.11 Field distribution on the parabolic mirror radiated from a Vlasov launcher.

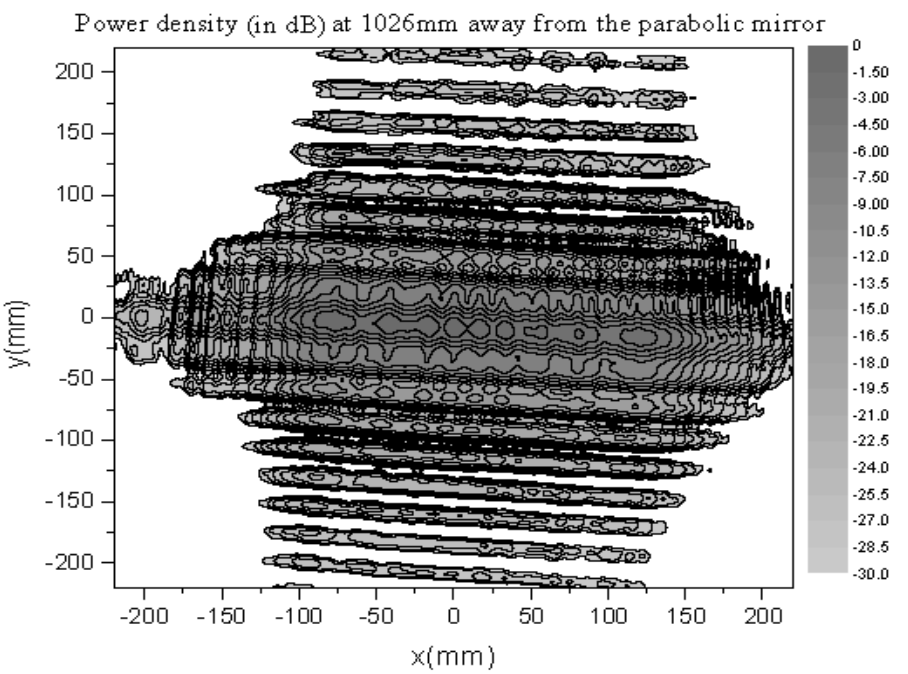

Fig.2.12 Field distribution on the aperture at 1026mm away from the parabolic mirror.

As an example, the field radiated from a Vlasov launcher with helical cut on a parabolic mirror surface is shown in Fig.2.11, where the launcher radius is 32.5mm, the operation mode is $TE_{34,19}$ mode, and the frequency is 170GHz. Reflected by two plane mirror, the field contour in Fig.2.12 is obtained at the output window of a gyrotron (see Fig.1.2b) which is 1026mm away from the parabolic mirror. In order to obtain the Gaussian mode content of the RF beam, a Gaussian mode fitting code has been developed for the analysis of the RF beam, and the results show a fundamental Gaussian mode content of 83.2% in the wave beam shown in Fig.2.12. This is a verification for our computer code developed for the synthesis of q.o. mode converters.

2.3 Denisov launcher

In order to depress the fields at the edges of cuts, the wave beam in a Vlasov-type launcher should be pre-shaped to provide a focused field distribution. A waveguide with transverse dimension large compared to the wavelength is called "overmoded" since more than one waveguide mode can propagate. Power can be coupled to desirable modes through wall distortions such as diameter change, curvature, ellipticity and triangularity. A Denisov-type launcher is an improved version of the Vlasov-type launcher and is also known as a dimpled-wall waveguide antenna intended for operation at a given mode mixture, since the dimples at the surface of the radiator are designed for transformation of the gyrotron cavity mode into a wave beam with a Gaussian profile of the intensity [68]. The principle of the transformation can be explained as follows: since the boundary condition is changed, the eigenmode of a Vlasov-type launcher is coupled to its satellite modes, that is to say the wall distortions (scattering surface) transform the input eigenwave to an eigenwave of the weakly perturbed transmission line. This leads to a variation of the mode spectrum which is defined as the complex amplitude distribution of the waveguide modes. In a waveguide unit with a continuous change of the cross section the mode spectrum is also changing continuously. The deformations of the launcher wall surface should be well designed to convert the input eigenmode to a mixture of modes such that the power in the waveguide is contained in a bundle with a Gaussian-like amplitude profile so that the spectrum of a Gaussian wave beam should be achieved after the conversion. The length of dimpled-wall launcher should be short enough to avoid interception with the expanding spent electron beam, so the profile must be achieved within a short distance.

To achieve a sidelobe-free fundamental Gaussian beam (TEM_{00} mode) as the output mode, the launcher wall must have waveguide deformations such that the incident rotating TE mode is converted to a mode mixture generating a Gaussian beam distribution [59,60,69]. The Gaussian distribution can be approximated by a raised-cosine distribution given in one-dimension as [70]

$$\frac{\sqrt{2}}{\sqrt{\pi w}}\exp\left(-\frac{2z^2}{w^2}\right)\approx\frac{b}{3\pi}(1+\cos bz)^2 \tag{2.26}$$

and $$f(z)=1+\cos bz=\left(1+\frac{1}{2}\exp(jbz)+\frac{1}{2}\exp(-jbz)\right) \tag{2.27}$$

The initial conversion of the input mode into the two other modes inherently starts with a phase shift of 90 degree. However, according to the spectrum of a Gaussian beam wave the initial relative phases of all the components must be zero. Hence the minimum length of the converter is defined by the restriction that the three modes must have the same phase after conversion. This leads to the minimum length of

$$L_{\min}=\frac{\pi}{\left|2k_{z1}-k_{z2}-k_{z3}\right|} \tag{2.28}$$

where k_{z1}, k_{z2} and k_{z3} are the propagation constants of the modes in the unperturbed circular waveguide.

A raised-cosine tapered field distribution for an astigmatic Gaussian beam can be obtained by means of a superposition of nine specific waveguide modes with matched amplitudes and relative phases, which are easier to generate for volume modes than for whispering gallery modes. Therefore modern high-power gyrotrons operate in volume modes rather than in whispering gallery modes like in earlier times.

$$f(\phi,z)=\left(1+\frac{1}{2}\exp\left(\frac{j\pi\phi}{\theta}\right)+\frac{1}{2}\exp\left(\frac{-j\pi\phi}{\theta}\right)\right)\left(1+\frac{1}{2}\exp\left(\frac{j2\pi z}{L}\right)+\frac{1}{2}\exp\left(\frac{-j2\pi z}{L}\right)\right) \tag{2.29}$$

The interference of the nine waveguide modes creates an RF-field bunching in the axial and azimuthal directions. The relative power of satellite modes forming the Gaussian wave beam corresponds to Table 2.1. Requirements for this bunching are: (a) longitudinal bunching—modes must have equal caustic radii and an interference length close to the launcher cut length; (b) azimuthal bunching—modes must have equal caustic radii and similar Bessel zeros. This leads to the following mode selection rules:

$$\Delta m=\frac{\pi}{\theta},\qquad \Delta\beta=\pm\frac{2\pi}{L} \tag{2.30}$$

These wall distortions (scattering surface) can transform the input eigenwave to an eigenwave of the weakly perturbed transmission line. The helical converter is described by the following wall perturbation:

$$R(\phi, z) = a + \delta_1 \cos\left(\Delta\beta_1 z - \ell_1 \phi\right) + \delta_2 \cos\left(\Delta\beta_2 z - \ell_2 \phi\right) \tag{2.31}$$

where $\Delta\beta_1 = k_{z\,m,n} - k_{z\,m\pm1,n}$, $\quad \ell_1 = \pm 1$ (2.32)

$\Delta\beta_2 = k_{z\,m,n} - k_{z\,m\pm\Delta m,n\mp\Delta n}$, $\quad \ell_2 = \pm\Delta m$ (2.33)

Here, $k_{zm,\mathrm{n}}$ is the longitudinal wave number of the TE_{mn} mode, m and n are the azimuthal and radial indexes, respectively. In equation (2.31), the term with $\ell_1 = \pm 1$ describes the longitudinal bunching, and that with $\ell_1 = \pm\Delta m$ the azimuthal bunching. If ℓ_1 and ℓ_2 in equations (2.32-33) are positive, $R(\phi, z)$ in equation (2.31) gives helical deformations with right hand rotation, otherwise with left hand rotation. The required minimal launcher length is [71]

$$L_{\min} = \frac{\pi}{\left|2k_{z\,mn} - k_{z\,m+\Delta m,n\ \Delta n} - k_{z\,m\ \Delta m,n+\Delta n}\right|} \tag{2.34}$$

Owing to the fact that the root of the Bessel function derivative for the $TE_{m,n-1}$ mode is not exactly equal to that for the $TE_{m,n+1}$ mode, $\Delta\beta_1$ has two different values in equation (2.32), and also two values for $\Delta\beta_2$ in equation (2.33). We use the average of the two different values to evaluate $\Delta\beta_1$, and the same processing to $\Delta\beta_2$.

Table 2.1 Set of TE modes to generate a Gaussian-like field distribution (with relative power according to equation (2.29)).

	→ azimuthal bunching		
↓ axial bunching	$TE_{m-2,n+1}$ 1/36	$TE_{m+1,n}$ 1/9	$TE_{m+4,n-1}$ 1/36
	$TE_{m-3,n+1}$ 1/9	$TE_{m,n}$ 4/9	$TE_{m+3,n-1}$ 1/9
	$TE_{m-4,n+1}$ 1/36	$TE_{m-1,n}$ 1/9	$TE_{m+2,n-1}$ 1/36

This results in the following equations for a TE_{mn} mode gyrotron

$$\Delta\beta_1 = \frac{1}{2}\left(\beta_{m-1,n} - \beta_{m+1,n}\right) = \frac{1}{2}\left[\sqrt{k_0^2 - \left(\frac{X_{m-1,n}}{a}\right)^2} - \sqrt{k_0^2 - \left(\frac{X_{m+1,n}}{a}\right)^2}\right] \tag{2.35}$$

$$\Delta\beta_2 = \frac{1}{2}\left(\beta_{m-\Delta m,n+\Delta n} - \beta_{m+\Delta m,n-\Delta n}\right) = \frac{1}{2}\left[\sqrt{k_0^2 - \left(\frac{X_{m-\Delta m,n+\Delta n}}{a}\right)^2} - \sqrt{k_0^2 - \left(\frac{X_{m+\Delta m,n-\Delta n}}{a}\right)^2}\right] \tag{2.36}$$

As an example, the results of numerical simulation for a dimpled-wall launcher with a radius of 20mm operating in the $TE_{22,6}$ mode at 118GHz are shown in Figs.2.13-15. The helical perturbations can be found in Fig.2.13(a), and the focused field with a nearly Gaussian beam distribution is plotted in Fig.2.13(b). The longitudinal and azimuthal bunchings are demonstrated in Figs.14-15.

The principle of a highly oversized Denisov-type launcher can be explained in the frame of geometrical optics. A mode in a circular waveguide can be regarded as a superposition of plane waves represented by rays as described in section 2.1. Among the rays composing the initial mode let us appoint one to be "chief". The deformed launcher wall surface focuses the rays near the reflection points of the chief and defocuses them at the remaining area. Then, successively reflected from the walls, the rays will converge to the chief and finally, will compose an eigenmode of an open mirror waveguide with the transverse distribution of the RF field depending on the mirror profile.

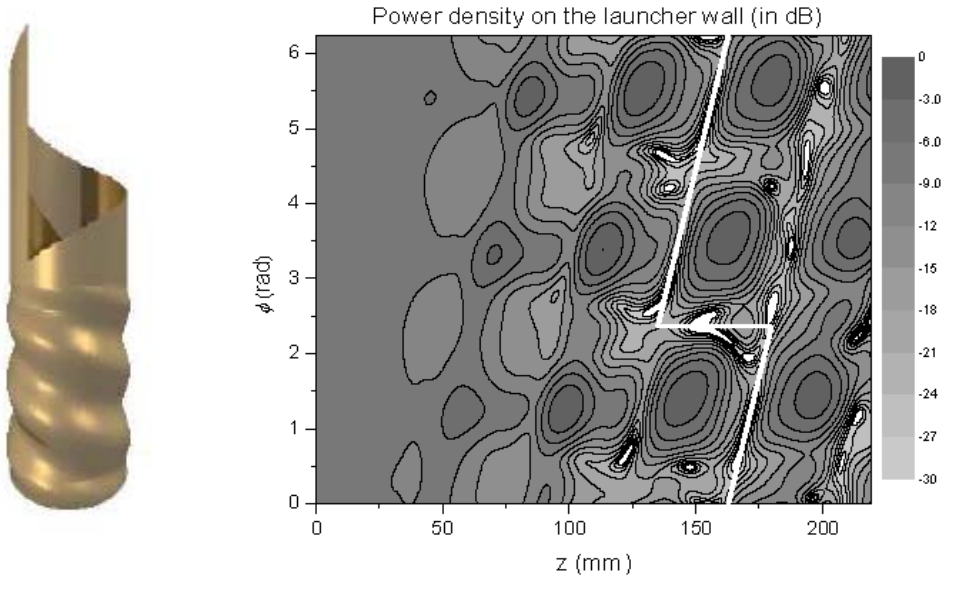

(a) (b)

Fig.2.13 Dimpled-wall launcher ($TE_{22,6}$ mode): (a) schematic drawing; (b) amplitude contours of fields on the unfolded launcher wall. The edges of cuts are indicated.

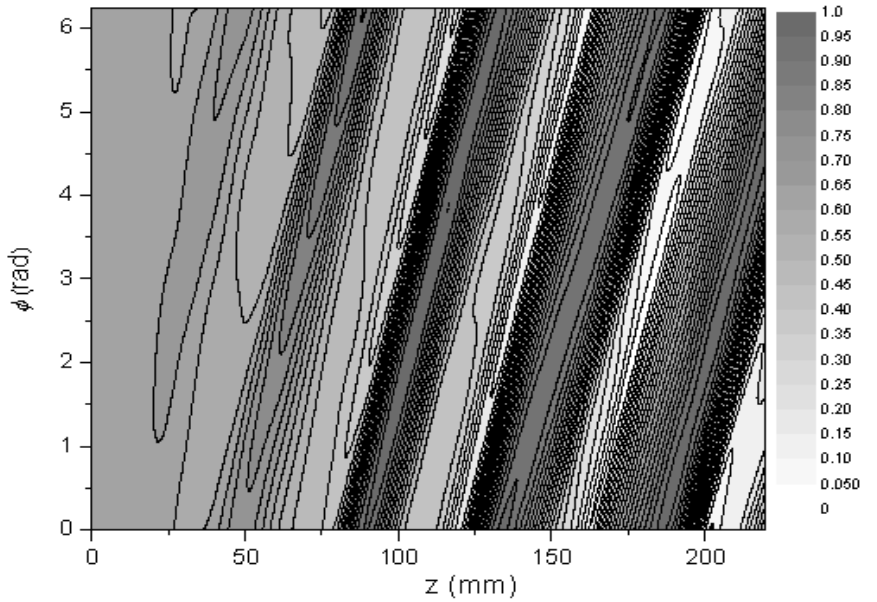

Fig.2.14 Longitudinal bunching ($TE_{22,6}$ mode) with only $\ell_1 = 1$ (δ_2=0) in the wall deformations.

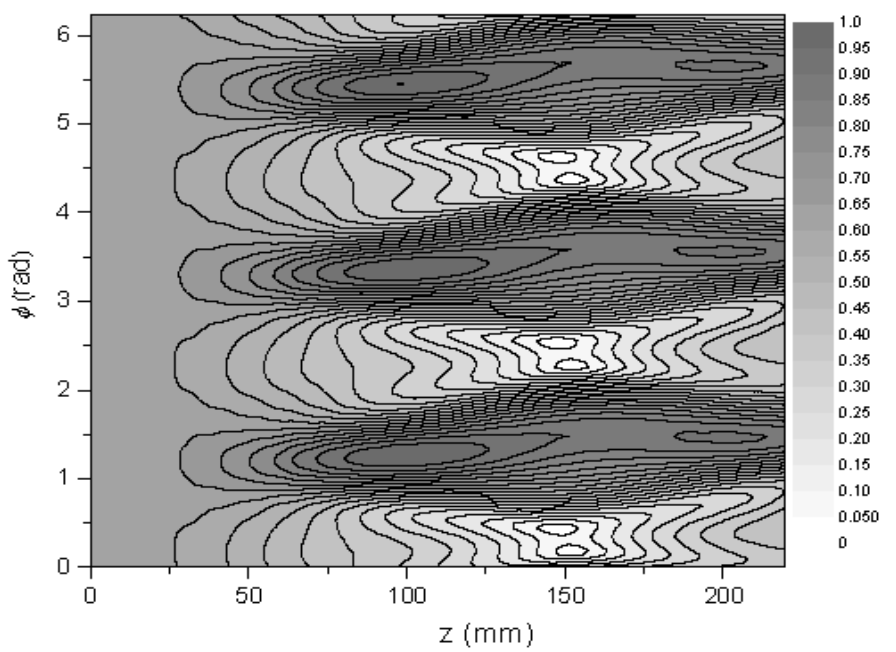

Fig.2.15 Azithumal bunching ($TE_{22,6}$ mode) with only $\ell_2 = 3$ (δ_1=0) in the wall deformations.

2.4 Slope of Launcher Diameter Taper

In order to prevent wave reflection at some perturbed positions, and thus to prevent spurious oscillations in the converter region of the launcher excited by the spent electron beam, a positive slope taper α is usually introduced on the wall radius of the launcher [70]. Taking the slope of the taper into account, the launcher wall surface is described by

$$\begin{aligned} R(\phi,z) &= a+\alpha z+\delta_1\cos(\Delta\beta_1 z-\ell_1\phi)+\delta_2\cos(\Delta\beta_2 z-\ell_2\phi) \\ &= R(z)+\delta_1\cos(\Delta\beta_1 z-\ell_1\phi)+\delta_2\cos(\Delta\beta_2 z-\ell_2\phi) \end{aligned} \tag{2.37}$$

In the case of $\alpha\neq 0$, $R(z)=a+\alpha z$, $\Delta\beta_i$ in equations (2.35-36) is no longer a constant and becomes [75]

$$\begin{aligned} &\int_0^z \Delta\beta_i(z)dz = \frac{1}{2}\left(\int_0^z \beta_{mn}(z)dz - \int_0^z \beta_{lp}(z)dz\right) \\ &\int_0^z \beta_{ij}(z)dz = \frac{1}{\tau}\left[\sqrt{k_0(a+\alpha z)^2} - X_{ij}\arccos\left(\frac{X_{ij}}{k_0(a+\alpha z)}\right)\right]\Bigg|_{z=0}^{z} \end{aligned} \tag{2.38}$$

If the slope of the taper is very small, for instance α=0.002, equation (2.38) can be well approximated by

$$\int \Delta\beta_i(z)dz \approx \Delta\beta_i z = \frac{z}{2}\left[\sqrt{k_0^2-\left(\frac{X_{mn}}{a+\alpha z}\right)^2}-\sqrt{k_0^2-\left(\frac{X_{lp}}{a+\alpha z}\right)^2}\right] \tag{2.39}$$

In a tapered launcher the inclination angle τ of the helical line shown in Figs.2.5 and 2.7-9 is variable along the longitudinal position. The expression for the helical cut of the up-tapered launcher has been derived and published in refs. [75,76], it can be described as:

$$\begin{aligned} g = \frac{\theta}{\sin\theta}\frac{X_{mn}}{k_0\alpha}\Bigg\{&\ln\left[\alpha(z-z_s)+R_s+\sqrt{[\alpha(z-z_s)+R_s]^2-\left(\frac{X_{mn}}{k_0}\right)^2}\right] \\ &-\ln\left[R_s+\sqrt{R_s^2-\left(\frac{X_{mn}}{k_0}\right)^2}\right]\Bigg\} \end{aligned} \tag{2.40}$$

$$\varphi = \begin{cases} \dfrac{g}{R_s + \alpha(z - z_s)} + \varphi_s & for \quad g < 2\pi\left[R_s + \alpha(z - z_s)\right] \\ \dfrac{g}{R_s + \alpha(z - z_s)} + \varphi_s - 2\pi & for \quad g \geq 2\pi\left[R_s + \alpha(z - z_s)\right] \end{cases} \tag{2.41}$$

where g is a parameter that connects between equations (2.40) and (2.41), $z \geq z_s$, (φ_s, z_s) and R_s are the coordinate and radius at the beginning of the cut, respectively. The coordinates (φ, z) describe the helical cut shown in Fig.2.13(b). In the case when the slope α of the taper is very small, equation (2.40) can be well approximated by

$$g = \frac{\theta}{\sin\theta} \frac{(z - z_s) X_{mn}}{R_m \sqrt{k_0^2 - \left(\dfrac{X_{mn}}{R_m}\right)^2}} \tag{2.42}$$

where R_m is the radius at the middle of the straight cut.

2.5 Method for the Synthesis of Denisov-Type Launcher

The efficiency of a q.o. mode converter is usually defined as the content of the fundamental Gaussian component in the outgoing wave beam at the output window. For achieving a high conversion efficiency and high power transmission, the launcher should be well designed to depress the diffraction from the edges of the launcher cuts, and to obtain a high quality radiated field distribution with high Gaussian contents to decrease the power losses in the open mirror transmission line. Hence, the deformations of the launcher wall surface should be well designed to provide a set mixture of modes to generate a Gaussian-like field distribution.

Several methods have been proposed which employ tailored aperture distributions, such that the sidelobes in the beam wave are reduced [53,72,73]. Recently, A.A. Bogdashov and G.G. Denisov have reported their excellent researches on dimpled-wall launchers [74]. The approximations for the longitudinal wavenumbers of very high order modes are given in [74]:

$$\begin{cases} k_{z\,m+\Delta m, n-\Delta n} \approx k_{z\,mn} - \dfrac{X_{mn}\nu}{k_{z\,mn} a^2} - \dfrac{\nu^2}{2k_{z\,mn} a^2 \cos^2\psi} - \dfrac{\nu\mu}{k_{z\,mn} a^2} \\ k_{z\,m-\Delta m, n+\Delta n} \approx k_{z\,mn} + \dfrac{X_{mn}\nu}{k_{z\,mn} a^2} - \dfrac{\nu^2}{2k_{z\,mn} a^2 \cos^2\psi} - \dfrac{\nu\mu}{k_{z\,mn} a^2} \end{cases} \tag{2.43}$$

where a is the radius of the launcher. The formula for the perturbation length is the same as equation (2.34)

$$L_{\min} = \frac{\pi}{2\Delta}, \qquad \Delta = \frac{\left|2k_{z\,mn} - k_{z\,m+\Delta m,n-\Delta n} - k_{z\,m-\Delta m,n+\Delta n}\right|}{2} \tag{2.44}$$

The roots of the Bessel functions or their derivatives in correspondence to the main and to two satellite modes can be approximated by

$$X_{m+\Delta m,n-\Delta n} = X_{mn} + \nu + \mu, \qquad X_{m-\Delta m,n+\Delta n} = X_{mn} - \nu + \mu \tag{2.45}$$

If only the azimuthal or radial number of a high-order mode (e.g. TE_{mn} mode, m>>1 and n>>1) is changed, the spectrum of the Bessel-function roots is almost equidistant and leads to $\mu \approx 0$. For the nearest quasi-degenerate mode ($X_{m+\Delta m,n-\Delta n} - X_{mn} \approx X_{mn} - X_{m-\Delta m,n+\Delta n}$, $\Delta m \neq 0$, $\Delta n \neq 0$), from equation (2.45) one can obtain $\nu \approx 0$. Based on the approximations for the longitudinal wavenumbers, the amplitudes and lengths of the launcher wall deformations for different approaches have been derived and published in IEEE on MTT, Mar., 2006 [75], and the formulas for the amplitudes and lengths can be described as follows [75].

2.5.1 Adiabatic Conversion

Adiabatic conversion is realized in a dimpled-wall launcher with gradually increasing deformations. The condition of adiabatic conversion is the absence of strong energy exchange between the operating mode and the satellite modes, it requires a very large length of the launcher as shown in Fig.2.16 [74].
The perturbation amplitude σ and launcher length L can be derived as:
a) For higher-order modes (e.g. TE_{mn} mode, m>>1 and n>>1) where only the azimuthal or the radial index is different, a Gaussian field structure is formed along the longitudinal coordinate. Note that for $\mu \approx 0$, combining equation (2.43) and $L \cdot \Delta = \pi$ (see Fig.2.16) the launcher length L and the perturbation amplitude δ can be obtained.

In the case of $\Delta m = 0, \Delta n \neq 0$

$$L = 2a^2 \frac{k_{zm,n}^3}{\pi k_0{}^2 (\Delta n)^2} \left(1 - \frac{m^2}{X_{mn}{}^2}\right) \tag{2.46}$$

$$\delta = \frac{(\Delta n \pi k_0)^2}{\left(X_{mn}{}^2 - m^2\right) k_{zm,n}^2} \tag{2.47}$$

In the case of $\Delta m \neq 0, \Delta n = 0$

$$L = 2\pi a^2 \frac{k_{zm,n}^3}{k_0{}^2 (\Delta m\theta)^2}\left(1 - \frac{m^2}{X_{mn}{}^2}\right) \tag{2.48}$$

$$\delta = \frac{(\Delta m\theta k_0)^2}{\left(X_{mn}{}^2 - m^2\right) k_{zm,n}^2} \tag{2.49}$$

b) For the nearest quasi-degenerate mode, where $\nu \approx 0$, a Gaussian structure is formed along the azimuth of the circular waveguide

$$L = \frac{2\pi k_{zm,n} a^2}{(\Delta m)^2}\left(1 - \frac{m^2}{X_{mn}^2}\right) \tag{2.50}$$

$$\delta = \frac{(\Delta m)^2}{X_{mn}^2 - m^2} \tag{2.51}$$

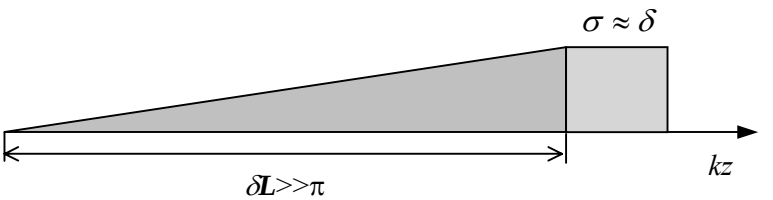

Fig.2.16 Gradually increasing deformation and length of launcher. The deformation $\sigma = \delta$ corresponds to the transmission line with a Gaussian wave structure.

2.5.2 Shortened Launcher

The launcher with gradually increasing deformations is not used in practice due to the large length, which leads to high ohmic losses on the launcher wall surfaces and the extending electron beam inside of the ultra high vacuum of the gyrotron requires a minimum distance to the launcher. Therefore, the maximum length of the launcher is restricted and limits the conversion efficiency of the periodically dimpled-wall launcher. In terms of equation (2.44), the launcher length L should be larger than L_{min}. Generally, the length L of the dimpled-wall launcher is in the interval [74]

$$L_{\min} = \frac{\pi}{2\Delta} \le L \le \frac{\pi}{\sqrt{1.5}\Delta} \tag{2.52}$$

The partial deformation is shown in Fig.2.17. The perturbation amplitude and exact length of the launcher can be derived as [75]:

a) If only the azimuthal or the radial index of a high-order mode is changed:
In the case of $\Delta m = 0, \Delta n \neq 0$

$$L = 2\hbar a^2 \frac{k_{zm,n}^3}{\pi k_0^{\,2} (\Delta n)^2} \left(1 - \frac{m^2}{X_{mn}^{\,2}}\right) \tag{2.53}$$

$$\delta = \frac{\lambda a (\Delta n \pi k_0)^2}{\left(X_{mn}^{\,2} - m^2\right) k_{zm,n}^2} \tag{2.54}$$

In the case of $\Delta m \neq 0, \Delta n = 0$

$$L = 2\hbar \pi a^2 \frac{k_{zm,n}^3}{k_0^{\,2} (\Delta m \theta)^2} \left(1 - \frac{m^2}{X_{mn}^{\,2}}\right) \tag{2.55}$$

$$\delta = \frac{\lambda a (\Delta m \theta k_0)^2}{\left(X_{mn}^{\,2} - m^2\right) k_{zm,n}^2} \tag{2.56}$$

b) For the nearest quasi-degenerate mode

$$L = \frac{2\hbar \pi k_{zm,n} a^2}{(\Delta m)^2} \left(1 - \frac{m^2}{X_{mn}^{\,2}}\right) \tag{2.57}$$

$$\delta = \frac{\lambda a (\Delta m)^2}{X_{mn}^{\,2} - m^2} \tag{2.58}$$

where, $1 > \lambda \geq 0.25$, $\frac{1}{\sqrt{1.5}} \geq \hbar \geq 0.5$. The perturbation length is $L_p = 0.5L$.

If the value of π/θ is approximately equal to an integer, the ray presentation of a waveguide mode forms an almost closed polygon in the cross section of launcher, this can be found from Fig.2.3(b). For such a waveguide mode, a dimpled-wall launcher with wall surface described by equations (2.31) and (2.37) can be designed in terms of equations (2.55-58) to transform the mode into to a nearly Gaussian distribution in both the longitudinal and azimuthal directions. As an example, considering the $TE_{22,6}$ mode which gives π/θ=2.94, θ =61.2 degree, the mode selection rule is Δm=3. The deformation amplitudes and lengths are shown in Fig.2.18. The fields inside the launcher are calculated by means of the coupled-mode

method, the power densities on the wall are shown in Fig.2.13(b). The appropriate amplitude relation can be achieved with a short perturbed section of 90 mm. A longer smooth section follows and allows for the development of the optimum phase relations. The cuts are around a Gaussian bundle, where the wall currents are at a minimum. The relative powers of satellite modes at the aperture of the launcher are given in Table 2.2. Comparing Table 2.1 in section 2.3 and Table 2.2, we can see that a wave beam with good appropriate relative amplitudes is achieved at the aperture of launcher.

Due to the low fields on the edges of the straight and helical cuts and the Gaussian bundle at the aperture, the dimpled-wall launcher generates a well-focused, Gaussian-like radiation pattern with low diffraction. The mode composition coefficients vary along the z-axis are shown in Fig.2.19.

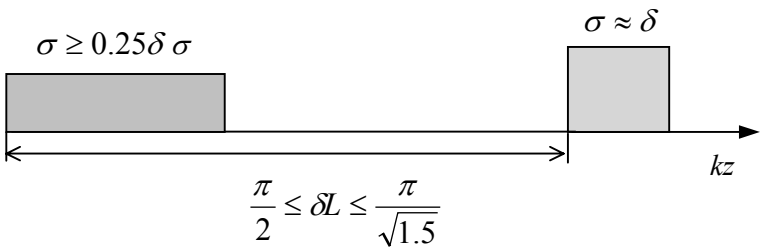

Fig.2.17 Partial deformation and length of launcher. The deformation $\sigma = \delta$ corresponds to the transmission line with a Gaussian wave structure.

Table 2.2 Relative powers of the satellite modes at the aperture of the $TE_{22,6}$-mode launcher.

	azimuthal bunching →		
axial bunching ↓	$TE_{20,7}$ 3.41%	$TE_{23,6}$ 11.53%	$TE_{26,5}$ 3.58%
	$TE_{19,7}$ 10.58%	$TE_{22,6}$ 44.27%	$TE_{25,5}$ 10.75%
	$TE_{18,7}$ 1.93%	$TE_{21,6}$ 10%	$TE_{24,5}$ 1.97%

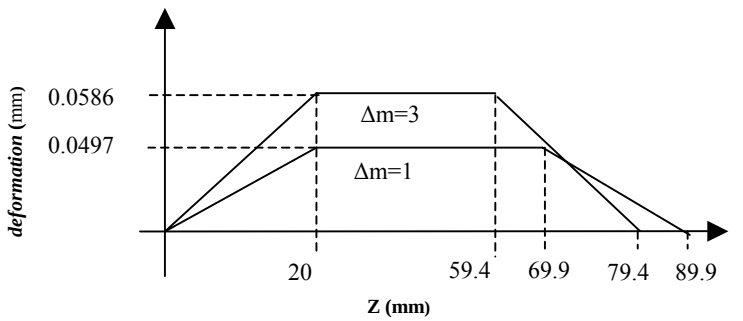

Fig.2.18 Schematic drawing of the wall deformations of the launcher for the $TE_{22,6}$ mode.

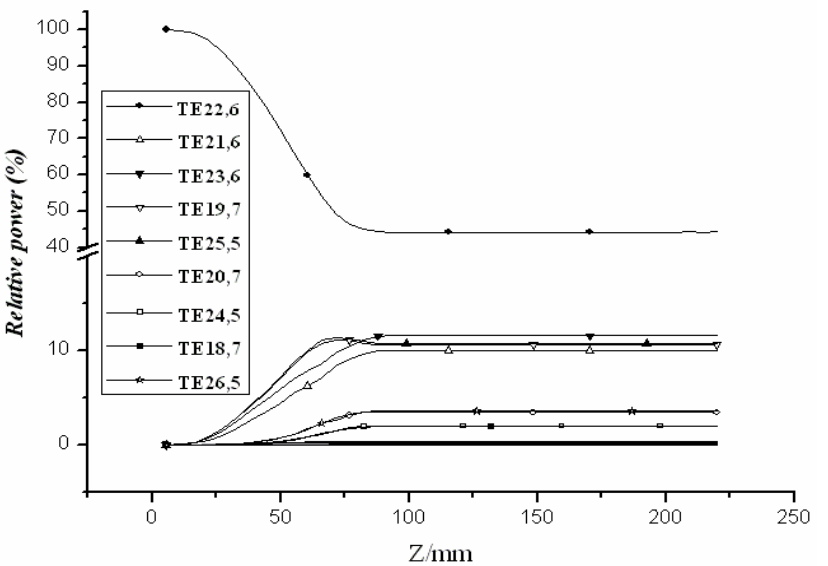

Fig.2.19 Mode composition (relative power) coefficients vary along the z-axis of the launcher for the $TE_{22,6}$ mode.

2.6 Power Density on the Launcher Wall

In the design of launchers for megawatt gyrotrons, as the power is relatively high, the thermal deformations of the launcher wall should be investigated. Especially in a dimpled-wall launcher, the fields on the launcher wall are focused and the maximum power density on the dimpled wall must meet the technical requirement of the cooling system for the launcher.

The power density can be calculated according to the power at the input of the launcher and the field distribution on the launcher wall [77]. Considering the input power as P_N, then the power density p_{in} at the beginning of the launcher is:

$$p_{in} = F_m \frac{R_s}{2} \left| H_{\tan} \right|^2 \tag{2.59}$$

where F_m is a factor with respect to the material that the launcher made from, for instance F_m=1.5 for Glidcop. The surface resistivity R_s and tangential magnetic field H_{tan} are given respectively by

$$R_s = \sqrt{\frac{\omega \mu_0}{2\sigma_0}} \tag{2.60}$$

$$\left| H_{\tan} \right|^2 = \left| H_r \right|^2 + \left| H_\theta \right|^2 + \left| H_z \right|^2 \approx \left| H_\theta \right|^2 + \left| H_z \right|^2 \tag{2.61}$$

here ω represents the angular frequency, μ_0 the permeability, σ_0 the electrical conductivity, and H_r, H_ϕ and H_z are the magnetic fields in radial, azimuthal and longitudinal directions, respectively. Expressions of field components for a TE_{mn} mode are indicated below

$$H_\theta = -j \frac{m}{a} \sqrt{\frac{2 \cdot P_N \cdot \beta}{\pi \cdot \omega \cdot \mu_0}} \frac{e^{jm\phi}}{\sqrt{X_{mn}^2 - m^2}} \tag{2.62}$$

$$H_z = -j \frac{X_{mn}^2}{a^2} \sqrt{\frac{2 \cdot P_N}{\pi \cdot \omega \cdot \mu_0 \cdot \beta}} \frac{e^{jm\phi}}{\sqrt{X_{mn}^2 - m^2}} \tag{2.63}$$

where β is the propagation constant. So, we get

$$\left| H_{\tan} \right|^2 = \frac{2 \cdot P_N}{a^2 \cdot \pi \cdot \omega \cdot \mu_0 \cdot \left(X_{mn}^2 - m^2 \right)} \left(\beta \cdot m^2 + \frac{X_{mn}^4}{\beta \cdot a^2} \right) \tag{2.64}$$

$$p_{\max} = p_{in} 10^{-\frac{r_p}{10}} \tag{2.65}$$

In equation (2.65), r_p is the relative power in dB at the beginning of launcher.

2.7 Coupled Mode Method

In a dimpled-wall launcher, due to the corrugations of the wall surface, the fields in the launcher are no longer exactly orthogonal modes. As described in section 2.3 and 2.4, the corrugations can couple the energy between the gyrotron cavity mode and the desirable satellite modes. The fields and the change of the mode spectrum in a dimpled-wall launcher can be accurately analyzed by means of the mode coupling theory. In general, the equation for coupling between the modes is given by [78-80]

$$\frac{\partial A^k}{\partial z} = jk_{zk}(z)A^k + j\sum_{l=1}^{L} C_{k,l}(z)A^l \tag{2.66}$$

where the superscripts k and l denote TE or TM modes (mode k: TE_{mp} or TM_{mp}, mode l: TE_{nq} or TM_{nq}), A^k is the complex amplitude of the k-th mode, $C_{k,l}$ is called coupling coefficient between the modes k and l and can be calculated as [81]

$$C_{k,l}(z) = K_{k,l}\frac{\alpha_{k,l}(z)}{R(z)} \tag{2.67}$$

$$\alpha_{k,l}(z) = \frac{1}{2\pi}\int_0^{2\pi} d_h(\phi,z)\exp\big(-j(m-n)\phi\big)d\phi \tag{2.68}$$

$R(z)$ is the launcher radius, $d(\phi,z)$ represents the distortions of launcher wall surface which can be described as

$$\begin{aligned} r(\phi,z) &= R(z) + d(\phi,z) = R(z) + \sum_{h=1}^{H} d_h(\phi,z) \\ &= a + \alpha z + \sum_{h=1}^{H} \delta_h \cdot \cos\big(\ell_h\phi + \Delta\beta_h z\big) \end{aligned} \tag{2.69}$$

a and α are the radius at the beginning and the slope of taper of the launcher, respectively.

If $|\ell_h| = |m-n|$ (it denotes the ℓ_h th-order wall perturbation) has the form of a periodic interference pattern between the two coupling modes, then $\alpha_{k,l}(z)$ becomes

$$\alpha_{k,l}(z) = \frac{dR(z)}{dz} = \alpha, \qquad \text{when} \quad \ell_h = m-n = 0 \tag{2.70}$$

$$\alpha_{k,l}(z) = \frac{\delta_n}{2}\exp(j\Delta\beta_h z) \qquad \text{when} \quad \ell_h = m - n \tag{2.71}$$

$$\alpha_{k,l}(z) = \frac{\delta_n}{2}\exp(-j\Delta\beta_h z) \qquad \text{when} \quad \ell_h = n - m \tag{2.72}$$

In the case of $|\ell_h| \neq |m-n|$, $\alpha_{k,l}(z) = 0$.

In equation (2.66), $K_{k,l}$ is the so-called the coupling factor. The coupling theory is discussed in ref. [78] in detail, the general forms for the coupling coefficient are presented in equations (78), (84) and (85) in [78]. From these equations, the coupling factor for the periodically corrugated launcher can be derived as [81].

$$K_{k,l} = \frac{mn\left(k_0^2 - k_{zm,p}k_{zn,q}\right) - \left(\dfrac{X_{mp} - X_{nq}}{R(z)}\right)^2}{\sqrt{k_{zm,p}k_{zn,q}\left(X_{mp}^2 - m^2\right)\left(X_{nq}^2 - n^2\right)}} \qquad \text{for } TE_{mp} \text{ to } TE_{nq} \tag{2.73}$$

$$K_{k,l} = \frac{jmk_0\left(k_{zm,p} - k_{zn,q}\right)}{\sqrt{k_{zm,p}k_{zn,q}\left(X_{mp}^2 - m^2\right)}} \qquad \text{for } TE_{mp} \text{ to } TM_{nq} \tag{2.74}$$

$$K_{k,l} = \frac{jnk_0\left(k_{zm,p} - k_{zn,q}\right)}{\sqrt{k_{zm,p}k_{zn,q}\left(X_{nq}^2 - n^2\right)}} \qquad \text{for } TM_{nq} \text{ to } TE_{mp} \tag{2.75}$$

$$K_{k,l} = \frac{k_0^2 - k_{zm,p}k_{zn,q}}{\sqrt{k_{zm,p}k_{zn,q}}} \qquad \text{for } TM_{mp} \text{ to } TM_{nq} \tag{2.76}$$

Finally, the variation of the mode spectrum along the z-position can be calculated in terms of the equations (2.66-76). The fields in the dimpled-wall launcher were calculated for the $TE_{22,6}$ mode by using the coupled-mode method, the power densities on the unfolded launcher wall are shown in Fig.2.13(b).

2.8 Brief Summary

In this chapter the methods for the analysis of a circular waveguide antenna and for the synthesis of a dimpled-wall launcher is presented. A well-focused wave beam with a good mode composition can be obtained at the aperture of a dimpled-wall launcher. The wave beam quality is usually described as the correlation coefficient of the wave beam to an ideal fundamental Gaussian mode (TEM_{00} mode). There are two ways to define the correlation coefficient: the amplitude correlation coefficient η_s called scalar correlation coefficient, and the vector correlation coefficient η_v including the amplitude and phase, which can be given as

$$\eta_s = \frac{\int_S |u_1| \bullet |u_2| ds}{\sqrt{\int_S |u_1|^2 ds \bullet \int_S |u_2|^2 ds}} \tag{2.77}$$

$$\eta_v = \frac{\int_S |u_1| \bullet |u_2| \exp[j(\varphi_1 - \varphi_2)] ds \bullet \int_S |u_1| \bullet |u_2| \exp[j(\varphi_2 - \varphi_1)] ds}{\int_S |u_1|^2 ds \bullet \int_S |u_2|^2 ds} \tag{2.78}$$

where $|u_1|\exp(j\varphi_1)$ represents an ideal fundamental Gaussian beam and $|u_2|\exp(j\varphi_2)$ the field distribution of the wave beam. If the mode purity is 100%, that means there is no high order mode in the wave beam, η_s and η_v are equal to 1. Unfortunately, although a well-designed dimpled-wall launcher can convert a cavity mode into a nearly Gaussian beam, there are still some high-order modes in the wave beam. As example, η_s and η_s are 98.5% and 95.3% at the aperture of the dimpled-wall launcher for the $TE_{22,6}$ mode (see Fig.2.13(b)). In the frame of geometrical optics, the phase distribution of the high-order mode are different from that of the ideal fundamental Gaussian mode, the ray-presentations of the high-order modes (see equation (2.10)) propagate at relatively large angles to the beam direction and are usually lost in open transmission lines. Accordingly, a phase criterion should be proposed to measure the wave beam quality—the conversion efficiency of the q.o. mode converter should include the phase distributions of the corrected wave beam. It is accurate to define the conversion efficiency as the Gaussian mode content of the wave beam, which can be calculated using some methods such as the Hermite-Gaussian expansion to get the complex amplitudes of each component and the percentage of the fundamental Gaussian mode to all the modes in the wave beam. However, the method is very complicated, because it needs very long computer time to expand the fields of the wave beam into the Hermite-Gaussian series. In the design of a q.o. mode converter, the wave beam

quality should be monitored at many positions in the converter, especially for the iterative optimization of a phase correction mirror, it is actually impossible to do the Hermite-Gaussian analysis so many times because of the long computer time and the problems in the design cannot be found promptly.

The conversion efficiency can be defined as the vector correlation coefficient η_v used as a simple and effective parameter to approximately describe the beam quality, in which both the amplitude and the phase of the wave beam are included in equation 2.78. In chapter 3, 4 and 5, the equation 2.78 is used as a criterion for obtaining the optimums of parameters of the mirror system in which the phases of the outgoing RF beam are included.

Chapter 3 Phase Correction Mirror System

A q.o. mode converter is a proper combination of a launcher together with a few beam-forming mirrors [55,56]. Generally, the radiated fields from the launcher are quite different from the desirable distribution, and then a mirror system is needed to form the paraxial wave beam with the required structure. The mirror system usually consists of a quasi-parabolic or quasi-elliptical reflector and one or two specially shaped mirrors. The mirror system is integrated into the gyrotron to form a spatial field structure over the output window surface; it can be called as an internal mirror system. In fact, the output wave beam before its use practically in all cases passes through a so-called matching optics which adjust the beam to the following transmission line. Fig.3.1 shows the schematic arrangement of the matching optic. To do this accurate wave beam measurements are needed. High-power beam structure measurements may be performed by means of an infrared camera recording thermal traces of the beam passing through thin dielectric films [82]. Having measured intensity distributions one can perform phase front retrieval [83] and after that mirror synthesis for the beam conditioning. This chapter presents the analysis and the synthesis method for the internal mirror system. Formed by the internal mirror system, the output wave beam should satisfy the requirement of matching to the HE_{11} waveguide mode or the fundamental Gaussian beam with conversion efficiencies higher than 95%.

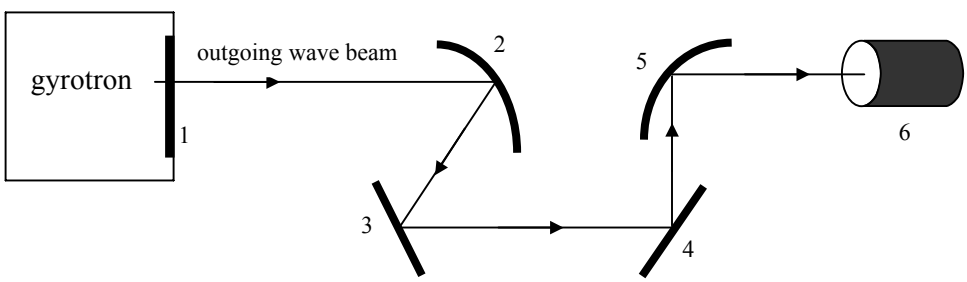

1. output window of gyrotron
2. reflector A
3. polarizer 1
4. polarizer 2
5. reflector C
6. waveguide

Fig.3.1 Schematic arrangement of the matching optic.

3.1 General Description

The conversion of the very high order cavity mode into a free space Gaussian mode is a very complex task. Some experimental investigations on q.o. mode converters have been reported. The q.o. mode converter in the FZK 165GHz, $TE_{31,17}$-mode

coaxial-cavity gyrotron consisted of a Vlasov-type launcher, one quasi-elliptical mirror and one adapted phase correction mirror with a non-quadratic surface contour function [84]. For this system the microwave losses inside the tube have been measured to be as high as 9%. There are two methods to depress the losses: pre-shaping of the wavebeam before its launching from the launcher cut, and improvement of the internal beam-forming mirror system to provide a high quality wave beam with low stray radiation. For a gyrotron operating in high-order volume mode whose ray-representation forms a nearly closed trajectory in the cross section of the launcher, a dimpled-wall launcher can be designed to pre-bunch the field distribution to provide a nearly Gaussian beam and to generate a well-focused Gaussian radiation pattern with low diffraction losses. A 140-GHz 1-MW CW gyrotron operating at the $TE_{28,8}$ mode has been developed at FZK [63], where the azimuthal spread angle is $\theta \approx 62.2$ degree (see Fig.2.3(b)). The internal mirror system used in this gyrotron is shown in Fig.3.2, which is a combination of a quasi-elliptical mirror with two toroidal mirrors to couple the wave beam out of the gyrotron with a desired beam pattern. Experimental measurements showed that a conversion efficiency of more than 98% has been achieved to convert the rotating $TE_{28,8}$ cavity mode at 140 GHz into a fundamental Gaussian beam (TEM_{00} mode) [63]. If the ray trajectory is not closed or even nearly closed, the azimuthal wall perturbation cannot match the azimuthal ray propagation very well in the launcher and it is very difficult to design a dimpled-wall launcher to obtain a well-focused field distribution with high Gaussian mode content. The mode (TEM_{00} mode) purity of the radiated beam wave from the cut of this launcher is low and the outgoing wave beam contains too many high-order modes. In this case, toroidal mirrors are not sufficient to obtain a desired output beam pattern. In order to satisfy the requirement to match the output-wave beam to the HE_{11} waveguide mode or the fundamental Gaussian beam with efficiencies higher than 95%, some non-quadratic phase correcting mirrors should be used instead of the toroidal mirrors to amend the phase distribution of the wave beam and then to improve the conversion efficiency [85].

The helical-cut launcher radiates the RF power via its straight cut onto a quasi-optical reflector (Fig.3.3). Care should be taken here that the center ray is reflected onto the gyrotron axis avoiding a transverse offset of the following mirrors. The power reflected from the first mirror propagates as an astigmatic beam onto a series of quasi-optical reflectors where the astigmatism is removed and the output beam transverse dimensions are matched to the window size [53,86].

In the synthesis of non-quadratic phase correction mirrors, the mirror surfaces are iteratively optimized according to the desired field distributions. The positions and the orientations of the mirrors are found by evaluating the moments of the first and second order of the power distribution. This design technique requires knowledge of both the amplitude and the phase distribution of the input beam and the desired

output beam [87]. The structure of a q.o. mode converter with a quasi-elliptical and two phase correcting mirrors is similar to Fig.3.2, where the toroidal mirrors are replaced by non-quadratic mirrors. The design procedure is: 1) back propagate the desired beam onto the last mirror, the field distributions on the mirror surface is used as the reference for the optimization of the middle mirror; 2) propagate the wave beam forward from the middle mirror to the last mirror, the differences between the wave beam input onto the last mirror and the reference field distributions are calculated. Based on the differences, if the middle mirror is a toroidal one, the major and/or minor radii are changed to match the reference field pattern; for a middle mirror with non-quadratic contour function, the mirror surface are iteratively amended according to the differences. The optimized first and second mirrors generate the resulting amplitude distribution on the last mirror; 3) the optimization procedure for the last mirror is the same like that for the middle mirror, the desired phase distribution can be obtained with the last mirror. The procedure for the numerical optimization of the mirror system is shown in Fig.3.4 [88,89], where KSA is the acronym of Katsenelenbaum-Semenov Algorithm and will be described in section 3.3. This design procedure incorporates a fast scalar diffraction code for a nonparallel aperture, which allows for a rapid synthesis of the mirror profiles [63].

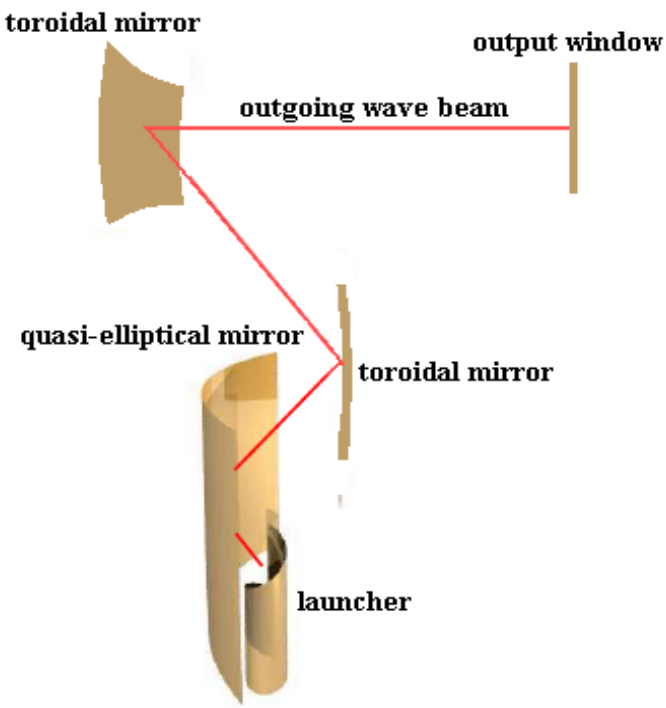

Fig.3.2 Schematic of the q.o. mode converter in the 140GHz TE28,8 mode gyrotron.

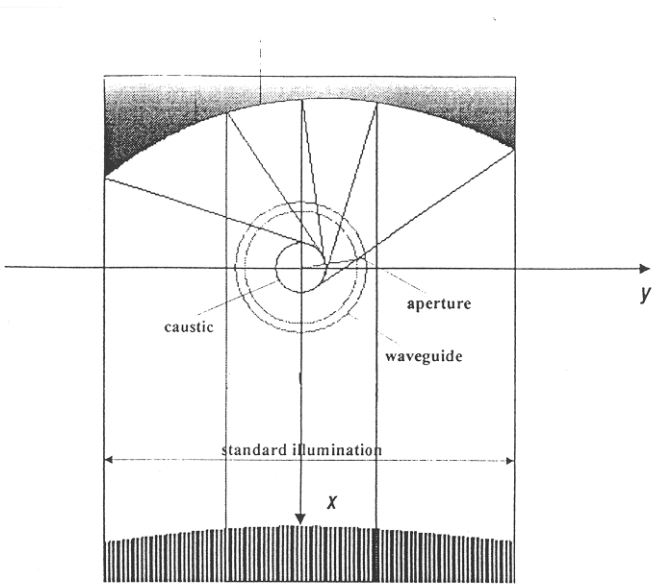

Fig.3.3 Cross-section of the launcher and the standard quasi-parabolic mirror

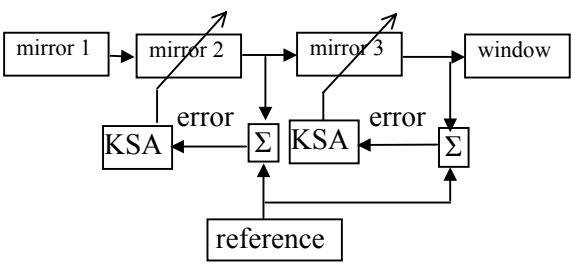

Fig.3.4 Principle of procedure for the numerical optimisation of the mirror system.

3.2 Beam-Forming Mirror System

In the case that the power densities on the edges of cuts are very low, this leads to small reflections at the cut edges and the fields in the launcher can be well approximated by waveguide modes. Diffraction losses can be neglected. The radiation on the first quasi-optical reflector from the aperture of the launcher can be calculated in terms of the scalar diffraction integral. In section 3.2.1, the radiated fields from the launcher cuts are investigated on a quasi-elliptical mirror, and section 3.2.2 presents the principle of phase correcting mirrors with non-quadric surfaces.

3.2.1 Quasi-Elliptical Mirror

According to the Huygens' Principle, the fields on the launcher aperture can be regarded as the second sources for the calculation of the radiated fields. The aperture is close to the launcher cuts (see Fig.2.11(b), the first bundle outside the cuts), its size is equal to the Brillouin region. The radiated field can be calculated in terms of the scalar diffraction integral:

$$u(\vec{r}_0) = \iint_{Sa} \left(u(\vec{r}) \frac{\partial g(\vec{r} - \vec{r}_0)}{\partial n} - g(\vec{r} - \vec{r}_0) \frac{\partial u(\vec{r})}{\partial n} \right) ds \tag{3.1}$$

where $u(\vec{r})$ is the field on the launcher aperture, $g(\vec{r})$ denotes the Green's function in the free space, S_a gives the area of aperture, $\frac{\partial}{\partial n}$ represents the partial derivative along the direction normal to the aperture surface. From equation (3.1), the fields $u(\vec{r}_0)$ on the quasi-elliptical mirror can be obtained, where $\vec{r}_0$ describes the profile of the mirror surface. The profile of the quasi-elliptical mirror surface is described in the following.

In order to calculate the fields reflected by the quasi-optical mirror, one needs to known the unit vector normal to the mirror surface. The quasi-elliptical mirror is a kind of bifocal mirror. The geometric structure of the cross section of the launcher and the quasi-elliptical mirror is shown in Fig.3.5, the global coordinate is indicated, where the center of the launcher aperture is set on the x-coordinate, the launcher axis is arranged along the z-coordinate, l_1 and l_1+l_2 denote the two focal lengths of the quasi-elliptical mirror [90]. The launcher axis is usually set at one of the focal line, and then the wave beam radiated from the launcher will be focused by the quasi-elliptical mirror to another focal line. In Fig.3.5, as an example, two ray representations of the outgoing wave beam are shown and marked as "0" and "1". If the gyrotron operates in the TE_{mn} mode, the phase difference between the two rays is:

$$\arg^{out}(r, \phi, z) - \arg^{out}(r, \phi_0, z) = m(\phi - \phi_0) \tag{3.2}$$

The curve length on the caustic is

$$\Delta s(\phi_0, \phi) = R_c(\phi - \phi_0) = \frac{m}{k_r}(\phi - \phi_0) \tag{3.3}$$

The propagation length of the ray to the focal point is

$$L(\phi) = l(\phi) + \sqrt{(x(\phi) + l_2)^2 + y(\phi)^2} \tag{3.4}$$

where

$$x(\phi) = R_c \cos\phi - l(\phi)\sin\phi \tag{3.5}$$

$$y(\phi) = R_c \sin\phi + l(\phi)\cos\phi \tag{3.6}$$

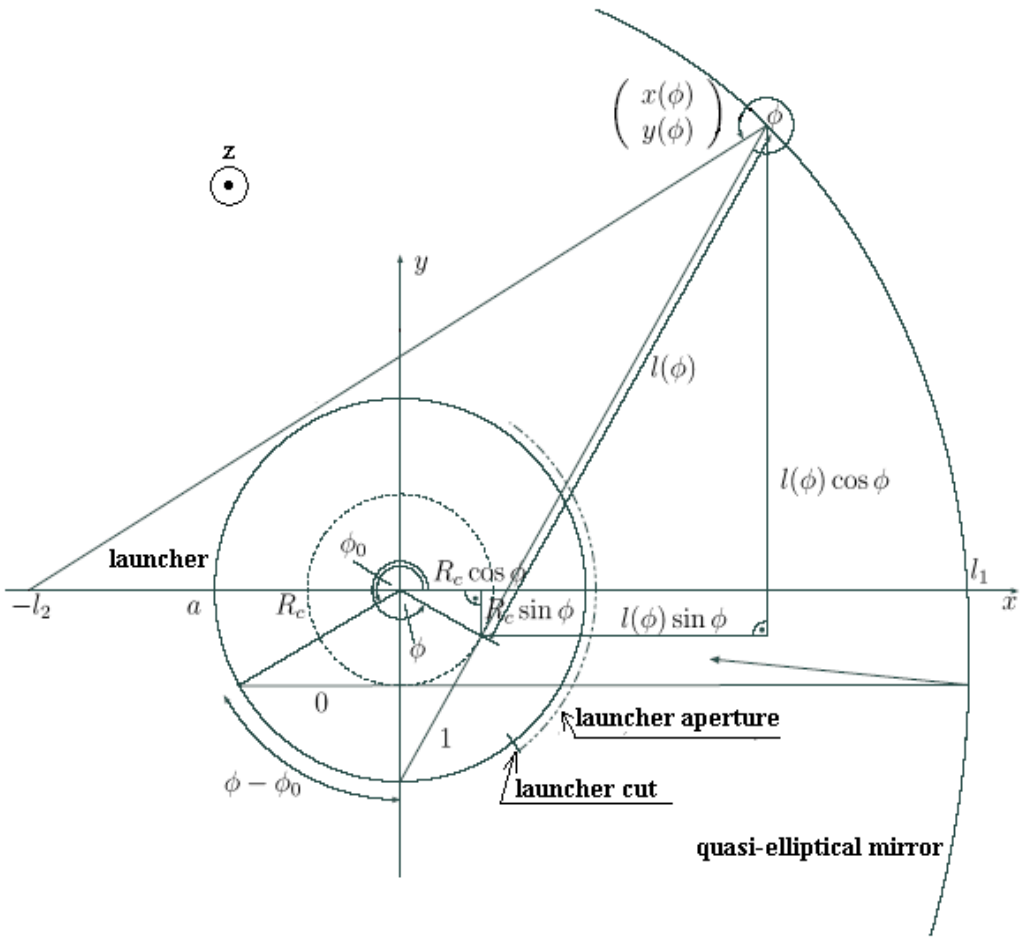

Fig.3.5 Schematic of the geometric structures of launcher and quasi-elliptical mirror [90].

The surface of the quasi-elliptical mirror reflects all the rays to the same line, and all the rays should have the same phase at the focal line, it can be called zero relative phase and accordingly the profile of the quasi-elliptical mirror surface is given. With

regard to the rays "0" and "1" shown in Fig.3.5, to satisfy the requirement of zero relative phase it gives

$$\Delta s(\phi_0, \phi) + L(\phi) - L(\phi_0) = 0 \tag{3.7}$$

Substitute the equations (3.3-6) into the equation (3.7), one can get

$$l(\phi) = \frac{8R_c l_2 \cos\phi - 4\phi^2 R_c^2 - 4\phi R_c^2 \pi + 8\phi R_c l_g - \pi^2 R_c^2 + 4\pi R_c l_g + 8l_1 l_g - 8l_1 l_2}{8l_2 \sin\phi + 8\phi R_c + 4\pi R_c + 8l_g} \tag{3.8}$$

where

$$l_g = L(-\pi/2) \tag{3.9}$$

From equations (3.5-6) and (3.8), the coordinates of the points on the quasi-elliptical mirror surface can be obtained: $\vec{r}_0 = (x(\phi), y(\phi), z)$.

In the case of $l_2 \to \infty$, the quasi-elliptical mirror becomes a quasi-parabolic mirror:

$$\lim_{l_2 \to \infty} l(\phi) = \frac{2R_c \cos\phi - 4l_1 + 2R_c\phi + \pi R_c}{2\sin\phi - 2} \tag{3.10}$$

If the caustic radius is R_c=0 (TE_{0n} modes), the equation (3.7) becomes

$$L(\phi) = L(\phi_0) \tag{3.11}$$

It describes an elliptical or parabolic mirror as anticipated.

In terms of the coordinate of $\vec{r}_0 = (x(\phi), y(\phi), z)$, the vector $\vec{n}$ normal to the quasi-elliptical mirror surface can be given as:

$$\vec{n} = \frac{\partial \vec{r}_0}{\partial z} \times \frac{\partial \vec{r}_0}{\partial \phi} = \left(-\frac{\partial y(\phi)}{\partial \phi}, \frac{\partial x(\phi)}{\partial \phi}, 0 \right) \tag{3.12}$$

The fields reflected from the quasi-elliptical mirror can be calculated by means of the scalar diffraction integral.

3.2.2 Phase Correcting Mirror

Usually the fields reflected by the quasi-elliptical mirror contain some high-order modes which propagate at relatively large angles to the transmission line. This produces the power losses in the transmission. In the frame of g.o., the wavefront of the beam is not in a good structure so its gradients are not in the direction of the transmission line at some points. Some phase correcting mirrors are needed to amend the phase distribution of the wave beam according to the desirable mode, so that the high-order modes can be suppressed. The principle of phase correcting mirrors is shown in Fig.3.6. An incoming wave beam hits a mirror with a smooth surface (S-plane in Fig.3.6), the field distributions $u(\vec{r})$ are different from $u_m(\vec{r})$ which represents the fields on the perturbed surface of the mirror, $\Delta z(\vec{r})$ describes the changing of the mirror surface. On the observation plane which is far away from the S-plane (in the far field) and perpendicular to the rays, the phase shift due to the surface variation of the mirror is given as

$$\Delta\psi = k_0 \Delta l \tag{3.13}$$

where

$$\Delta l = \frac{\Delta z}{\cos\gamma}(1+\cos 2\gamma) = 2\Delta z \cos\gamma \tag{3.14}$$

This can be found from Fig.3.7. The fields on the perturbed surface become

$$u_m(\vec{r}) = u(\vec{r})\exp(j2k\Delta z(\vec{r})\cos\gamma) \tag{3.15}$$

The fields propagated from the S-plane to a point $\vec{\mathrm{r}}_0$ on S_0-plane can be calculated by means of the scalar diffraction integral shown in equation (3.1)

$$u_r(\vec{\mathrm{r}}_0) = 2\iint_S u_m(\vec{\mathrm{r}})\frac{\partial}{\partial z}G(\vec{\mathrm{r}}_0 - \vec{\mathrm{r}})dxdy \tag{3.16}$$

where G represents the Green's function in free space

$$G(\vec{r}_0 - \vec{r}) = \frac{\exp\left(-jk(\vec{r}_0 - \vec{r})\right)}{4\pi\left|\vec{r}_0 - \vec{r}\right|} \tag{3.17}$$

In order to achieve the desirable distribution $u_g(\vec{r}_0)$ on the observation plane (S_0-plane in Fig.3.6), $\Delta z(\vec{r})$ should be optimized according to the differences between the input field and the desirable one on the S_0-plane. By changing the profile of the mirror, the differences should be minimized. There are many methods which can be used to analyze the differences and thus to optimize the mirror surface to achieve minimum errors on the observation plane. For example, the Gradient Algorithm which is an effective method to find the minimum error in terms of the gradients of the error according to its distributions, and the Fast Self Adaptive Algorithm which is widely applied in the self adaptive filter and self adaptive optics. The error correction Katsenelenbaum-Semenov Algorithm (KSA) [91] can be used for the synthesis of a particular distribution by means of phase correctors. This is now an established method in gyrotron technology for the formation of a microwave beam with desired characteristics.

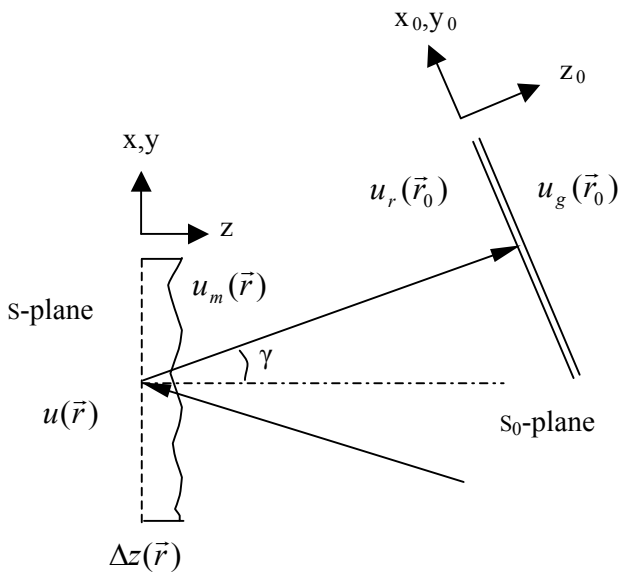

Fig.3.6 Principle of phase correcting mirror.

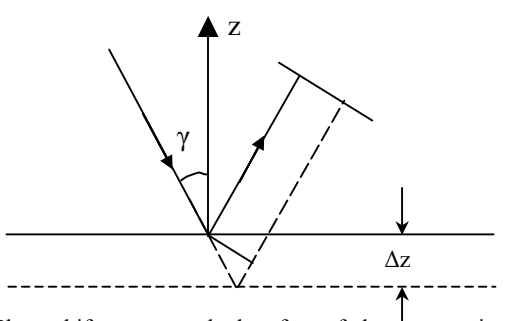

Fig.3.7 Phase shift on a perturbed surface of phase correcting mirror.

3.3 Error Correction Algorithm—Katsenelenbaum-Semenov Algorithm

In the design of mirror systems at FZK, the KSA is used for the synthesis of adapted phase correcting mirrors with non-quadratic contour function. The KSA is described in detail in ref. [91]. The main idea of the KSA is to find the minimum of the error

$$E(\Delta z) = \int_{-\infty}^{+\infty}\int \left| u_g(\vec{r}_0) - u_r(\vec{r}_0) \right|^2 dx_0 dy_0 \tag{3.18}$$

where $u_g(\vec{r}_0)$ is the desired field distribution in the observation plane (see Fig. 3.6), and usually is the fundamental Gaussian mode (TEM_{00}). In the S_0-plane, the input fields can be described as

$$u_r(\vec{r}_0) = |u_r(\vec{r}_0)| \exp(j\theta(\vec{r}_0)) \tag{3.19}$$

From equation (3.15-16) we can find that the input fields are relative to the surface of S-plane. At the discrete sample points in the S-plane, the position $\vec{r}$ and perturbation Δz can be written as

$$\vec{r} = (v\Delta x, w\Delta y, z) \tag{3.20}$$

$$\Delta z(\vec{r}, \vec{a}) = \sum_{v=1}^{V}\sum_{w=1}^{W} a_{vw}\delta(\vec{r} - \vec{r}_{vw}) \tag{3.21}$$

where v and w are the mesh numbers, Δx and Δy are the mesh lengths in x- and y-directions, respectively. The plane is perpendicular to z-axis in the local coordinate as shown in Fig.3.6. In equation (3.21), δ represents the Dirac function, a_{vw} is the perturbation amplitude at the point $\vec{r}_{vw}$. Substituting the equations (3.20-21) into equation (3.18), the error in the S_0-plane can be expressed as

$$E(\vec{a}) = \sum\sum \left| u_g(\vec{r}_0) - u_r(\vec{a}, \vec{r}_0) \right|^2 \Delta x_0 \Delta y_0 \tag{3.22}$$

Setting the gradient $\nabla E(\vec{a}) = 0$, it results in

$$\frac{\partial E(\vec{a})}{\partial a_{vw}} = 0, \quad \begin{matrix} v = 1, \cdots, V \\ w = 1, \cdots, W \end{matrix} \tag{3.23}$$

From equation (3.23), the iteration formula can be derived as

$$\Delta z^{i+1}(\vec{r}) = \frac{1}{2k_0 \cos\gamma}\left[\frac{\pi}{2} - \arg\left(j2k_0 u(\vec{r}) q^i(\vec{r}) \cos\gamma\right)\right] \tag{3.24}$$

$$q^i(\vec{r}) = -4\iint_{S_0}\left(u_g(\vec{r}_0) - u_r^i(\vec{r}_0)\right)^* \frac{\partial}{\partial z} G(\vec{r}_0 - \vec{r}) dx_0 dy_0 \tag{3.25}$$

Here k_0 is the wave number in free space and the superscript "*" represents the complex conjugate. The field propagated from the mirror to the point $\vec{r}_0$ is described as

$$u_r^i(\vec{r}_0) = 2\iint_S u_m^i(\vec{r}) \frac{\partial}{\partial z} G(\vec{r}_0 - \vec{r}) dxdy \tag{3.26}$$

$$u_m^i(\vec{r}) = u(\vec{r}) \exp\left(j2k_0 \Delta z^i(\vec{r}) \cos\gamma\right) \tag{3.27}$$

Notice that the equations (3.1), (3.16) and (3.25-26) have the form:

$$W(\vec{r}_0) = 2\iint_S U(\vec{r}) V(\vec{r}_0 - \vec{r}) dxdy \tag{3.28}$$

According to the Signal Processing Theory, equation (3.28) can be calculated using the Fourier Transform of the functions:

$$W(\vec{r}_0) = F^{-1}(W_f) = F^{-1}\left(U_f V_f\right) \tag{3.29}$$

$$U_f = F(U) \tag{3.30}$$

$$V_f = F(V) \tag{3.31}$$

where F and F^{-1} denote the Fourier Transform and the reverse Fourier Transform, respectively. For the partial derivative of $V(\vec{r})$, its Fourier Transform becomes:

$$F\left(\frac{\partial V}{\partial z}\right) = -j2\pi\Omega_z V_f \tag{3.32}$$

where Ω_z is the frequency with respect to the variable z.

Finally, in terms of the equations (3.24-27), the phase correcting mirror can be iteratively optimized to provide a field distribution in the observation plane which is similar to the desired field structure. If the requirement is to achieve a fundamental Gaussian distribution, the vector Gaussian mode content shown in equation (2.78) can be used to monitor the quality of the corrected wave beam in the iterative optimization.

Chapter 4 Design and Experiment: Prototype of the Quasi-Optical Mode Converter for the $TE_{34,19}$-Mode Coaxial-Cavity Gyrotron

A 2MW, CW, 170GHz, $TE_{34,19}$-mode coaxial-cavity gyrotron is under development in cooperation between European Research institutes (FZK Karlsruhe, CRPP Lausanne, HUT Helsinki) and European tube industry (TED, Velizy, France), which is foreseen to be used for electron cyclotron resonance heating (ECRH) of magnetically confined plasmas in the International Thermonuclear Experimental Reactor (ITER). For such a high-order waveguide mode, it is necessary to employ a q.o. mode converter for transmission of the volume mode transformation into a fundamental Gaussian mode. A pre-prototype of the q.o. mode converter has been investigated and integrated into the coaxial-cavity gyrotron. This q.o. mode converter for the coaxial-cavity gyrotron consists of a dimpled-wall launcher, a quasi-elliptical mirror, a toroidal mirror and a non-quadratic phase correcting mirror [92-94]. This chapter presents the design and the experimental verification of the pre-prototype q.o. mode converter and provides information about an improved prototype.

4.1 First Approach of a Launcher for the $TE_{34,19}$-Mode Coaxial-Cavity Gyrotron

By means of the conventional method presented in section 2.4.2, a first approach for a dimpled-wall launcher has been designed for the 2MW, CW, $TE_{34,19}$-mode coaxial-cavity gyrotron at FZK. The perturbation amplitudes and lengths are shown in Fig.4.1 [75].

The field distribution on the unfolded launcher wall and the mode composition coefficients which are calculated using the coupled-mode method are shown in Fig.4.2 and Fig.4.3. In agreement with Fig.2.19, we can see that a good mode composition along the longitudinal axis is obtained as shown in Fig.4.3. Table 4.1 gives the relative powers of the satellite modes at the aperture of the launcher, from which we can find that a good Gaussian mode amplitude composition is achieved. However, the Gaussian output pattern requires a certain amplitude and phase relation between the main mode and the satellite modes. The appropriate amplitude

relation can be achieved in a short perturbed section of 271 mm, but the phases are not in appropriate relations, even after a length of approximately 480mm.

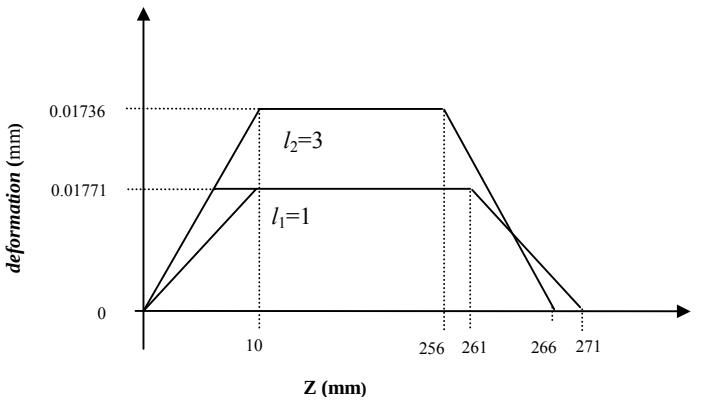

Fig.4.1 Schematic drawing of wall deformations of a dimpled-wall launcher for the $TE_{34,19}$-mode coaxial-cavity gyrotron with $\ell_1 = 1$ and $\ell_2 = 3$

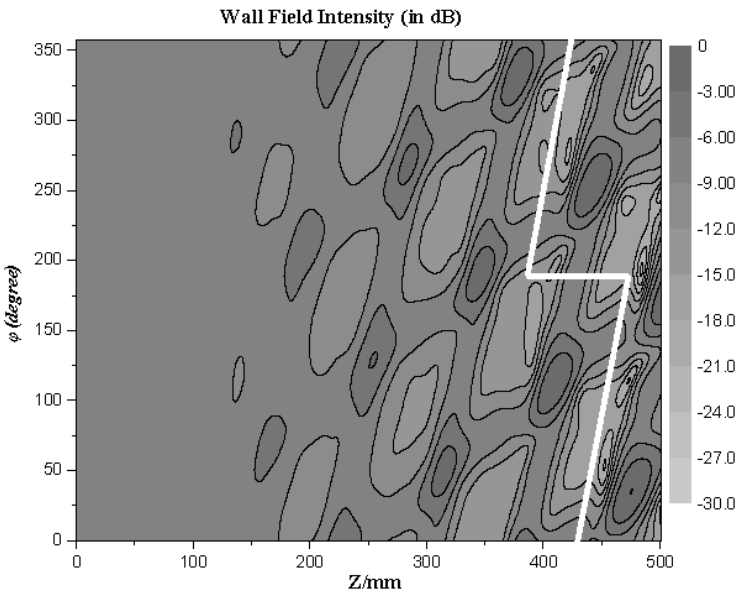

Fig.4.2 Field distribution on the unfolded wall of the launcher for the $TE_{34,19}$ mode coaxial cavity gyrotron with $\ell_1 = 1$ and $\ell_2 = 3$. The edges of the launcher cut are indicated.

For the 2MW, CW, $TE_{34,19}$-mode gyrotron, the power density at the beginning of the launcher is 57W/cm^2 and the factor F_m=1.5 in equation (2.59). On the cut edges of the dimpled-wall launcher with perturbation rules $\ell_1 = 1$, $\ell_2 = 3$ and the radius of 32.5mm shown in Fig.4.2, the average and peak of the power densities are –9.7dB and –6.7dB, the corresponding power densities are 32.3W/cm^2 and 63.8W/cm^2,

respectively. Although a good amplitude distribution for a Gaussian mode composition is obtained at the aperture, the dimpled-wall launcher fails to provide a well-focused field structure by means of the conventional method. The peak of the power densities on the cut edges is even larger than the input power density. Such strong fields on the cut edges will produce large diffraction and stray radiation losses. Moreover, the launcher is too long to be integrated into the gyrotron. As described in chapter 2, a mode in circular waveguide can be regarded as superposition of plane waves represented by rays. In the launcher for the $TE_{34,19}$-mode coaxial-cavity gyrotron, the azimuthal angle θ between the adjoining reflection points of a ray on the launcher wall can be obtained from equation (2.17): $\theta \approx 71.1$ degree, the ratio of the caustic to the cavity radius is $R_c/a \approx 0.323$. According to equation (2.30), the selection rule for the azimuthal bunching is $\Delta m = \pi/\theta = 2.53$ and has to be approximated by $\ell_2 = 3$ in equation (2.31). Due to the ratio of caustic to cavity radius of approximately 0.323, the transformation of the $TE_{34,19}$ mode into a nearly Gaussian distribution in the dimpled-wall launcher cannot be done as good as for the modes of conventional cavity 140GHz gyrotron [41,63,95,96], 170GHz gyrotron [97], and 110GHz gyrotron [73,98], where the ratio of caustic to cavity radius is approximately 0.5 and the ray representation of the waveguide mode forms an almost closed triangle in the cross section of launcher. In the launcher for the $TE_{34,19}$-mode gyrotron, the azimuthal wall perturbation with $\ell_2 = 3$ cannot match the azimuthal ray propagation in the launcher (see Fig.2.3) very well. This makes it very difficult both to transform the cavity mode into a nearly Gaussian beam mode and to obtain well-focused fields at the aperture to provide low diffraction at the cuts of the launcher.

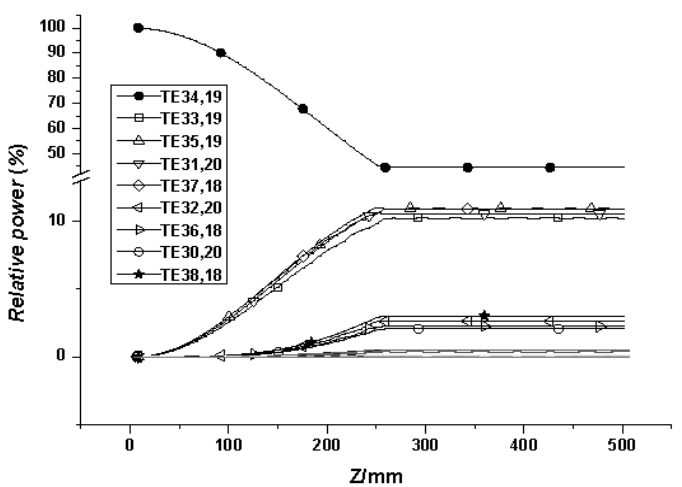

Fig.4.3 Mode composition (relative power) coefficients vary along the z-axis in the launcher for the $TE_{34,19}$-mode coaxial-cavity gyrotron with $\ell_1 = 1$ and $\ell_2 = 3$.

Table 4.1. Relative powers of the satellite modes at the aperture of the launcher with $\ell_1 = 1$ and $\ell_2 = 3$.

	azimuthal bunching		
axial bunching	$TE_{32,20}$ 2.63%	$TE_{35,19}$ 10.99%	$TE_{38,18}$ 3.02%
	$TE_{31,20}$ 10.53%	$TE_{34,19}$ 44.42%	$TE_{37,18}$ 10.95%
	$TE_{30,20}$ 2.08%	$TE_{33,19}$ 10.2%	$TE_{36,18}$ 2.26%

4.2 Analysis of the Pre-prototype Quasi-Optical Mode Converter for the $TE_{34,19}$-Mode Coaxial-Cavity Gyrotron

A pre-prototype of the q.o. mode converter has been developed for the 2MW, CW, $TE_{34,19}$-mode coaxial-cavity gyrotron and was tested in August, 2005 at FZK. The q.o. mode converter consists of a dimpled-wall launcher, a quasi-elliptical mirror, a toroidal mirror, and one non-quadratic mirror, which means that a second, external non-quadratic mirror must be employed in order to get a Gaussian beam with good amplitude and phase. The schematic arrangement of the designed q.o. mode converter is shown in Fig.4.4. Low power measurements of the q.o. mode converter have been performed with a $TE_{34,19}$-mode generator operated at 170.3 GHz. The experimental setup is shown in Fig.4.5 [94].

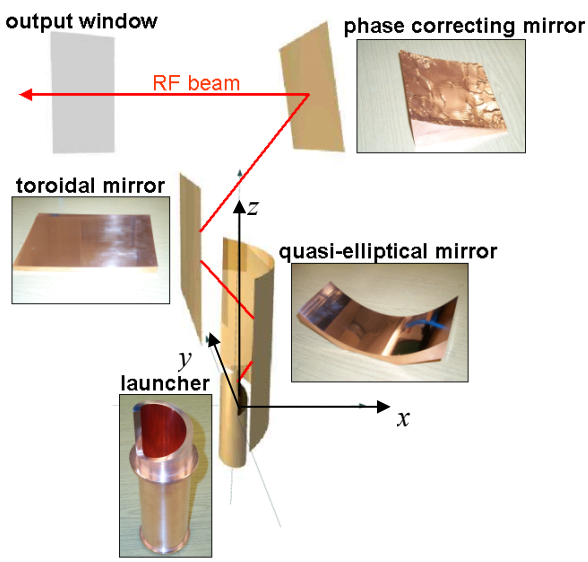

Fig.4.4 Arrangement of the q.o. mode converter for the $TE_{34,19}$ mode gyrotron.

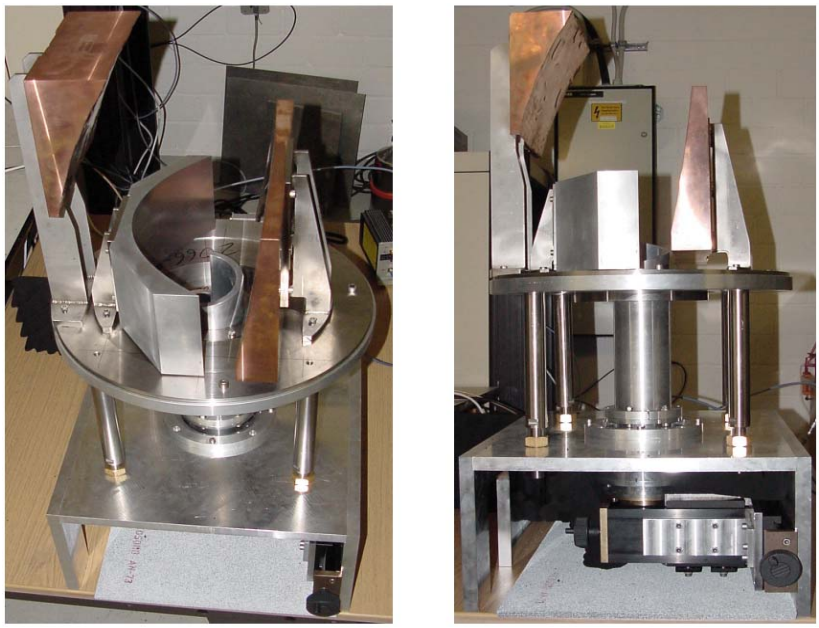

Fig.4.5 The q.o. mode converter as assembled for the low power measurement.

4.2.1 Launcher

In section 4.1, the analysis shows that the dimpled-wall launcher with $\ell_1 = 1$ and $\ell_2 = 3$ cannot provide a well-focused field at the aperture of launcher. In order to obtain a well-focused field structure, the second order harmonics ($\ell_2 = 2$) is included in the wall surface deformations of the launcher [76,99] to approximate together with a $\ell_3 = 3$ perturbation the $\Delta m = 2.53$ bunching. The slope of taper is 0.002 (see equation (2.44)), and the input radius of the launcher is 32.5mm which gives an oversize factor of 1.1, where the oversize factor is defined as

$$F_o = \frac{k_0 a}{X_{mn}} \tag{4.1}$$

where a is the launcher radius, X_{mn} is the root of the derivative of the Bessel function, k_0 is the wavenumber in free space. The perturbation amplitudes and lengths are shown in Fig.4.6, and the profile of the launcher wall surface is shown in Fig.4.7. Based on the coupled-mode method, the fields in the launcher are calculated. The power densities on the wall are shown in Fig.4.8, where the conversion efficiency η_v (see equation (2.78)) is 43% at the aperture. According to the equations (2.59) and (2.65) with the factor f_m=1.5, the average value and peak on the edges of cuts are 18.4W/cm^2 and 87.3W/cm^2, respectively.

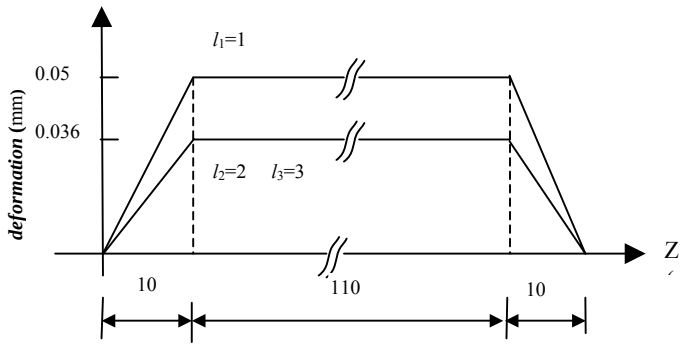

Fig.4.6 Schematic drawing of wall deformations of launcher for the $TE_{34,19}$-mode coaxial-cavity gyrotron with $\ell_1 = 1$, $\ell_2 = 2$ and $\ell_3 = 3$.

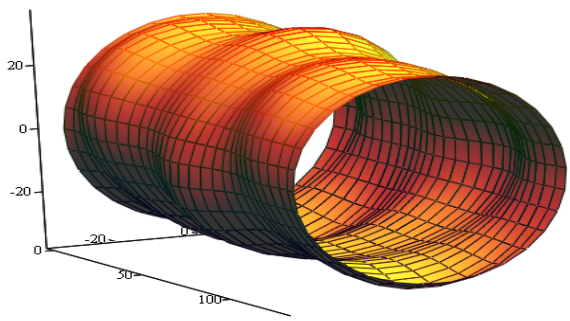

Fig.4.7 Schematic contour of the launcher wall ($\ell_1 = 1$, $\ell_2 = 2$, $\ell_3 = 3$ perturbations).

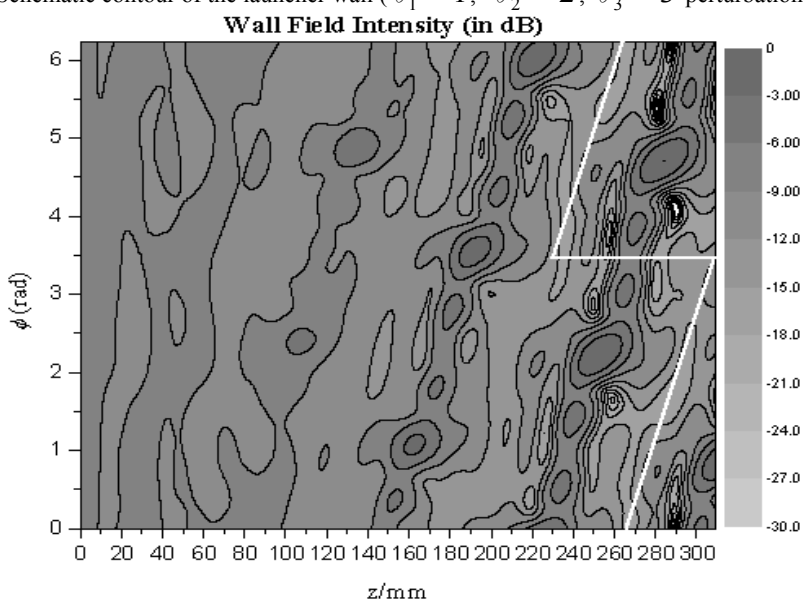

Fig.4.8 Field distribution on the unfolded launcher wall ($\ell_1 = 1$, $\ell_2 = 2$, $\ell_3 = 3$ perturbations),the edge of cut is indicated.

4.2.2 Mirror System

As shown in Fig.4.4, the mirror system is the combination of a quasi-elliptical mirror together with a toroidal mirror and an adapted phase correcting mirror with non-quadratic contour surface function. The center of the quasi-elliptical is set at the point (-100.0mm, 0.0mm, 95.0mm), the focal length l_1=100mm (see Fig.3.5) is selected to match the center of the launcher, and l_2=1200mm. The toroidal mirror is a focusing device which has two different radii whose axes are oriented at 90 degree to each other. They are utilized in cases where the beam must be focused and folded. Rather than using both a spherical mirror and a plane mirror for this purpose, both functions may be combined in one element. The small number of optical elements increases the energy throughput and also allows for more compact designs. Toroidal mirrors also correct for the astigmatism that results when a spherical mirror is used off axis. The major and minor focal lengths of the toroidal mirror used in the q.o. mode converter are 4000.0mm and 1500.0mm, respectively, and the coordinate (x,y,z) of its center point is (-70.0mm, 0.0mm, 176.0mm). By making use of the KSA, the surface of the last mirror has been optimized for amplitude matching according to a desirable field distribution. The coordinates of the centers of the last mirror and the output window are (130.0mm, 0.0mm, 350.0mm) and (-310.0mm, 0.0mm, 350.0mm), respectively. Using the scalar diffraction integral equation 3.1, the calculation result for the radiated fields on the quasi-elliptical mirror is shown in Fig.4.9.

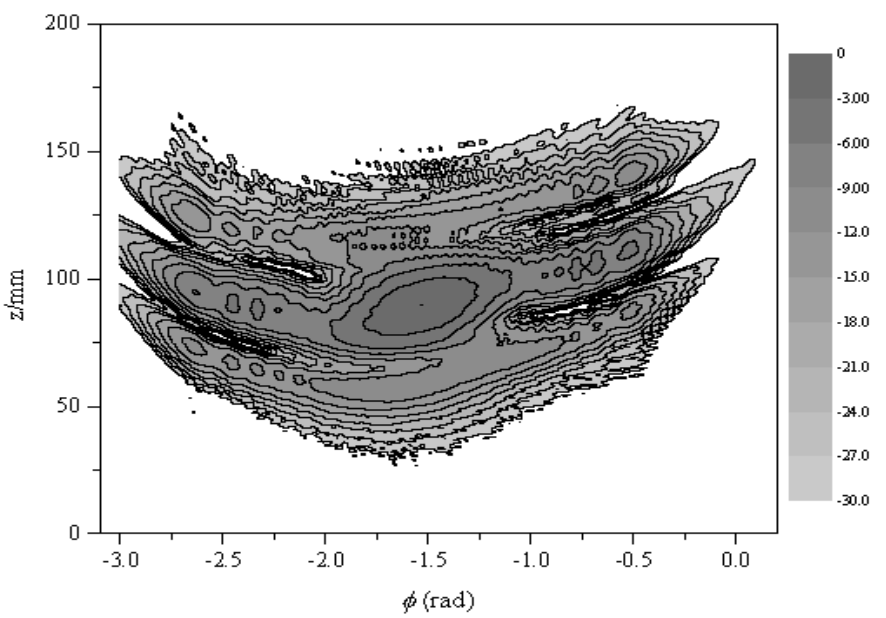

Fig.4.9 Power density on the quasi-elliptical mirror (in dB).

The field patterns radiated from the launcher have been measured after the quasi-elliptical mirror at the position of the second mirror, where the system is operated at the frequency of 170.3GHz. The results have been compared with the calculation results. From Fig.4.10 we can see that a good agreement is achieved between the calculation and the low power measurement result.

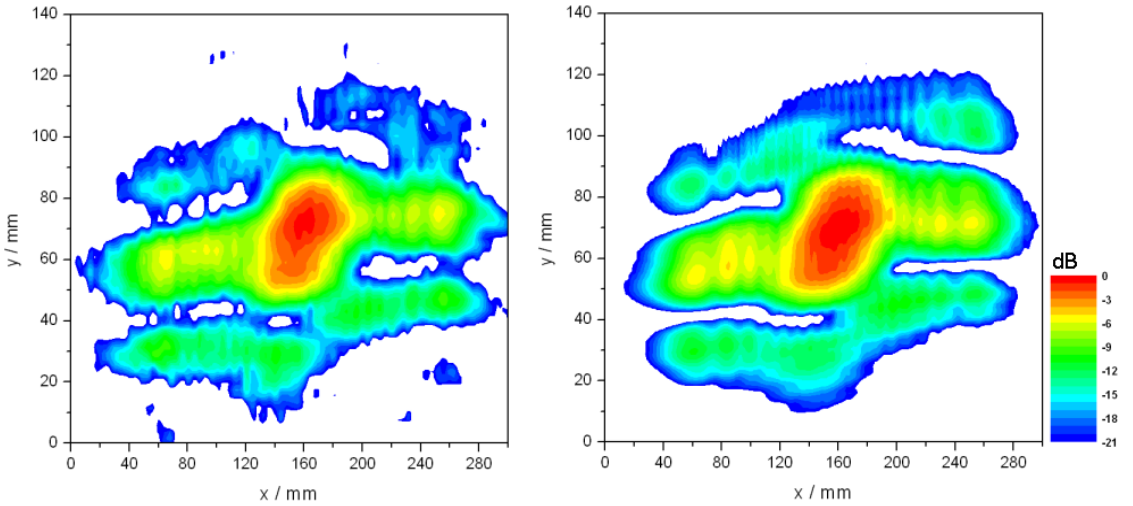

Fig.4.10 The field radiated from the launcher at the position of the second mirror measurement (left) and calculation (right) at 170.3 GHz [94].

In order to investigate the tolerance conditions of the q.o. mode converter, the system is measured with a second low power mode generator operating at 171.92GHz. Fig.4.11 shows the field patterns measured at the position of the second mirror and the calculated amplitude contours of the fields on the second mirror. It seems that although the frequency is 1.89GHz higher than the given value, the measured field is still in a relatively good agreement with the calculation results. That is, the launcher and the quasi-elliptical are of good tolerance conditions.

The second and third mirrors have been also tested. With the $TE_{34,19}$-mode generator operating at the frequency of 170.3GHz, the outgoing wave beam has been measure at different planes. The measurements are performed at three positions; the results are shown in Fig.4.12. The scalar correlation coefficient η_s (defined in equation (2.77)) of the measured to the calculated patterns is estimated to be 90% in the window plane [94]. At the position of 50mm outside the gyrotron, the measured beam pattern is very similar to the calculation result, but both the measured and the calculated patterns are quite different from those in the window plane. Using a Gaussian mode fitting code, the analysis shows that the fundamental Gaussian mode content of the RF output wave beam is approximately 65%. This can explain the big difference between the pattern at 50mm outside the gyrotron and that in the window

plane. As the RF wave beam propagates along the negative x-direction to 500mm outside the gyrotron, the beam becomes very large in the cross-section.

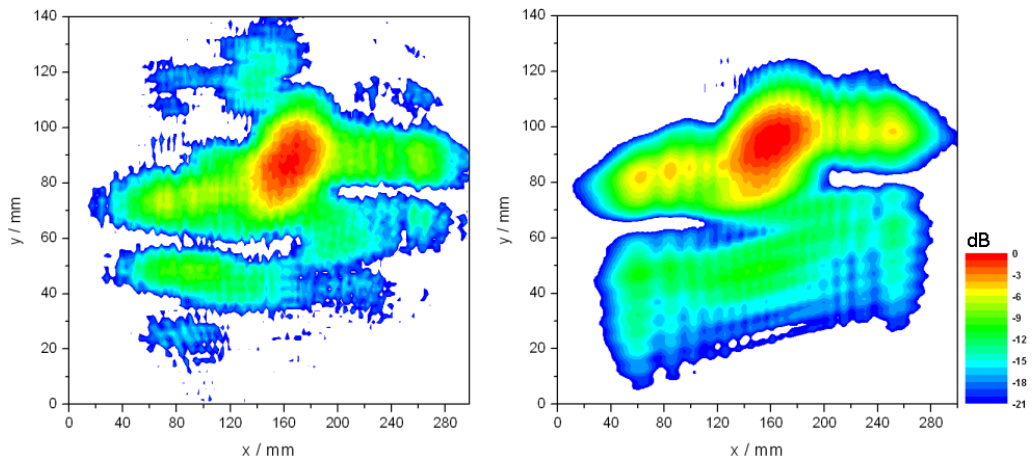

Fig.4.11 The field radiated from the launcher at the position of the second mirror measurement (left) and calculation (right) at 171.92 GHz [94].

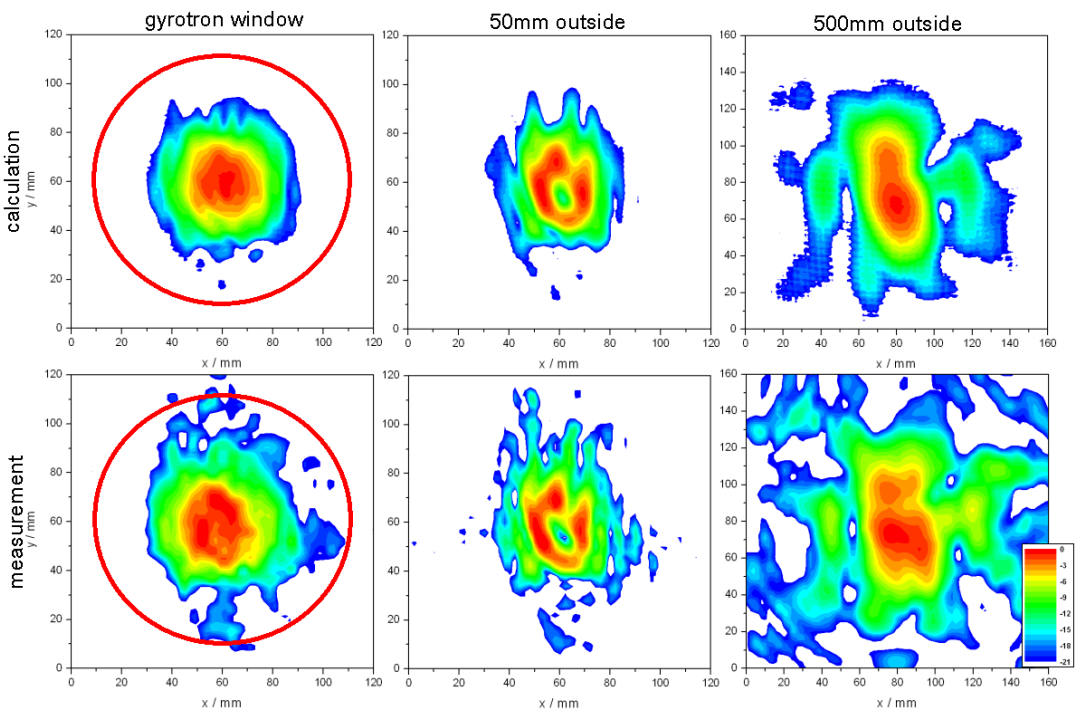

Fig. 4.12 Distribution of the RF output beam at three planes outside the gyrotron.
upper row: results of calculations; lower row: results of measurements performed with the $TE_{34,19}$-mode generator at 170.3 GHz. The window aperture (96 mm diameter) is indicated [94].

As the frequency increased to 171.92GHz, the beam patterns shown in Fig.4.14 are quite different in comparison to those in Fig.4.12. It seems the frequency of 171.92 GHz is slightly too high. Due to the frequency difference the Brillouin angle is decreased by approximately 1 degree. This results in a significant shift of the position of the microwave beam at each mirror. Consequently the beam pattern is modified mainly because the correct beam phase modification at the 3rd mirror is not feasible anymore. The properties of the microwave beam have been calculated for these conditions (Fig.4.14, upper row).

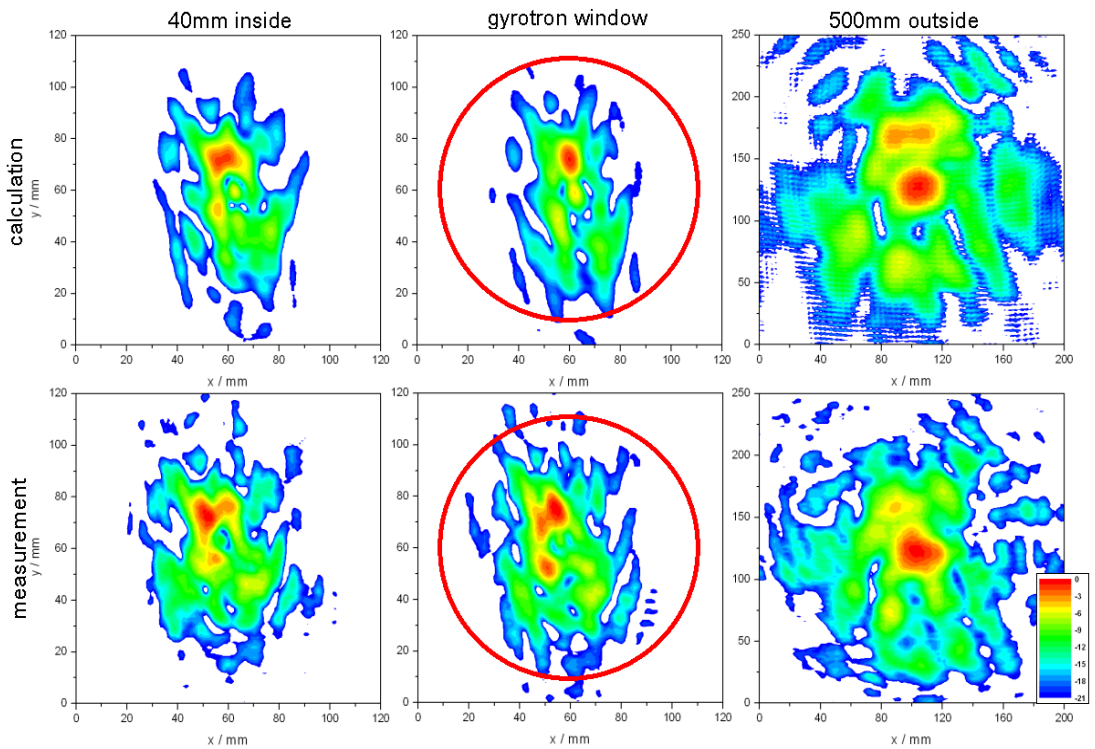

Fig.4.14 Results of cold tests at three planes in comparison with calculations performed with the second mode generator at 171.92 GHz. The window aperture (96 mm diameter) is indicated [94].

The radiated fields are calculated by making use of a Surface Integral Equation (SIE) code SURF3D developed at Calabazas Creek Research, Inc., USA [100], which can provide a 3-D full wave analysis of the field in the launcher. Power reflection and field diffraction at the launcher cuts can be evaluated in the calculation. The radiated fields on the cylindrical surface with a radius of 100m are shown in Fig.4.15. The size of the quasi-elliptical mirror in the azimuthal direction is 3.1 radian (from –3 to 0.1), the relative power on this mirror is about 94.87%, and so the diffraction loss is approximately 5.13%. This is due to the fields on the edges of launcher cuts are relatively strong, the maximum power density on the edges is as high as 87.3W/cm^2, which is even larger than the input power density of 57W/cm^2,

and the average power density of 18.4W/cm^2 is somewhat large. Moreover, the conversion efficiency is only 43% at the aperture of launcher, thus there are too many high-order modes embraced in the outgoing wave beam. This would make it very difficult to design the mirror system to correct the field distributions of the RF output wave beam and to achieve the desirable fundamental Gaussian structure. In order to satisfy the two requirements for megawatt gyrotrons, stray radiation losses in the tube of less than 5% and the matching to the HE_{11} waveguide mode or a fundamental Gaussian beam with conversion efficiencies higher than 95%, the q.o. mode converter must be improved.

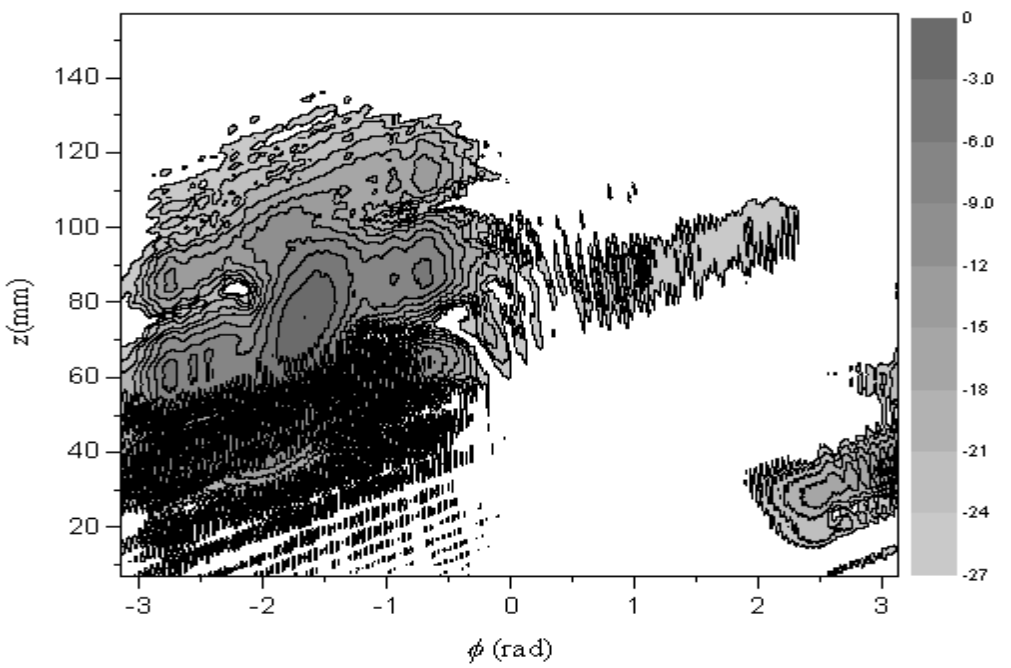

Fig.4.15 Field distribution on a cylindrical surface with 100mm radius.

4.3 Influence of the Focal Lengths of the Quasi-Elliptical Mirror on the Conversion Efficiency and First Improvement

The theoretical and experimental results show that the mirror system shown in Fig.4.4 fails to provide a high conversion efficiency to the desired fundamental Gaussian distribution with a given structure. The analyses in sections 3.1 and 4.1 show, as expected, that one toroidal mirror and one adapted phase correcting mirror are not sufficient to provide a high conversion efficiency for the transformation of

the $TE_{34,19}$ mode into a Gaussian distribution, a second phase correcting mirror with non-quadratic surface contour should be used instead of the middle toroidal mirror in Fig.4.4 or as an external mirror. Here we choose the first solution. With this new arrangement of the mirror system consisting of a quasi-elliptical and two non-quadratic mirrors, the focal lengths of the quasi-elliptical mirror on the conversion efficiency are investigated. In the coordinate system shown in Fig.4.4, the desirable fundamental Gaussian beam $|u_2|\exp(j\varphi_2)$ with required structure can be described as

$$u_2 = A_0 \frac{1}{w(x)} \exp\left(-\frac{r^2}{w^2(x)} - j\left(k_0 \left(x + \frac{r^2}{2R(x)} \right) - \tan^{-1}\left(\frac{\lambda_0 (x - x_0)}{\pi w_0^2} \right) \right) \right) \tag{4.2}$$

$$w(x) = w_0 \sqrt{1 + \left(\frac{\lambda_0 (x - x_0)}{\pi w_0} \right)^2} \tag{4.3}$$

$$R(x) = (x - x_0) + \frac{1}{(x - x_0)} \left(\frac{\pi w_0^2}{\lambda_0} \right)^2 \tag{4.4}$$

$$r = \sqrt{(y - y_0)^2 + (z - z_0)^2} \tag{4.5}$$

where A_0 represents the amplitude, w_0 is the beam waist, k_0 and λ_0 are the wave number and wave length in free space, respectively, x_0 describes the position of the beam waist in x-direction as shown in Fig.4.4, the coordinate (y_0, z_0) denotes the center of the fundamental Gaussian distribution in the y-z plane. In our simulation, the coordinates (x_0, y_0, z_0) are (-310.0mm, 0.0mm, 350.0mm) which is the center of the output window. The investigations show that there is a great influence of the focal length l_2 of the quasi-elliptical mirror (see Fig.3.5) on the conversion efficiency [89,101].

Since in the q.o. mode converter for the transformation of the $TE_{34,19}$ mode, the input field distribution on the quasi-elliptical mirror shown in Fig.4.9 is quite complicated, its focal length l_2 should be well selected to match the required asymptotic beam growth (ABG) angle $\theta_0 = \frac{\lambda_0}{\pi w_0}$ of the Gaussian beam in order to achieve a high conversion efficiency into a fundamental Gaussian wave beam with given

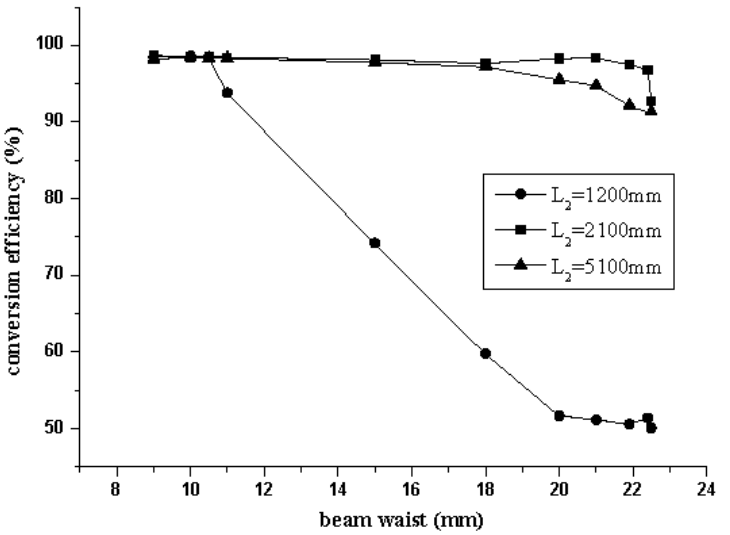

Fig.4.16 Conversion efficiency in the window plane.

structure [89,101]. In the procedure for the mirror system optimization as shown in Fig.3.4, the initial surfaces of the second and third phase correcting mirrors are plane. The optimization of the focal length l_2 of the quasi-elliptical mirror is carried out by changing the value of l_2 to match the ABG angle and then to obtain a high conversion efficiency to the desirable circular fundamental Gaussian distribution as described in equations 4.2-5. The optimized conversion efficiencies are shown in Fig.4.16, where the first focal length is l_1=100mm. For the second mirror, all the scalar correlation coefficients η_s could be improved from about 73-78% to 98-99% when l_2=1200mm, 69~75% to 98-99% when l_2=2100mm and 67-73% to 98-99% when l_2=5100mm, whereas the conversion efficiency η_v could not be enhanced [89,101]. This means that the second mirror can correct the amplitude distribution, but is unable to improve the phase distribution. Taking the wave beam corrected by the second mirror as the input, the third mirror is also optimized to provide a high conversion efficiency. For the focal length l_2 equal to 1200mm, which is same with that in Fig.4.4, an optimized conversion efficiency of more than 95% can be obtained only for a wave beam with an ABG angle larger than 3.0 degree; the corresponding beam waist is 11mm. This can explain that the existing mirror system could just provide a low scalar correlation coefficient η_s of 85% of the RF wave beam to the desired fundamental Gaussian distribution with the required beam waist of 25mm measured at the output window [94]. From Fig.4.16 we can also find that there is a great influence of the focal length of the quasi-elliptical mirror on the optimized conversion efficiency. As the focal length l_2 is increased to 2100mm, the smallest ABG angle of the wave beam with a high conversion efficiency of more than 95% could be decreased to 1.43 degree, and the corresponding beam waist is 22.4mm. The optimized conversion efficiencies with the focal length l_2 of 5100mm

are also shown in Fig.4.16. In this case the smallest ABG angle of the beam wave with high conversion efficiency is 1.6 degree. It seems that the focal length of 2100mm can best match the ABG angle.

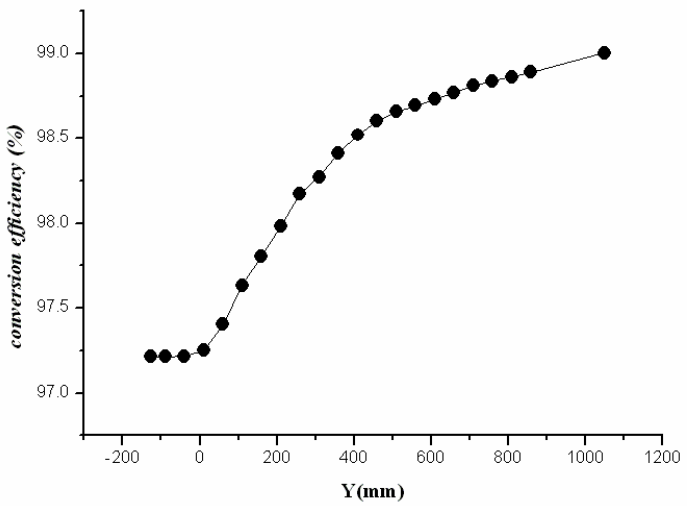

Fig.4.17 Conversion efficiencies along the path of propagation.

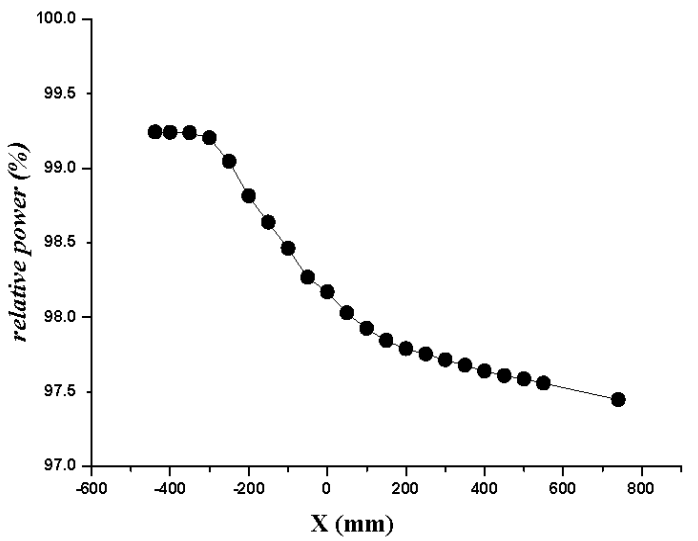

Fig.4.18 Relative power along the path of propagation.

In the case of l_2=2100mm, when the ABG angle is larger than 1.47 degree, the optimized conversion efficiency η_v is stable at the value of about 98%. As the beam waist increases to the value of 22.5mm, the optimised conversion efficiency η_v of the third mirror is decreased to 92.7%. The power transmission is determined as the relative power P_r

$$P_r = \frac{\iint_s |u|^2 \, ds}{P_{in}} \tag{4.6}$$

where P_{in} dedicates the input power on the quasi-elliptical mirror, S is an aperture and u is the field distribution on the aperture. In the window plane, the aperture size is πr^2, where r is the radius of the output window which is 50mm. At other position the aperture is $440*440mm^2$. As an example, the power transmission and the variation of the conversion efficiency along the propagation direction are plotted in Fig.4.17 and Fig.4.18, where the ABG angle is 1.6 degree, the corresponding beam waist is 20mm. From Fig.4.17 we can see that the conversion efficiency on the third mirror is 97.1% which means that the high-order modes in the outgoing wave beam are depressed and most of the outgoing wave beam has been converted into the desired fundamental Gaussian beam mode with required structure, the loss of power after correction is small as shown in Fig.4.18, the relative power is 98.2% at the output window. The conversion efficiency η_v is increased a little bit to 98.3% in the window plane and 99.0% at 740mm after the window due to the loss of high-order modes in the beam wave.

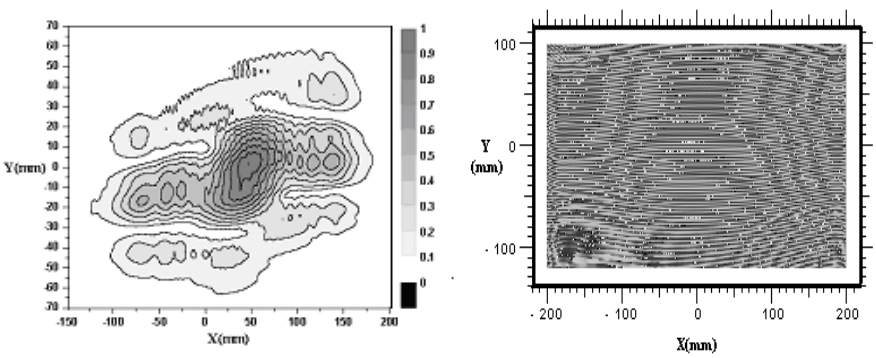

(a) (b)

Fig.4.19 Amplitude contour (a) and phase pattern (b) of the input field on the second mirror.

Fig.4.19 shows the amplitude contour and the phase pattern on the second mirror, where the field distribution is quite irregular and complicated with very low conversion efficiency of 43% and the scalar correlation coefficient of 70.6%. After correction by the second mirror, the amplitude contour and the phase pattern on the third mirror are shown in Fig.4.21. Comparing Fig.4.19(a) with Fig.4.20(a), it can be found that the amplitude distribution is rectified and the scalar correlation coefficient η_s is enhanced to 98.8%, whereas the phase pattern on the third mirror shown in Fig.4.20(b) is still very irregular in comparison to Fig.4.19(b).

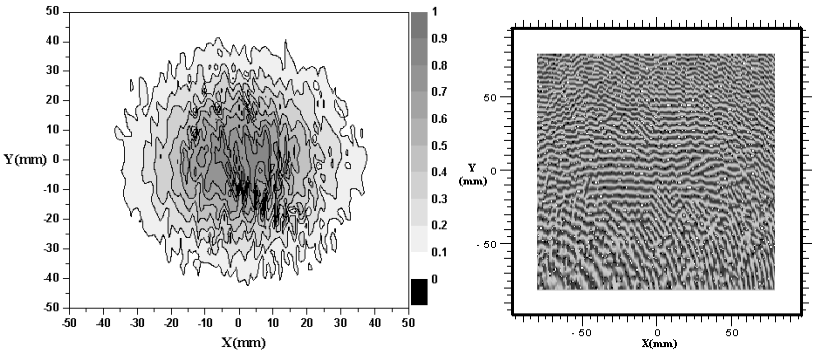

(a) (b)

Fig.4.20 Amplitude contour (a) and phase pattern (b) of the input field on the third mirror.

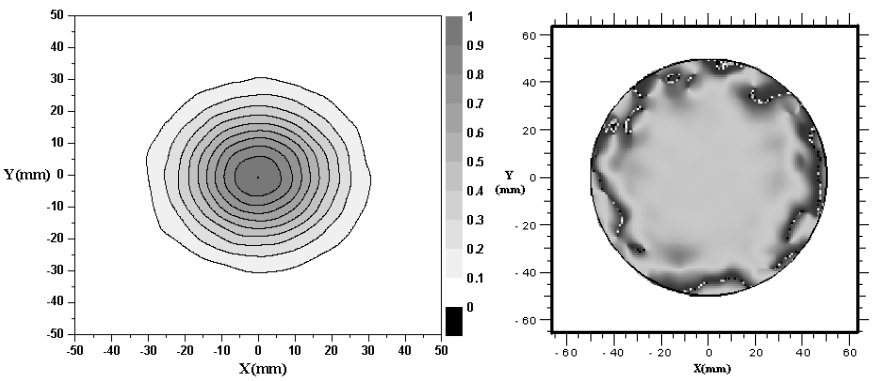

(a) (b)

Fig.4.21 Amplitude contour (a) and phase pattern (b) of the field in the window plane.

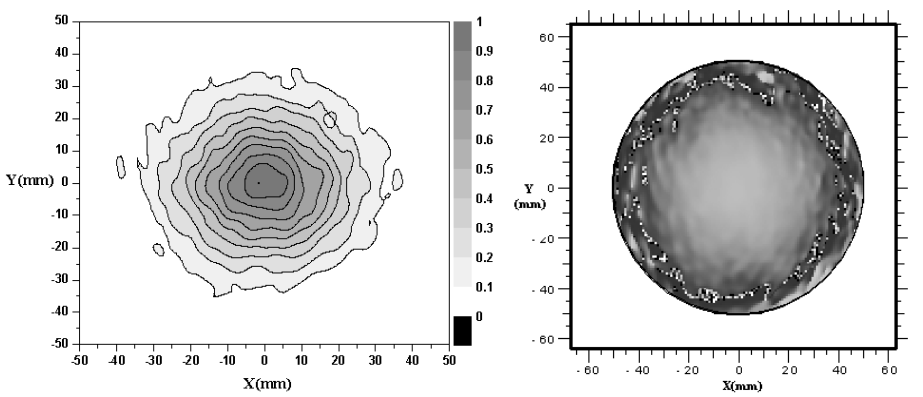

(a) (b)

Fig.4.22 Amplitude contour (a) and phase pattern (b) of the field at 300mm before the window.

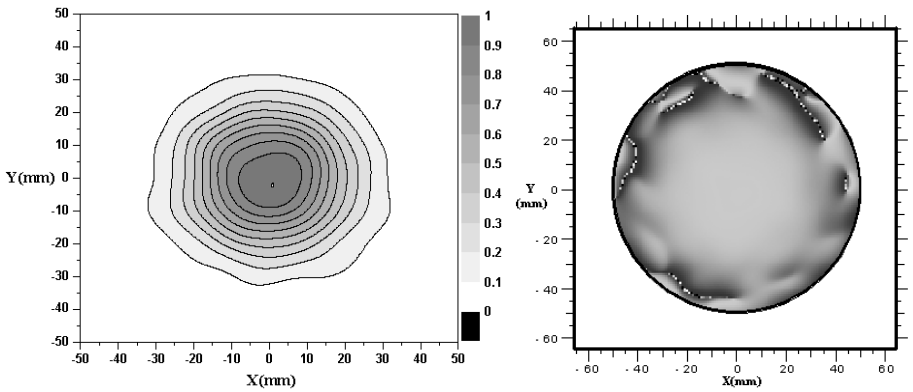

(a) (b)

Fig.4.23 Amplitude contour (a) and phase pattern (b) of the field at 300mm after the window.

Formed by the third mirror, both the amplitude contour and phase pattern in the window plane shown in Fig.4.21 are strongly improved and the conversion efficiency η_v is increased to 98.3%. The amplitude contours and phase patterns at 300mm before and after the window are also given in Fig.4.22-23, where the conversion efficiency η_v is 97.2% and 98.7%, respectively.

In this chapter, the theoretical and experimental investigations of the pre-prototype of the q.o. mode converter for the $TE_{34,19}$-mode coaxial-cavity gyrotron are presented. From the discussions we can conclude that it is a great challenge for the design of a q.o. mode converter for this gyrotron to provide a high quality wave beam with desired structure. Both the launcher and the mirror system are quite complicated; all the relative parameters should be well chosen and optimised to achieve a high conversion efficiency and high power-transmission.

Chapter 5 Improvement of the Quasi-Optical Mode Converter for the $TE_{34,19}$-Mode Coaxial-Cavity Gyrotron

In chapter 4, the analyses and experimental results of the prototype of the q.o. mode converter for the 170GHz, $TE_{34,19}$-mode coaxial-cavity gyrotron reveal that the dimpled-wall launcher designed by means of the conventional method fails to provide a high conversion efficiency of the volume cavity mode into a fundamental Gaussian distribution. In this case the mirror system is very complicated and very difficult for precise fabrication of the components with complicated surface structure. In this chapter, a dimpled-wall launcher with some high-order harmonics introduced to the wall deformations is investigated. By making use of a commercial computer code [100], the launcher wall surface is numerically optimized to provide a wave beam with high vector correlation coefficient η_v to a fundamental Gaussian mode. The mirror system is ameliorated, the tolerance conditions of the phase correcting mirrors with non-quadratic surface contours are improved.

5.1 Numerical Optimization of the Dimpled-Wall Launcher

In order to achieve a well-focused field distribution at the aperture of the dimpled-wall launcher for the $TE_{34,19}$-mode coaxial-cavity gyrotron, a launcher with high order perturbations included in the wall surface deformations are proposed [75]. The perturbation amplitudes and lengths are indicated in Fig.5.1.

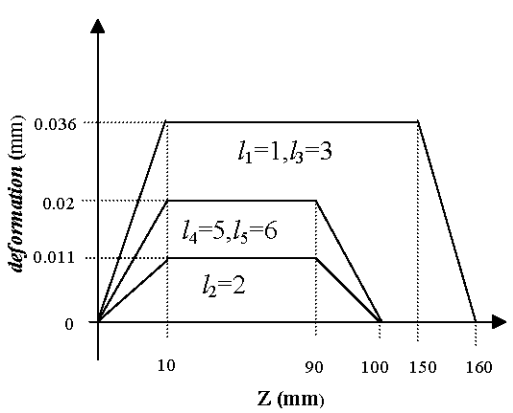

Fig.5.1 Schematic drawing of launcher wall deformations (l_1=1, l_2=2, l_3=3, l_4=5, l_5=6 perturbations).

The field distributions on the wall surface are simulated and shown in Fig.5.2, and the schematic contour of the wall is shown in Fig.5.3, where the slope of the

diameter taper is 0.002, the radius of the launcher is 32.5mm and therefore the oversize factor F_o is 1.1.

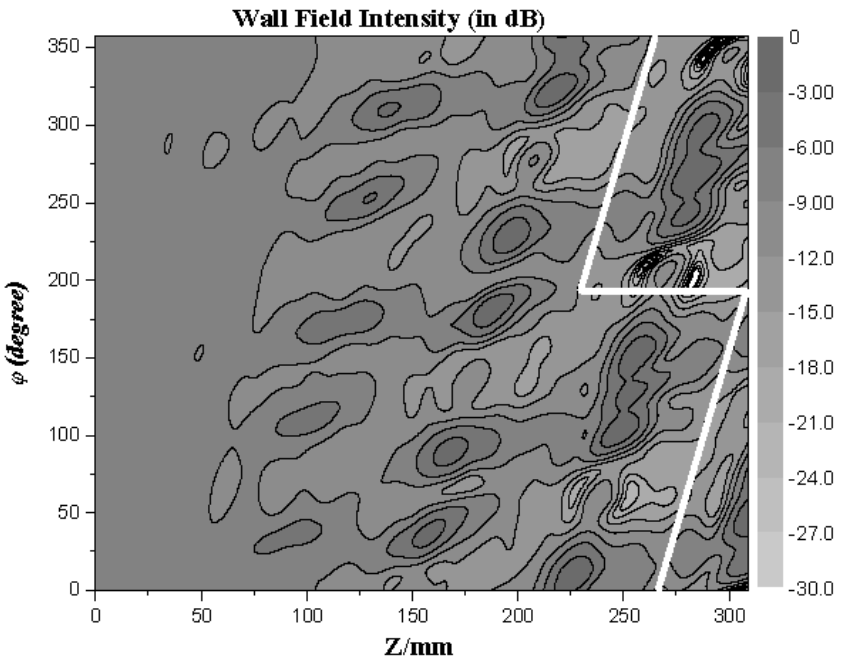

Fig.5.2 Field distribution on the unrolled waveguide wall of the launcher ($\ell_1 = 1, \ell_2 = 2, \ell_3 = 3, \ell_4 = 5, \ell_5 = 6$ perturbations). The edges of the launcher cut are indicated.

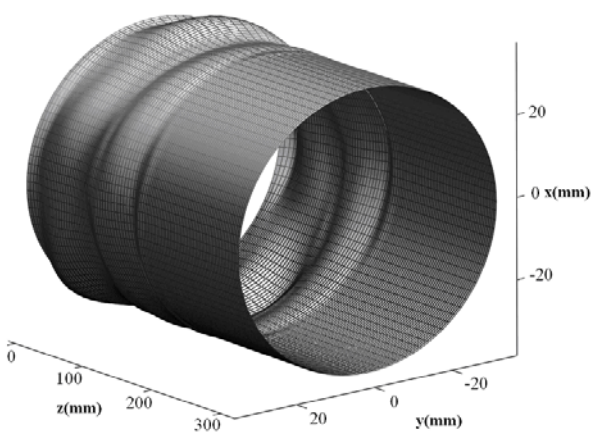

Fig.5.3 Schematic contour of the launcher wall
($\ell_1 = 1, \ell_2 = 2, \ell_3 = 3, \ell_4 = 5, \ell_5 = 6$ perturbations).

It is obvious that the fields on the aperture of the launcher shown in Fig.5.2 are not in good distributions in comparison to a fundamental Gaussian mode, the vector correlation coefficient is only 23%. The peak power density of the fields on the edges of cuts is as high as that of the input field of the launcher which is given as 57W/cm^2 in section 4.1, the launcher should be improved. Using the commercial computer code LOT developed at Calabazas Creek Research, Inc., USA [100], the launcher with high order perturbations is numerically optimized.

5.1.1 Launcher with Oversize Factor of 1.1

From Fig.5.2 we can see that the fields at the edges of the cuts are still relatively strong and the wave beam at the aperture is not good enough to provide high quality radiated fields. Notice that the amplitudes of the launcher wall perturbations are constant in the deformation section as shown in Fig.5.1, one can expect if the perturbation amplitude δ_i in equation (2.31) is variable along the z-axis, low fields at the edges of the cuts could be obtainable. We rewrite the equation as

$$R(\phi, z) = a + \alpha z + \sum_{i=1}^{N} \left[\xi_i(z) \cos(\ell_i \phi) + \zeta_i(z) \sin(\ell_i \phi) \right] \tag{5.1}$$

In equation (5.1), not only the amplitudes of the perturbations could be changed, but also the phases are variable, because ξ_i and ζ_i are independent to each other in the optimization. With both the amplitudes and phases of the perturbations optimized, the field patterns on the launcher wall are shown in Fig.5.5.

In comparison with Fig.4.2 and 4.8, we can find that the power densities on the edges of the cuts are decreased, the peak and average value are 5.4W/cm^2 and 1.9W/cm^2, respectively, and the maximum power density on the launcher wall is 400.8W/cm^2, which can satisfy the technical requirement for the cooling system of the launcher (<500W/cm^2). However, it should be pointed out that the vector correlation coefficient at the launcher aperture is not enhanced very much and is only 53% (see Fig.5.5). There are still too many and relatively strong high order modes in the radiated fields from this launcher. Thus it could be difficult to design a mirror system for the correction of the RF wave beam to achieve a desirable fundamental Gaussian distribution.

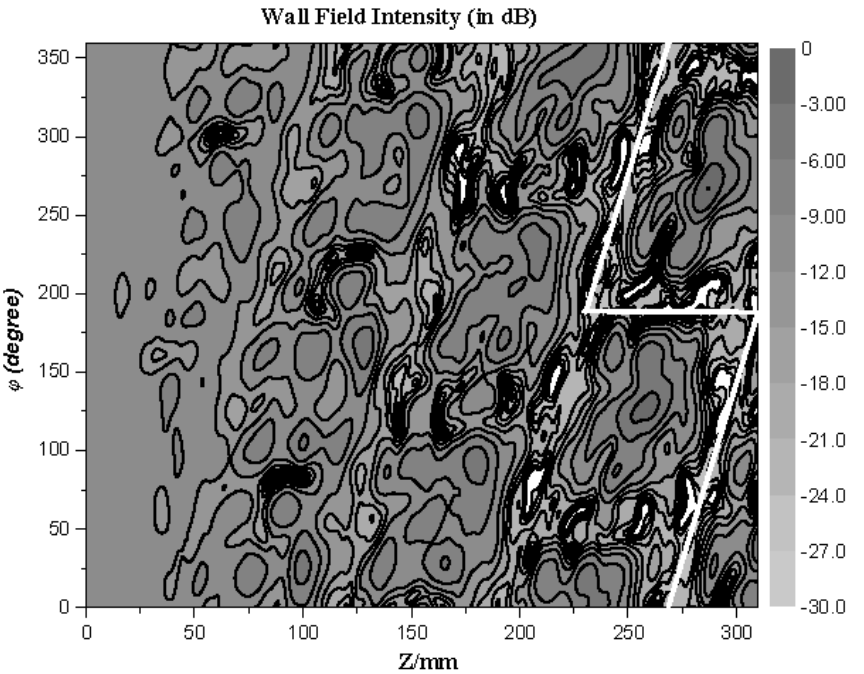

Fig.5.4 Field distribution on the unrolled waveguide wall of the optimized launcher ($\ell_1 = 1, \ell_2 = 2, \ell_3 = 3, \ell_4 = 5, \ell_5 = 6$ perturbations, f_o=1.1). The edges of the launcher cut are indicated.

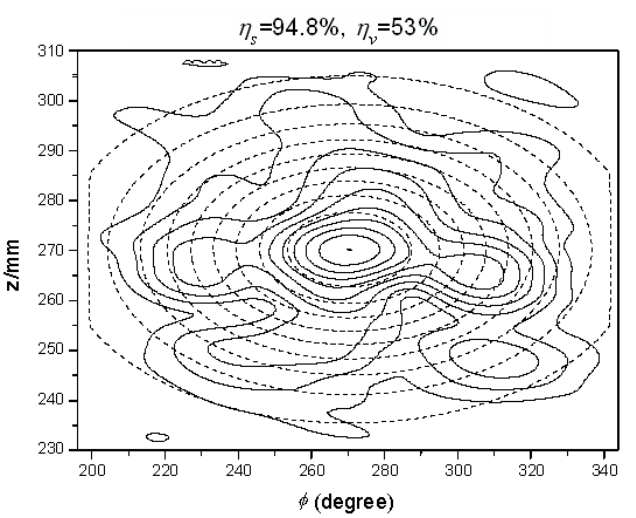

Fig.5.5 Contour of the strength of the field at the aperture of launcher in a linear step of 0.1, the solid and dashed lines represent the wave beam mode and ideal Gaussian distribution, respectively.

5.1.2 Launcher with Oversize Factor of 1.07

For the Denisov-type launcher, the oversize factor has a great influence on the field distributions inside the launcher. So a launcher with different radius is investigated to find an optimum value of the oversize factor in order to obtain a high quality wave beam at the launcher aperture. The optimizations are performed on a launcher with a smaller radius 31.6mm, where the oversize factor is decreased from 1.1 to 1.07. In this case, the power density at the input of launcher is 74.25W/cm^2 with F_m=1.5, so it becomes critical for the maximum power density to meet the technical requirement of the cooling system for the launcher. The optimized field patterns on the unrolled launcher wall are shown in Fig.5.6, and the amplitudes ξ_i and ζ_i are shown in Fig.5.7(a) and (b). The vector correlation coefficient to a fundamental Gaussian mode is increased to 82.3% at the aperture, the peak and average value of the power density at the edges of cuts are approximately 7.7W/cm^2 and 2.7W/cm^2, respectively, the maximum power density on the wall is 522W/cm^2, which is 22W/cm^2 larger than the requirement. An advance cooling system could be used for this launcher, which allows the maximum power density of 600W/cm^2 and accordingly is more expensive. The profile of the launcher wall surface shown in Fig.5.8 is much more complicated in comparison to Fig.5.3, it looks as if a large fabrication error would be produced. As a matter of fact, ξ_i(z) and ζ_i(z) shown in Fig.5.7 are continuous, and $R(\phi, z)$ in equation (5.1) is also a continuous function, the curvature radii of the perturbed wall surface are not very small so that the launcher can be fabricated in the same accuracy as that shown in Fig.5.3.

The fields in an opened-end launcher are not exactly waveguide modes due to diffraction and reflection at the edges of cuts. Only as the fields on the edges of cuts are very small, the fields inside the launcher can be well approximated by waveguide modes. In the computer code LOT [100], the fields inside the launcher are calculated using the coupled-mode method, which is based on the approximation to the fields in the launcher using the TE or TM modes. As the fields on the cuts edges of the optimized launcher are suppressed, both the reflection and the diffraction at the cut edges are all very low. This can be found from the similarity of the patterns of the field radiated from the optimized launcher shown in Fig.5.9 and 5.10 which are calculated using the computer code SUF3D [100] and the scalar diffraction integral equation (3.1), respectively. The algorithm used in the SUF3D code is the Moment of Method (MoM) to solve the Electric Surface Integral Equation (EFIE) for the launcher. It is a 3-D full wave analysis to the fields in the launcher, and thus the influences of the reflections and diffractions from the cuts edges are evaluated automatically in the calculation, and are all included in Fig. 5.9. Unfortunately, as the gyrotron operates at very high order mode and high frequency, it requires a large computer memory (8GB) and long computer time for the solution of the equivalent electric currents on the launcher wall using the SUF3D code.

Moreover, the convergence of the solutions becomes very critical as the convergence residual is small in the SUF3D code. So the solutions for the launcher in the $TE_{34,19}$-mode, 170GHz coaxial-cavity gyrotron cannot be done in a very high accuracy. The field pattern in the region z=7-60mm is quite irregular due to the calculation error as shown in Fig.5.9. The size of the quasi-elliptical mirror in the azimuthal direction is the same as that used in the pre-prototype of the q.o. mode converter (see section 4.1, page 58). The energy losses due to the diffraction is estimated as around 1.2%, which is just 23.4% of that given in section 4.1.

The optimized launcher with high-order harmonics introduced to the wall surface deformations and with an oversize factor of 1.07 can provide a relatively high vector correlation coefficient at the aperture and low diffraction losses at the launcher cuts. So the field distribution in the launcher can be well approximated by waveguide modes and the radiated fields can be calculated in terms of the scalar diffraction integral equation. Taking into account the calculation errors and complication, it seems that the scalar diffraction integral method is more effective and accurate for the analysis of the launchers operating with very high-order modes and high frequencies, so long as the fields on the launcher cuts are small enough to allow a good approximation of the fields inside the launcher by waveguide modes. This provides a simple way for the calculation of the field distributions inside the launcher and of the fields radiated from the launcher.

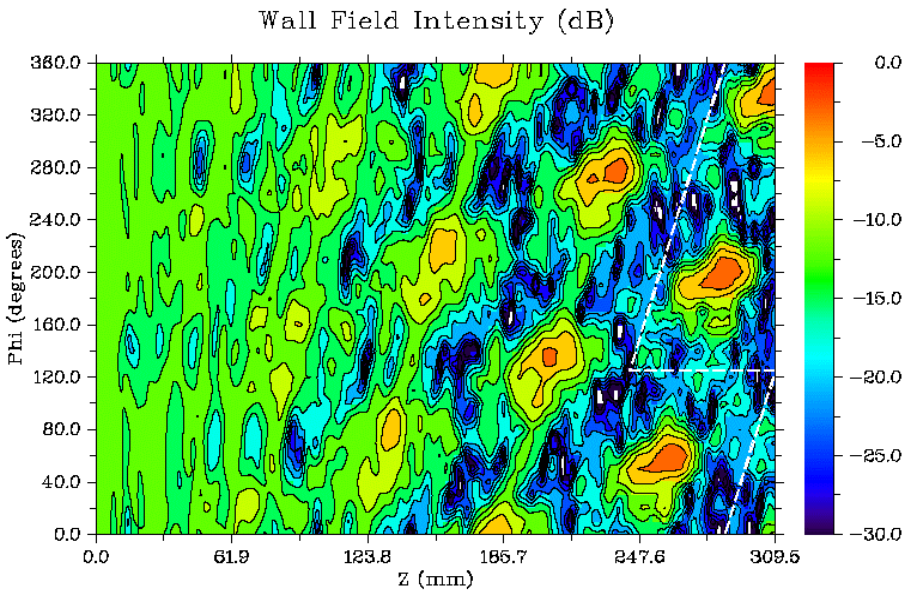

Fig.5.6 Field distribution on the unfolded wall of launcher for the $TE_{34,19}$-mode coaxial-cavity gyrotron with $\ell_1 = 1, \ell_2 = 2, \ell_3 = 3, \ell_4 = 5, \ell_5 = 6$ perturbations, and oversize factor F_o=1.07. The edges of the launcher cut are indicated.

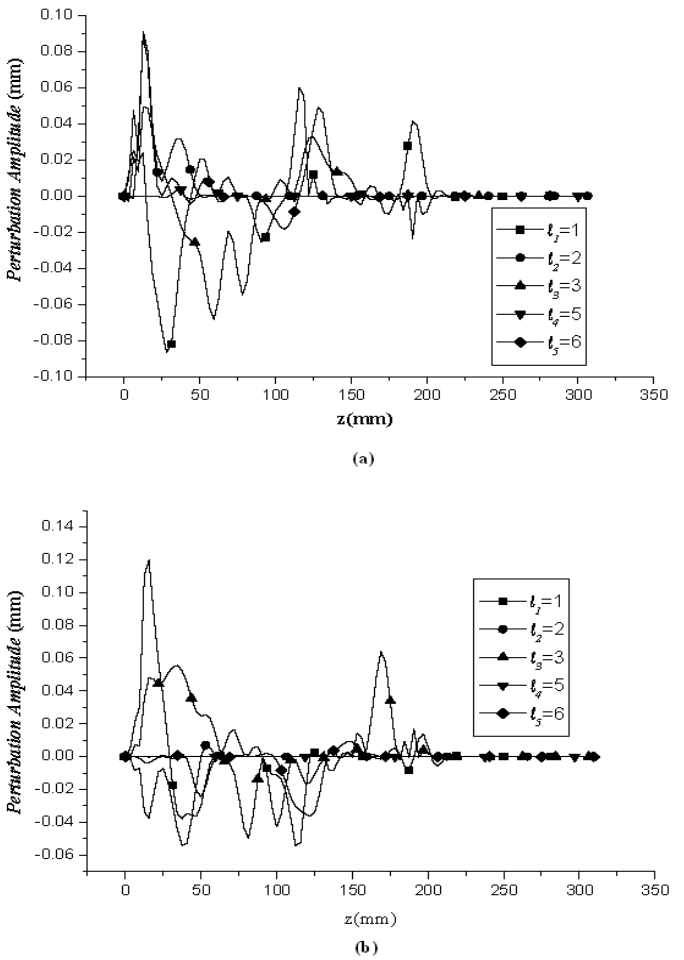

Fig.5.7 Perturbation amplitudes of the optimized launcher: (a) ξ_i(z); (b) ζ_i (z).

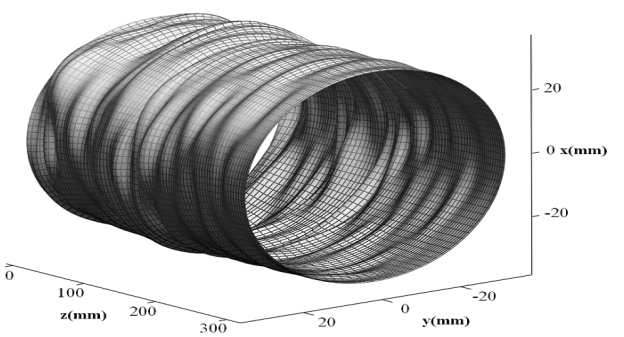

Fig.5.8 Schematic contour of the wall surface of the optimized launcher with $\ell_1 = 1, \ell_2 = 2, \ell_3 = 3, \ell_4 = 5, \ell_5 = 6$ perturbations, and oversize factor F_o=1.07.

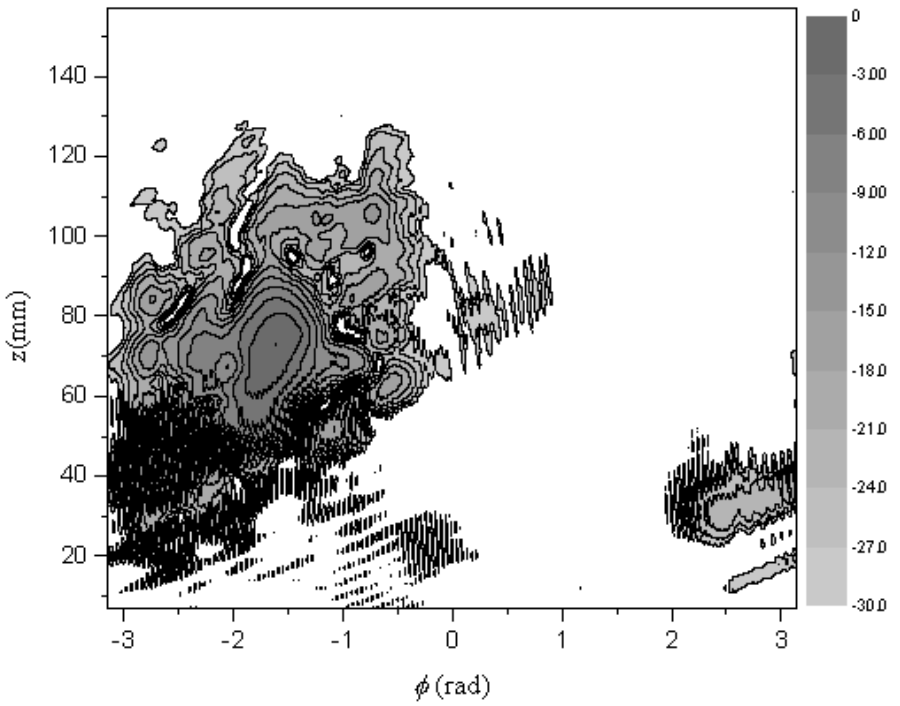

Fig.5.9 Field distribution on a cylindrical surface with 100mm radius and oversize factor F_o=1.07, which is calculated using the computer code SUF3D.

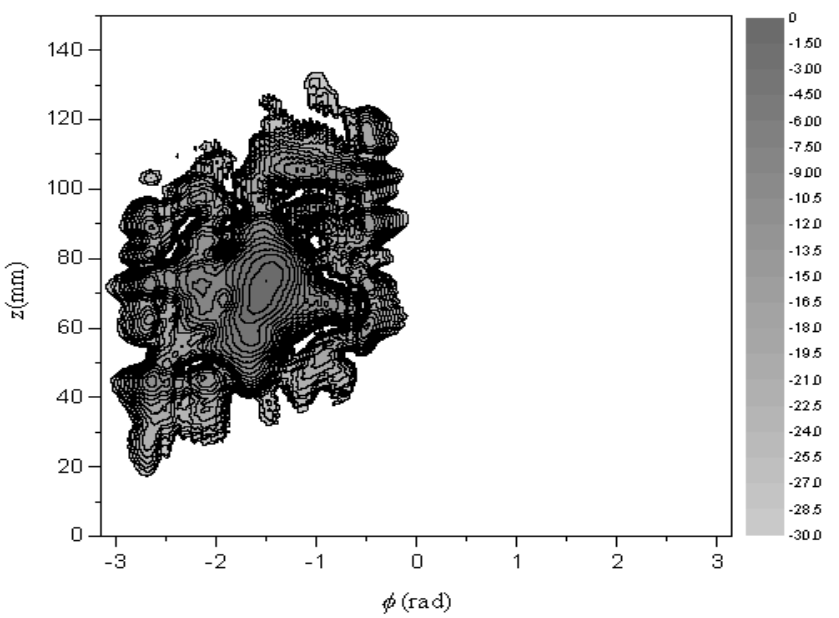

Fig.5.10 Field distribution on a cylindrical surface with 100mm radius and oversize factor F_o=1.07, which is calculated using the scalar diffraction integral equation.]

5.2 Improved Mirror System

In sections 3.1, 4.1 and 4.3, the beam forming mirror system for the $TE_{34,19}$-mode coaxial-cavity gyrotron is generally discussed. The focal length l_2 of the quasi-elliptical has been optimized in section 4.3. It has been pointed out that toroidal mirrors are not sufficient for the transformation of the field distribution radiated from the launcher into a desirable fundamental Gaussian mode. In the improved mirror system, there are three mirrors: the first one is a quasi-elliptical mirror with focal length l_1=100mm and l_2=2100mm, the second and third mirrors are phase correcting mirrors with non-quadratic surface contour functions. In order to investigate the tolerance conditions of the phase correcting mirrors, the procedure for the optimization of the phase correcting mirrors is improved as shown in Fig.5.11, where the mirror surfaces are smoothed in the iterative optimization algorithm. Accordingly, the equation (3.15) is changed as follows:

$$u_m(\vec{r}) = u(\vec{r}) \exp\left(j2kF_b\left(\Delta z(\vec{r}), r_c\right)\cos\alpha\right) \tag{5.2}$$

where F_b describes the smoothing function with respect to the perturbation $\Delta z(\vec{r})$ of the mirror surfaces and the curvature radius r_c of the milling tools. In the improved procedure, the fabrication errors are included in the optimization, so mechanically feasible mirror can be obtained. From the view of mathematics, the optimal mirror surfaces are related to the initial values of $\Delta z(\vec{r})$, so the choices of the initial shapes of the mirror surfaces are very important for the optimization of the phase correcting mirrors.

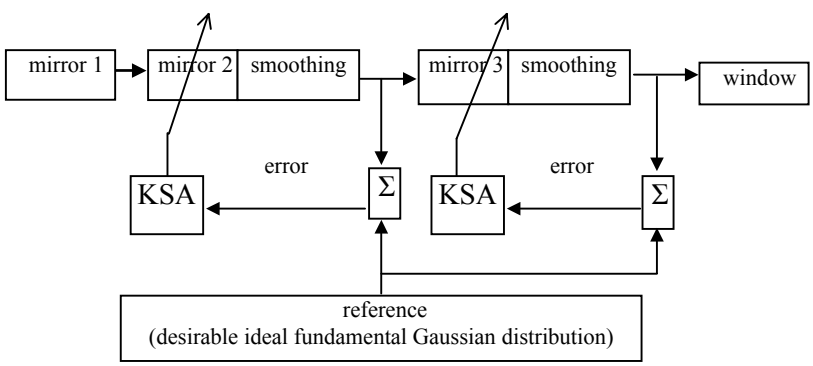

Fig.5.11 Principle of the improved procedure for the numerical optimisation of the mirror system.

As the maximum power density on the wall of the launcher with an oversize factor of 1.1 satisfies the requirement of the simple cooling system for the launcher, we first try to design a mirror system to correct the RF beam radiated from this launcher. With a curvature radius 0.5mm of the milling tools, an efficiency of 97% is achievable for conversion of the RF beam to the desirable fundamental Gaussian

mode in the window plane with a beam waist of 20mm. The power transmission is 96.8% at the output window. It seems a good mirror system has been obtained which can meet the requirements for the conversion efficiency and power transmission. However, the curvature radius of 0.5mm is too small, it needs too long time for the fabrication of the phase correcting mirrors. If the curvature radius increased to 1mm, the conversion efficiency decreases to 93.1%, and the power transmission is only 88.4%. The technical requirement for the curvature radius of the milling tools is $r_c \geq 2$mm. Setting the curvature radius r_c=2mm, the optimised mirror system could just provide a low conversion efficiency of 92% and a low power transmission of 81.9%. Since the vector correlation coefficient of the fields radiated from the launcher is just around 53%, the perturbed surfaces of the phase correcting mirrors are distorted very strongly in the optimisation and are very difficult to be machined.

It is expected that the fields radiated from the launcher with an oversize factor 1.07 can be transformed into the required fundamental Gaussian mode with high conversion efficiency by a mirror system optimised with a larger curvature radius of the milling tools. In the mirror system, the focal lengths of the quasi-elliptical are same as the optimum in section 4.3, and the initial values of $\Delta z(\vec{r})$ are zero for both the second and third mirrors, namely, the initial shapes of the second and third mirror are plane. Unfortunately, the phase correcting mirrors smoothed with curvature radius of 2mm could just provide a conversion efficiency of 93.2% to the fundamental Gaussian mode defined in equations (4.2-5) with 20mm beam waist in the window plane. Only as the value of r_c decreased to 1.4, the simulation results report the conversion efficiency is as high as 95.82% in the window plane. The field contour and phase pattern on the second and third mirrors are shown in Fig.5.12 and Fig.5.13, respectively. The size of the second mirror is 400mm×220mm, the power transmission on the second mirror is estimated to be 98.8%. Before corrected by the third mirror, the conversion efficiency of the field distribution shown in Fig.5.13 is 61%. The size of the third mirror is 160mm×160mm which is indicated in Fig.5.13. It can be found that the quality of the wave beam shown in Fig.5.13 is better than that shown in Fig.4.20 with the conversion efficiency of 23%. However, the power transmission on the third mirror is only 92.3%, there is too much power outside the mirror in Fig.5.13. Corrected by the third mirror, the field contour and phase pattern of the outgoing wave beam at 300mm before the window are plotted in Fig.5.14, from which we can see there are some high-order modes in the RF beam so that stray radiation is produced. Fig.5.15 gives the field distribution in the window plane, where the power transmission is reduced to 90%. The amplitude contour and phase pattern at 300mm after the window are also presented in Fig.5.16, the conversion efficiency and the relative power are 96% and 89.4%, respectively.

Although a conversion efficiency of more than 95% in the window plane is obtained, the power losses in the gyrotron are around 10% which is too large for the

$TE_{34,19}$-mode, 2MW,CW, coaxial-cavity gyrotron. The curvature radius of the milling tools used in the optimisations cannot satisfy the technical requirement. The analyses show that the power losses in the propagation from the second mirror to the third one is 6.5%, so it is very important to improve the second mirror further more.

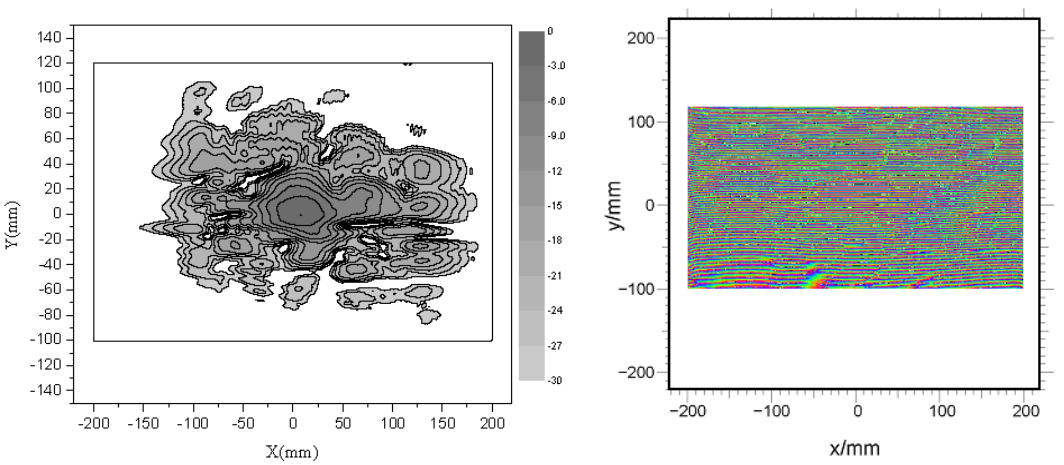

(a) (b)

Fig.5.12 Amplitude contour (a) and phase pattern (b) of the field on the second mirror, the size of the mirror is indicated.

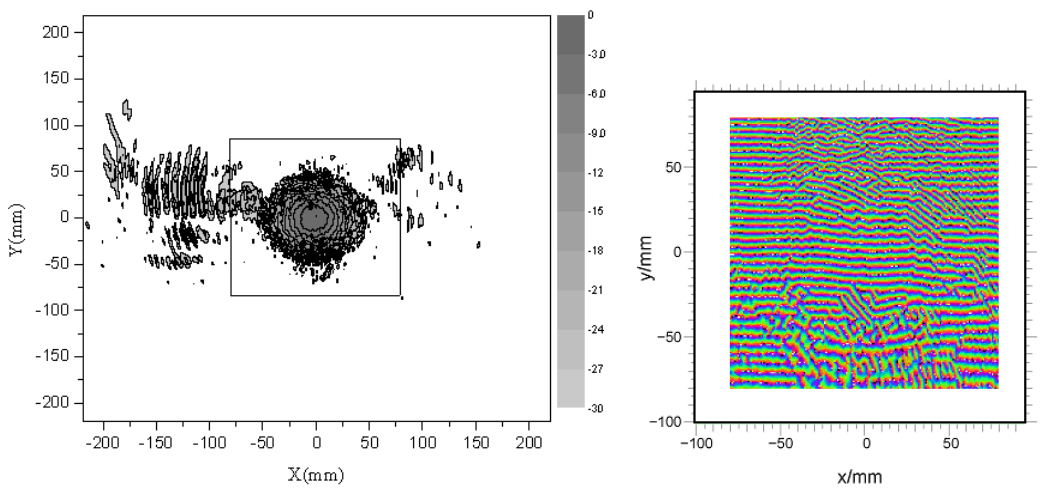

(a) (b)

Fig.5.13 Amplitude contour (a) and phase pattern (b) of the field on the third mirror, the size of the mirror is indicated.

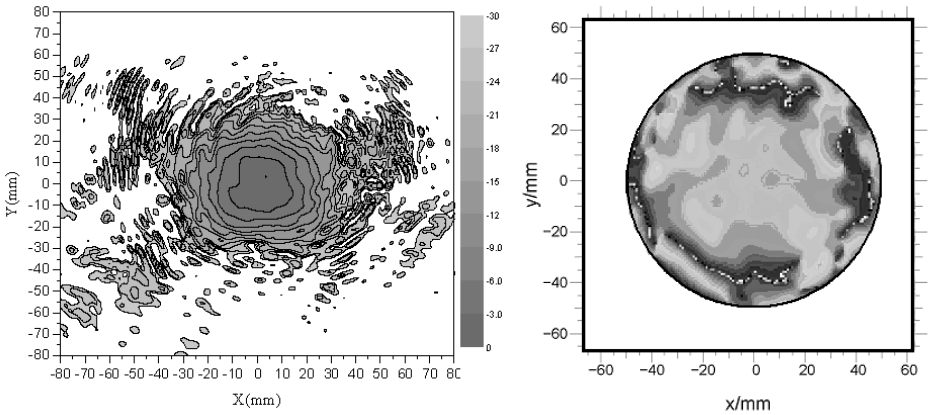

(a) (b)

Fig.5.14 Amplitude contour (a) and phase pattern (b) of the field at 300mm before the window.

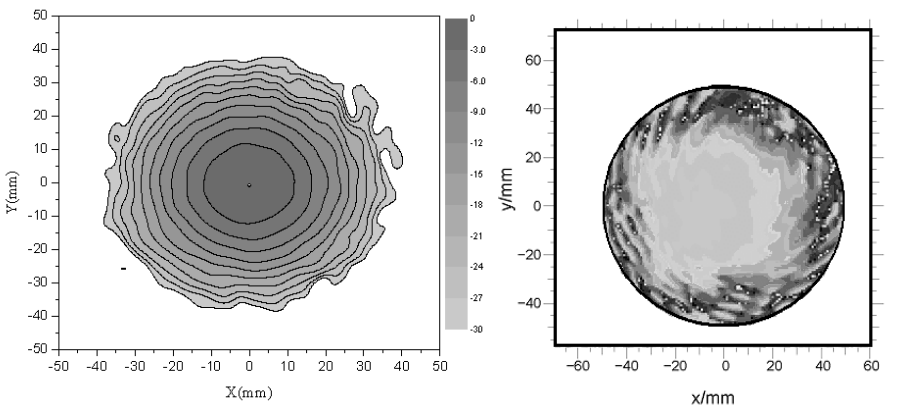

(a) (b)

Fig.5.15 Amplitude contour (a) and phase pattern (b) of the field in the window plane.

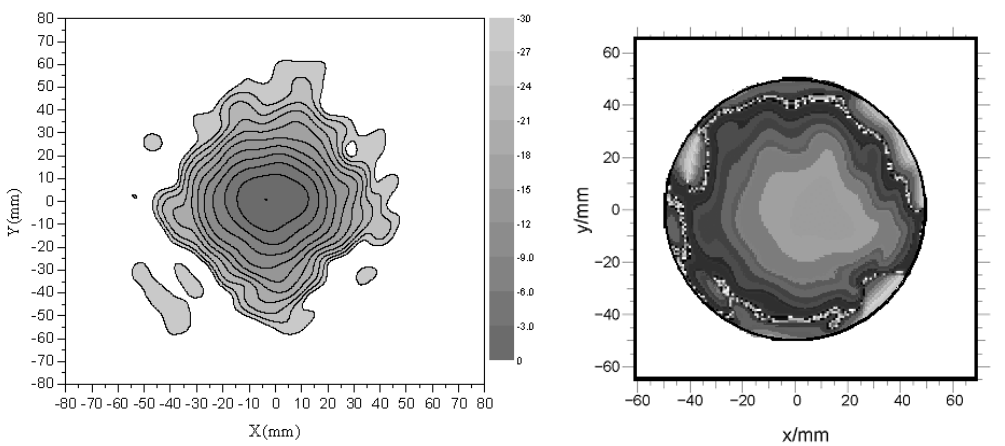

(a) (b)

Fig.5.16 Amplitude contour (a) and phase pattern (b) of the field at 300mm after the window.

Notice that the astigmatism of the RF wave beam before correction by the second mirror is relatively strong in the x-direction in Fig.5.11. It seems that the second mirror fails to remove the astigmatism in the wave beam as shown in Fig.5.13, so that a large stray radiation is produced in the x-direction.

The following approaches can be used for the improvement of the mirror system:

- Setting the initial values of $\Delta z(\vec{r})$ according to toroidal shapes instead of $\Delta z(\vec{r})=0$ before the optimization of the phase correcting mirrors. That is, the phase correcting mirrors are optimized from toroidal shapes;
- Making use of the Gaussian mode fitting code to choose the parameters of the desirable fundamental Gaussian mode, so that a higher vector correlation coefficient can be obtained before the optimisation;
- Finding the optimum value of the major and minor radii of the initial toroidal shapes to provide a minimum error defined in equation (3.18) before the optimisation.

It can be anticipated that by making use of the three methods, the mirror system can be improved to achieve a high conversion efficiency and high power transmission of more than 95% and the technical requirement for the curvature radius of the milling tools $r_c \geq 2$mm can be satisfied.

Chapter 6 Summary

As megawatt gyrotrons operate in high-order volume cavity modes, it is necessary to use a quasi-optical mode converter to transform the operating mode into a fundamental Gaussian beam. This work concentrates on the synthesis of the quasi-optical mode converter for the $TE_{34,19}$-mode, 2MW, CW coaxial-cavity gyrotron at FZK.

A quasi-optical mode converter is the combination of a launcher and a mirror system. In order to pre-shape the fields in the launcher, the launcher wall surface is perturbed to suppress the fields on the cut edges and to achieve a nearly Gaussian distribution at the aperture. The general method for the design of such dimpled-wall launcher is improved in this thesis. By means of the improved method very short perturbation lengths can be obtained with matched perturbation amplitudes. Using the improved method, a dimpled-wall launcher operating in the $TE_{22,6}$ mode at 118 GHz has been designed to provide a focused wave beam with a Gaussian mode content of 95.3% at the aperture.

For coaxial-cavity gyrotrons operating in very high-order cavity modes such as the $TE_{34,19}$ mode, due to the ratio of caustic to cavity radius of 0.323, the ray-representation of the $TE_{34,19}$ mode cannot form a closed or even almost closed polygon in the cross-section of the launcher. In this case, the dimpled-wall designed using the general method can provide a good amplitude composition. However, the phases are not in appropriate relations between the main mode and the satellite modes. The dimpled-wall launcher fails to transform the high-order cavity mode into a nearly Gaussian distribution. Moreover, the mirror system becomes very complicated. The synthesis of the q.o. mode converter for this gyrotron becomes very difficult and is a great challenge to obtain a high-quality RF beam with high conversion efficiency and low power losses. The setting of the parameters used in the q.o. mode converter for this gyrotron becomes very critical. The phase rule is proposed as a quality criterion to monitor the optimization of phase correcting mirrors and to find the optimum parameters for the q.o. mode converter.

Numerical calculations show that some high-order harmonics have to be introduced to the launcher wall deformations. The investigation shows that there is a great influence of the oversize factor of the launcher on the vector correlation coefficient of the outgoing wave beam to a fundamental Gaussian distribution. The optimum of the oversize factor is obtained (1.07), the fields on the cut edges are suppressed and a high vector correlation coefficient of 82.3% is achieved. The calculation results report low power diffraction losses around 1.2%. The field distributions in the optimized launcher can be well approximated by waveguide modes and radiated

fields can be calculated using the scalar diffraction integral. It provides a simple way for the simulation of the field distribution in an opened-end waveguide antenna and for the calculation of the radiated field from the opened-end waveguide antenna with low fields on the opened-end edges.

By taking the fabrication accuracy into account, the procedure for the numerical optimization of the mirror system is improved and the tolerance conditions of the phase correcting mirrors are investigated. The mirror system is numerically optimized, the conversion efficiency of 95.82% to the circular fundamental Gaussian distribution with 20mm beam waist, where the curvature radius of the milling tools is 1.4mm and is somewhat small. The power transmission is only 90% in the window plane. As the initial shapes of the phase correcting mirrors are plane, the astigmatism in the outgoing beam is not removed. So if the initial profiles of the phase correcting mirrors are toroidal functions, it is anticipated the conversion efficiency and power transmission would be enhanced. Optimal major and minor radii should be used. The parameters of the desired fundamental Gaussian distribution need to be adjusted. By ameliorating the initial conditions, a high conversion efficiency should be obtained. Finally, the q.o. mode converter is anticipated to provide a conversion efficiency of more than 95% and a power transmission of also > 95% even in the case if the curvature radius of the milling tools is larger than 2mm.

References

[1] R. S. Symons, "Tubes: still vital after all these years", *IEEE Spectrum.*, April 1998, vol. 35, pp. 52-63.

[2] A.S. Gilmour, "*Microwave Tubes*", Artech House, Norwood, MA, 1986.

[3] A.L. Goldenberg and A.G. Litvak, "Recent progress of high-power millimeter wavelength gyrodevices*", Phys. Plasmas 2*, June 1995, vol. 2, pp. 2562-2572.

[4] J. L. Hirshfield and J. M. Wachtel, "Electron cyclotron masers," *Phys. Rev. Lett*., 1964, vol. 12, no. 19, pp. 533–536.

[5] Flyagin V.A., Gaponov A.V., Petelin I., Yulpatov V.K., "The gyrotron", *IEEE Trans. on Microwave Theory and Techniques*, 1978, Volume 25, Issue 6, pp. 514 – 521.

[6] A.A Andronov, V.A. Flyagin, A.V. Gaponov, A.L. Goldenberg, M.I. Petelin, V.G. Usov, V.K. Yulpatov, "The gyrotron: high power sources of millimeter and submillimetre waves.", *Infrared Physics*, 1978, 18, pp. 385-393.

[7] M.I. Petelin, "Physics of advanced gyrotrons", *Plasma Phys. & Contr. Nucl. Fusion*, 1993, 35, Supplement B, pp. 343-351.

[8] V.A. Flyagin, A.L. Goldenberg, G.S. Nusinovich, "Powerful gyrotrons", in *Infrared and Millimeter Waves*, vol. 11, ed. K.J. Button, Academic Press, New York, 1984, pp. 179-226.

[9] V.A. Flyagin and G.S. Nusionvich, "Gyrotron oscillators", *Proceedings of the Institute of Electrical and Electronics Engineers*, 76, 1988, pp. 644-656 and, Powerful gyrotrons for thermonuclear research, in Infrared and Millimeter Waves, vol. 13, ed. K.J. Button, Academic Press, New York, 1985, pp. 1-17.

[10] K. Felch, H. Huey and H. Jory, "Gyrotrons for ECH application", *J. Fusion Energy*, 1990, 9, pp. 59-75.

[11] A.L. Goldenberg, G.G. Denisov, V.E. Zapevalov, A.G. Litvak and V.A. Flyagin, "Cyclotron resonance mesers: state of the art", *Radiophys. And Quantum Electronics*, 1996, 39, pp. 423-446.

[12] S.H. Gold and G.S. Nusinovich, "Review of high-power microwave source research", *Rev. Sci. Instrum.*, 1997, 68, pp. 3945-3974.

[13] V.L. Granatstein, B. Levush, B.G. Danly and R.K. Parker, "A quarter century of gyrotron research and development", 1997, *IEEE Trans. On Plasma Science*, PS-25, pp. 1322-1335.

[14] S.-C. Zhang and J. Elgin, "Propagation of the equilibrium electron beam in a free electron laser with axial guide magnetic field", *Physical Review E55*, 1997, pp. 4684-4693.

[15] S.-C. Zhang and J. N. Elgin, "A method of suppressing velocity spreads of the electron beam in the combination of helical wiggler and axial guide magnetic field", *Physics Letters A 198*, 1995, pp. 89-93.

[16] J.-B. Jin, Z.-B. Ouyang, C.-R. Qiu, X.-P. Liang, H.-B. Zhang, L. Hu and S.-C. Zhang, "Efficiency enhancement of coaxial-cavity electron cyclotron resonance maser by tapering guide magnetic field", *Int. Journal of Infrared and Millimeter Waves*, Jan. 2003, vol. 24, no. 1, pp. 35-41.

[17] V.G. Zorin, "Review of investigations on plasma creation by gyrotrons in Nizhny Novgorod", 15th International Workshop on ECR Ion Sources (ECRIS'02), Department of Physics, University of Jyväskylä, Finland, June 12-14, 2002.

[18] K.E. Kreischer and R.J. Temkin, "Single-mode operation of a high-power, step-tunable gyrotron", Physical Review Letters, Aug. 1987, vol. 59, pp. 547-550.

[19] D.R. Whaley, M.Q. Tran, S. Alberti and T.M. Tran, "Startup methods for single-mode gyrotron operation", Physical Review Letters, Aug. 1995, vol. 75, pp. 1304-1307.

[20] B. Piosczyk, A. Arnold, G. Dammertz, O. Dumbrajs, M. Kuntze and M. Thumm, "Coaxial cavity gyrotron – recent experimental results", IEEE Trans. on Plasma Science, Jun. 2002, vol. 30, pp. 819-827.

[21] T. Idhara, S. Mitsudo, S. Sabchevski, M. Glyavin and I. Ogawa, "Gyrotron FU series – current status of development and applications", Vacuum, 2001, vol. 62, pp. 123-132.

[22] T.C. Luce, "Application of high-power millimeter waves in fusion energy research", IEEE Trans. on Plasma Science, 2002, PS-30, pp. 734-754.

[23] T. Imai, N. Kobayashi, R. Temkin, M. Thumm, M.Q. Tran, V. Alikaev, "ITER R&D: auxiliary systems: electron cyclotron heating and current drive system", Fusion Engineering and Design, 2001, vol. 55, pp. 281-289.

[24] H. Zohm, G. Gantenbein, G. Giruzzi, S. Günter, F. Leuterer, M. Maraschek, J. Meskat, A.G. Peeters, W. Suttrop, D. Wagner, M. Zabiégo, ASDEX Upgrade Team, ECRH Group, "Experiments on neoclassical tearing mode stabilization by ECCD in ASDEX Upgrade", Nuclear Fusion, 1999, vol. 39, pp. 577-580.

[25] G. Gantenbein, H. Zohm, G. Giruzzi, S. Günter, F. Leuterer, M. Maraschek, J. Meskat, Q. Yu, ASDEX Upgrade Team, ECRH-Group (AUG), "Complete suppression of neoclassical tearing modes with current drive at the electron-cyclotron-resonance frequency in ASDEX Upgrade tokamak", Phys. Rev. Lett, 2000, vol. 85, pp. 1242-1245.

[26] H. Zohm, G. Gantenbein, A. Gude, S. Günter, F. Leuterer, M. Maraschek, J. Meskat, W. Suttrop, Q. Yu, ASDEX Upgrade Team, ECRH-Group (AUG), "The physics of neoclassical tearing modes and their stabilization by ECCD in ASDEX Upgrade", Nuclear Fusion, 2001, vol. 41, pp. 197-202.

[27] H. Zohm, G. Gantenbein, A. Gude, S. Günter, F. Leuterer, M. Maraschek, J. Meskat, W. Suttrop, Q. Yu, ASDEX Upgrade Team, ECRH-Group (AUG), "Neoclassical tearing modes and their stablization by electron cyclotron current drive in ASDEX Upgrade", Physics of Plasmas, 2001, vol. 8, pp. 2009-2016.

[28] R. Prater, "Heating and current drive by electron cyclotron wave", Physics of Plasma, 2004, vol. 11, pp. 2349-2376.

[29] V. Erckmann, WVII-AS Team, W. Kasparek, G.A. Müller, P.G. Schüller and M. Thumm, "Electron cyclotron resonance beating transmission line and launching system for the Wendelstein VII-AS stellarator", Fusion Technology, 1990, vol. 17, pp. 76-85.

[30] V. Erckmann, G. Dammertz, D. Dorst, L. Empacher, W. Förster, G. Gantenbein, T. Geist, W. Kasparek, H.P. Laqua, G.A. Müller, M. Thumm, H. Weissgerber, H. Wobig, W7-X and W7-AS Teams at IPP Gerching, W7-X Team at FZK Karlsruhe, W7-X Team at IPF Stuttgart, "ECRH and ECCD with high power gyrotrons at the stellarators, W7-AS and W7-X" IEEE Trans. on Plasma Science, 1999, PS-27, pp. 538-546.

[31] W. Kasparek, V. Erckmann, H.P. Laqua, E. Borie, G. Dammertz, L. Empacher, W. Förster, G. Gantenbein, S. Illy, G. Michel, G. Müller, B. Piosczyk, M. Thumm, D. Wagner, M. Weißgerber, H. Zohm, W7-x and W7-AS Teams at IPP Garching, W7-X Team at FZK Karlsruhe, W7-X Team at IPF Stuttgart, "ECRH and ECCD with high power gyrotrons at the stellarators W7-X", Proc. 4th Int. Workshop on Strong Microwaves in Plasmas, Nizhny Novgorod, ed. A.G. Litvak, Inst. Of Applied Phasics, Russian Academy of Sciences, Nizhny Novgorod, 2000, vol. 1, pp. 185-204.

[32] V. Erckmann, H.P. Laqua, H. Maassberg, J. Geiger, G. Dammertz, W. Kasparek, M. Thumm, W7-x and W7-AS Teams IPP, W7-X Team FZK, W7-X Team IPF, "Electron cyclotron resonance heating and EC-current drive experiments at W7-AS, status at W7-X", Fusion Engineering and Design, 2001, vol. 53, pp. 365-375.

[33] M. Wanner, V. Erckmann, J.-H. Feist, W. Gardebrecht, D. Hartmann, R. Krampitz, H. Niedermeyer, H. Renner, Th. Rummel, F. Schauer, L. Wegener, F. Wesner, G.A. Müller, W. Kasparek, M. Thumm and G. Dammertz, "Status of WENDELSTEIN 7-X construction", Nucl. Fusion, 2003, vol. 43, pp. 416-424.

[34] G. Dammertz, H. Braune, V. Erckmann, G. Gantenbein, W. Kasparek, H.P. Laqua, W. Leonhardt, G. Michel, G. Müller, G. Neffe, B. Piosczyk, M. Schmid, M.K. Thumm, "Progress in the 10-MW ECRH system for the stellarator W7-X", IEEE Trans. on Plasma Science, 2004, vol. 32, pp. 144-151.

[35] K. Ohkubo, et al., "Electron cyclotron plasma production and heating on LHD: system and its application", Proc. 4th Workshon on Strong Microwave in Plasmas, Nizhny Novgorod, ed. A.G. Litvak, Inst. Of Applied Physics, Russian Academy of Sciences, Nizhny Novgorod, 2000, vol. 1, pp. 27-40.

[36] H. Idei, et al, "Electron cyclotron heating scenario and experimental results in LHD", Fusion Engineering and Design, 2001, vol. 53, pp. 329-336.

[37] T. Shimozuma, et al, "Recent results of ECRH experiment by an upgraded heating system in LHD", 5th Int. Workshop on Strong Microwaves in Plasmas,

Nizhny Novgorod, ed. A.G. Litvak, Inst. of Applied Physics, Russian Academy of Sciences, Nizhny Novgorod, 2002, H4.

[38] M. Thumm, "State-of-the-art of high power gyro-devices and free electron masers update 2004", Forschungszentrum Karlsruhe, Wissenschaftliche Berichte FZKA 7097, Februar 2005, pp.1, pp.20.

[39] V. Erckmann, "Electron cyclotron resonance heating in the Wendelstein 7-A stellarator," Plasma Phys. Control. Fusion, 1986, vol. 28, no. 9A, pp. 1277–1290.

[40] V. Erckmann, et al, "ECRH and ECCD with high power gyrotrons at the stellarators W7-AS and W7-X," IEEE Trans. Plasma Sci., Apr. 1999, vol. 27, pp. 538–546.

[41] G. Dammertz, S. Alberti, A. Arnold, E. Borie, V. Erckmann, G. Gantenbein, E. Giguet, R. Heidinger, J. P. Hogge, S. Illy,W. Kasparek, K. Koppenburg, M. Kuntze, H. P. Laqua, G. LeCloarec, Y. LeGoff, W. Leonhardt, C. Lievin, R. Magne, G. Michel, G.Müller, G. Neffe, B. Piosczyk, M. Schmid, K. Schwörer,M. Thumm, and M. Q. Tran,, "Development of a 140-ghz 1-mw continuous wave gyrotron for the w7-x stellarator", IEEE Transactions on Plasma Science, 2002, 30, pp. 808-818.

[42] K. Koppenburg, G. Dammertz, M. Kuntze, B. Piosczyk, and M. Thumm, "Fast frequency-step-tunable high-power gyrotron with hybrid-magnet-system", IEEE Trans. on Electron Devices, Jan. 2001, vol. 48, pp. 101-107.

[43] K. Koppenburg, A. Arnold, E. Borie, G. Dammertz, O. Drumm, M. Kartikeyan, B. Piosczyk, M. Thumm, and X. Yang, "Design of a step-tunable 105-140 GHz, 1 MW gyrotron at FZK", Proceedings 10th International Conference Displays and Vacuum Electronics, ITG-Fachbericht 183, pp. 55-59, Garmisch-Partenkirchen, Germany, May 2004

[44] B. Piosczyk, O. Braz, G. Dammertz, C.T. Iatrou, S. Illy, S. Kern, M. Kuntze, G. Michel, A. Möbius, M. Thumm, V.A. Flyagin, V.I. Khishnyak, A.B. Pavelyev, V.E. Zapevalov, "A 1.5 MW, 140 GHz, $TE_{28,16}$-coaxial cavity gyrotron, IEEE Trans. on Plasma Science", 1997, vol. 25, pp. 460-469.

[45] C.T. Iatrou, O. Braz, G. Dammertz, S. Kern, M. Kuntze, B. Piosczyk, M. Thumm, "Design and experimental operation of a 165 GHz, 1.5 MW coaxial cavity gyrotron with axial RF-output", IEEE Trans. Plasma Science, 1997, vol. 25, pp. 470-479.

[46] B. Piosczyk, A. Arnold, E. Borie, G. Dammertz, O. Drumm, O. Dumbrajs, S. Illy, M. Kuntze, K. Koppenburg, M. Thumm, "Development of Advanced High Power Gyrotrons at Forschungszentrum Karlsruhe", Frequenz, 2001, vol. 55, pp. 242-246.

[47] B. Piosczyk, A. Arnold, G. Dammertz, M. Kuntze, G. Michel, O.S. Lamba, M. Thumm, "Step-frequency operation of a coaxial cavity gyrotron from 134 to 169.5 GHz", IEEE Trans. on Plasma Science, 2000, vol. 28, pp. 918-923.

[48] B. Piosczyk, "A novel 4.5 MW-electron gun for a coaxial cavity gyrotron", IEEE Trans. Electron Devices, 2001, vol. 48, pp. 2938-2944.

[49] S.N. Vlasov et al., "Open coaxial resonators for gyrotrons", Radio Eng. Electrn. Phys., 1976, vol. 21, pp. 96-102.
[50] C.T. Iatrou, S. Kern, A. Pavelyev "Coaxial cavities with corrugated inner conductor for gyrotrons", IEEE Microwave Theory Tech, 1996, vol. 41, no. 1, pp56-64.
[51] B. Piosczyk, G. Dammertz, O. Dumbrajs, O. Drumm, S. Illy, J. Jin, and M. Thumm, "A 2-MW, 170GHz Coaxial Cavity Gyrotron", IEEE Trans. Plasma Sci., June 2004, vol. 32, pp. 413-417.
[52] B. Piosczyk, O. Dumbrajs, S. Illy, J. Jin, G. Michel, T. Rzesnicki, M. Thumm, X. Yang, "Final report: $TE_{34,19}$, 170 GHz, 2 MW, CW Coaxial Cavity Gyrotron - design and experimental results with the short pulse pre-prototype", Efda reference: TW3-THHE-CCGDS1, Association: FZK, Dec. 2004.
[53] A. Möbius and M. Thumm, "Gyrotron output launchers and output tapers", in Gyrotron Oscillators – Their Principles and Practice, C. Edgcombe, Ed. London: Taylor & Francis, 1993, Chapter 7, pp. 179-222.
[54] L.A. Weinstein, Open waveguides and resonators, Golem Press, Boulder Colorado, 139, 1969.
[55] S.N. Vlasov and I.M. Orlova, "Quasi-optical transformer which transforms the waves in a waveguide having a circular cross-section into a highly-directional wave beam", Radio Phys. and Quantum Electronics, 1974, vol. 17, pp. 115-119.
[56] S.N. Vlasov, L.I. Zagryadskaya, and M.I. Petelin, "Transformation of a whispering gallery mode, propagating in a circular waveguide into beam of waves", Radio Eng. and Electron Physics, 1975, vol. 20, pp. 14-17.
[57] M. Thumm, "High-power microwave transmission systems, external mode converters and antenna technology", in Gyrotron Oscillators - Their Principles and Practice, C. Edgcombe, ed., London: Taylor & Francis, 1993, chapter 13, pp. 365-401.
[58] S.V. Kuzikov and M.I. Petelin, "Conversion of paraxial waveguide mode to Gaussian beam", Proc. Int. Workshop on Strong Microwaves in Plasma, Nizhny Novgorod, 1996, ed. A.G. Litvak, Russian Academy of Sciences, 1997, vol. 2, pp. 877-885.
[59] G. G. Denisov, A. N. Kuftin, V. I. Malygin, N. P. Venediftov, D. V. Vinogradov, and V. E. Zapevalov, "110 GHz gyrotron with built-in high efficiency converter," Int. J. Electron., vol. 72, pp. 1079–1091, 1992.
[60] J. Pretterebner, A. Mübius, and M. Thumm, "Improvement of quasioptical mode converters by launching an appropriate mixture of modes," in Conf. Dig. 17th Int. Conf. Infrared and Millimeter Waves, vol. 1929, Pasadena, CA, 1992, pp. 40–41.
[61] M. Thumm, A. Arnold, E. Borie, O. Braz, G. Dammertz, O. Dumbrajs, K. Koppenburg, M. Kuntze, G. Michel, and B. Piosczyk, "Frequency step-

tunable (114–170 GHz) megawatt gyrotrons for plasma physics applications," Fusion Eng. Des., vol. 53, pp. 407–421, 2001.
[62] G. Dammertz, S. Alberti, A. Arnold, E. Borie, V. Erckmann, G. Gantenbein, E. Giguet, R. Heidinger, J. P. Hogge, S. Illy,W. Kasparek, K. Koppenburg, M. Kuntze, H. P. Laqua, G. LeCloarec, Y. LeGoff, W. Leonhardt, C. Lievin, R. Magne, G. Michel, G.Müller, G. Neffe, B. Piosczyk, M. Schmid, K. Schwörer,M. Thumm, and M. Q. Tran, "Development of a 140 GHz 1 MW continuous wave gyrotron for the W7-X stellarator," IEEE Trans. Plasma Sci., vol. 30, no. 3, pp. 808–818, Jun. 2002.
[63] M. Thumm, X. Yang, A. Arnold, G. Dammertz, G. Michel, J. Pretterebner, and D. Wagner, "A high-efficiency quasi-optical mode converter for a 140-Ghz 1-MW CW gyrotron", IEEE Trans. on Electron Devices, May 2005, vol. 52, pp. 818-824.
[64] L. A.Vainshtein, Open Resonators and Open Wavequides, Golem Press, Boulder, Colorado (1969).
[65] V.M.Babich and V. S.Buldyrev, Short-Wavelength Diffraction Theory. Asymptotic Methods, Springer-Verlag, Berlin, 1991.
[66] G. Michel, "Field profile analysis and synthesis in the millimeter wave range", PhD thesis (in German), Forschungzentrum Karlsruhe, Germany, Wissenschaftliche Berichte FZKA 6216, 1998, pp. 19-21.
[67] A. Wien and M. Thumm, "Numerical analysis of quasi-optical mode converters. Part 1: Backscattering analysis of shaped-end radiators". Int. J. Electronics, 1999, vol. 86, pp. 739-745.
[68] G.G Denisov, M.I. Petelin, and D.V. Vinogradow, "Converter of high-mode of a circular waveguide into the main mode of a mirror line", 1990, WO90/0780 H01P1/16, PCT Gazette, 16, pp.47-49.
[69] G.G Denisov, M.I. Petelin, and D.V. Vinogradow, "Effective conversion of high waveguide modes to eigenmodes of open mirror lines", Proc. 10th Summer-Seminar on Wave Diffraction and Propagation, Moscow, SRIRP, pp. 96-128, 1993.
[70] M. Thumm: Modes and mode conversion in microwave devices. In "Generation and Application of High Power Microwaves", Ed. R.A.Cairns and A.D.R.Phelps, IOP, Bristol, 121, 1997.
[71] A. Wien, "Contribution to the analysis of quasi-optical mode converters in high-power gyrotrons", PhD thesis (in German), Forschungzentrum Karlsruhe, Germany, Wissenschaftliche Berichte FZKA 5638, September 1995, pp. 22.
[72] Yosuke Hirata, Y. Mitsunaka, K. Hayashi, Y. Itoh, K. Sakamoto and T. Imai, "The design of a tapered dimple-type mode converter/launcher for high-power gyrotrons", IEEE Trans. Plasma Sci., Feb. 2003, vol. 31, pp. 142-145.
[73] M. Blank, K. Kreischer, R.J. Temkin, "Theoretical and experimental investigation of a quasi-optical mode converter for a 110-GHz gyrotron", IEEE Trans. Plasma Sci., Jun. 1996, vol. 24, pp. 1058-1066.

[74] A.A. Bogdashov and G.G. Denisov, “Asymptotic theory of high-efficiency converters of high-order waveguide modes into eigenwaves of open mirror lines”, Radiophysics and Quantum Electronics, 2004, vol. 47, no. 4, pp.283-296.

[75] J.B. Jin, M. Thumm, B. Piosczyk, and T. Rzesnicki, “Theoretical investigation of an advanced launcher for a 2-MW, 170GHz, $TE_{34,19}$ coaxial cavity gyrotron”, IEEE Trans. on Microwave Theory and Technique, vol.54, no. 3, March 2006, pp. 1139-1145.

[76] J.B. Jin, B. Piosczyk, G. Michel, M. Thumm, O. Drumm, T. Rzesnicki, and S.C. Zhang, “The Design of a Quasi-Optical Mode Converter for a Coaxial-Cavity Gyrotron”, Joint 29th Int. Conf. on IRMMW & 12th Int. Conf. on Terahertz Elect., Karlsruhe, Germany, pp. 669-670, 2004.

[77] D. Bariou, private communication, TED, Velizy, France, Mar. 26, 2005.

[78] J. L. Doane, Propagation and mode coupling in corrugated and smooth-wall circular waveguides, Infrared and Millimeter Waves, 13, ed. K.J. Button, Acad Press, Ch 5, pp. 123-170, 1985.

[79] M. Thumm, “High-power millimeter-wave mode converters in overmoded circular waveguides using periodic wall perturbations”, Int. J. of Electronics, 1984, Bd.57, no.6, pp. 1225-1246.

[80] M. Blank, K. Kreischer, and R.J. Temkin, “Theoretical and experimental investigation of a quasi-optical mode converter for a 110-GHz gyrotron”, IEEE Trans. on Plasma Science, 1996, vol. 24, no. 3, pp. 1058-1066.

[81] J. Pretterebner, “Compact quasi-optical antennas in oversized waveguide”, Phd thesis (in German), Institut für Plasmaforschung, Universität Stuttgart, 2003, pp. 108-109.

[82] A.G.Litvak, V.V.Alikaev, G.G.Denisov, V.I.Kurbatov, V.E.Myasnikov, E.M.Tai, and V.E.Zapevalov, “Gyrotrons for fusion. status and prospects”, http://www.iaea.org/programmes/ripc/physics/fec2000/pdf/ftp1_31.pdf.

[83] A.V. Chirkov, G.G. Denisov, N.L. Aleksandrov, “3D wavebeam field reconstruction from intensity measurements in a few cross sections”, Optics Communication, 1995, 115, pp. 449-452.

[84] B. Piosczyk, et al.; "165-GHz coaxial cavity gyrotron.", IEEE Trans. on Plasma Science, 2004, vol. 32, pp.853-60.

[85] J.B. Jin, M. Thumm, B. Piosczyk, T. Rzesnicki, and G. Dammertz, "Investigation of an Advanced Quasi-Optical Mode Converter for a Coaxial Gyrotron”, Proc. The Joint 30th Int. Conf. on Infrared and Millimeter Waves and 13th Int. Conf. On Terahertz Electronics”, Williamsburg, USA, 2005, pp. 299-300.

[86] S.N. Vlasov and M.A. Shapiro, "Bievolvent mirror for transfer of caustic surfaces", Soviet Technical Physics Letters, 1989, vol. 15, pp. 374-375.

[87] G. Michel and M. Thumm, “Spectral domain techniques for field pattern analysis and synthesis,” Surveys Math. Ind., 1999, vol. 8, pp. 259–270.

[88] J.B. Jin, B. Piosczyk, M. Thumm, T. Rzenicki, S.C. Zhang, "Investigation of a mirror system for a high power coacial-cavity gyrotron", Proc. 6th International Vacuum Electronics Conference IVEC 2005, Noordwijk, Netherland, April 20-22, 2005, WPP-246, pp. 275-278.

[89] J.B. Jin, B. Piosczyk, M. Thumm, T. Rzesnicki, and S. Zhang, "Quasi-optical mode converter/mirror system for a high power coaxial-cavity gyrotron", IEEE Trans. on Plasma Science,vol. 34, no. 4, August 2006, pp. 1508-1515.

[90] O. Drumm, "Numerical optimization of quasi-optical mode converter for grequency step-tunable gyrotron", Phd thesis (in German), Institut für Elektrotechnik und Informationstechnik der Universität Karlsruhe, Wissenschaftliche Berichte FZKA 6754, 2002, pp. 108-109.

[91] B.Z. Katsenelenbaum, V.V. Semenov, "Synthesis of phase correctors shaping a specified field", Radio Eng. and Electron Physics, 1967, vol. 12, pp. 223-231.

[92] T. Rzesnicki, J. Jin, B. Piosczyk, M. Thumm, G. Michel, and D. Wagner, "170GHz, 2MW coaxial cyvity gyrotron- design and experimental verification of the RF output system", Proc. 6th International Vacuum Electronics Conference IVEC 2005, Noordwijk, Netherland, April 20-22, 2005, WPP-246 , pp. 303-306.

[93] T. Rzesnicki, J. Jin, B. Piosczyk, M. Thumm, G. Michel, and D. Wagner, "170GHz, 2 MW coaxial cavity gyrotron –design verification of the new RF output system", Proc. The Joint 30th International Conference on Infrared and Millimeter Waves & 13th International Conference on Terahertz Electronics, Williamsburg, Virginia, USA, Sept. 19-23, 2005, pp. 519-520.

[94] T. Rzesnicki, J. Jin, B. Piosczyk, M. Thumm, G. Michel, and D. Wagner, "Low power measurements on the new RF output system of a 170GHz, 2MW coaxial cavity gyrotron", Int. Journal of Infrared and Millimeter Waves, Jan. 2006, vol. 27, no. 1, pp. 1-11.

[95] A.A. Bogdashov, A.V. Chirkov, G.G Denisov, D.V. Vinogradov, A.N. Kuftin, V.I. Malygin, and V.E Zapevalov, "Mirror synthesis for gyrotron quasi-optical mode converters", Int. J. Infrared and Millimeter waves, Apr. 1995, vol. 16, pp. 735-744.

[96] D.R. Denison, T.S. Chu, M.A. Shapiro, and R.J. Temkin., "Gyrotron internal mode converter reflector shaping from measured field intensity", IEEE Trans. Plasma Sci., vol.27, pp. 512-519, Apr. 1999.

[97] Y. Hirata, Y. Mitsunaka, K. Hayashi, and Y. Itoh, "Wave-beam shaping using multiple phase-correction mirrors", IEEE Trans. Microwave Theory Tech., vol.45, pp 72-77, Jan., 1997.

[98] B.M. Harper and R.J. Vernon, "Beam-shaping reflectors for gyrotrons - a technique based on measured amplitude distributions with reconstructed phase distributions", Antennas and Propagation Society International Symposium, IEEE, vol. 4, pp. 1926-1929, 2000.

[99] J.B. Jin, M. Thumm, T. Rzesnicki, B. Piosczyk, and G. Dammertz, "Investigation of an Advanced Quasi-Optical Mode Converter for a Coaxial Gyrotron", Proc. The Joint 30th Int. Conf. on Infrared and Millimeter Waves and 13th Int. Conf. On Terahertz Electronics", Williamsburg, USA, 2005, pp. 299-300.

[100] J. Neilson, "Surf3d and TOL: Computer codes for design and analysis of high-performance QO launchers in gyrotrons", pp. 667-668, Joint *29th Int. Conf. on IRMMW & 12th Int. Conf. on Terahertz Elect., Karlsruhe, Germany, 2004.*

[101] J.B. Jin, B. Piosczyk, M. Thumm, T. Rzesnicki, and S.C. Zhang, "Investigation of a mirror system for a high power coaxial-cavity gyrotron", Proc. 6th International Vacuum Electronics Conference IVEC 2005, Noordwijk, Netherland, April 20-22, 2005, WPP-246 , pp. 275-278.

List of Publications

1 Jianbo Jin, Bernhard Piosczyk, Manfred Thumm, Tomasz Rzesnicki, and Shichang Zhang
Quasi-optical mode converter/mirror System for a high power coaxial-cavity gyrotron
IEEE Trans. on Plasma Science, vol. 34, no. 4, August 2006, pp. 1508-1515.

2 Jianbo Jin, Manfred Thumm, Bernhard Piosczyk, and Tomasz Rzesnicki
Theoretical investigation of an advanced launcher for a 2MW, 170GHz, $TE_{34,19}$ coaxial cavity gyrotron
IEEE Trans. on Microwave Theory and Technique, vol.54, no. 3, March 2006, pp. 1139-1145.

3 Jianbo Jin, Zheng-Biao Ouyang, Chun-Rong Qiu, Xiao-Ping Liang, Hui-Bo Zhang, Li Hu, and Shichang Zhang,
Efficiency enhancement of coaxial-cavity electron cyclotron resonance maser by tapering guide magnetic field
Int. Journal of Infrared and Millimeter Waves, Jan. 2003, vol. 24, no. 1, pp. 35-41.

4 Tomasz Rzesnicki, Jianbo Jin, Bernard Piosczyk, Manfred Thumm, George Michel, and D. Wagner
Low power measurements on the new RF output system of a 170GHz, 2MW coaxial cavity gyrotron
Int. Journal of Infrared and Millimeter Waves, Jan. 2006, vol. 27, no. 1, pp. 1-11.

5 Chunrong Qiu, Zhengbiao Ouyang, Shichang Zhang, Huibo Zhang, and Jianbo Jin
Self-Consistent Nonlinear Investigation of an Outer-Slotted-Coaxial Waveguide Gyroton Traveling-Wave Amplifier
IEEE Trans. on Plasma Science, vol. 33, no. 3, June 2005

6 Chunrong Qiu, Zhengbiao Ouyang, Shichang Zhang, Huibo Zhang, Jianbo Jin and Ying-Xin Lai
Nonlinear theory of a cyclotron autoresonance maser (CARM) amplifier with outer-slotted-coaxial waveguide
Journal Phys. D: Appl. Phys. 38 (2005) 1571–1576

7 Bernard Piosczyk, Guenter Dammertz, Olgierd Dumbrajs, Oliver Drumm, Stefan Illy, Jianbo Jin, and Manfred Thumm
A 2-MW, 170GHz Coaxial Cavity Gyrotron

IEEE Trans. Plasma Sci., June 2004, vol. 32, pp. 413-417.

8 Jianbo Jin, Manfred Thumm, Tomasz Rzesnicki, Bernard Piosczyk, and Guenter Dammertz
Investigation of an Advanced Quasi-Optical Mode Converter for a Coaxial Gyrotron
Proc. The Joint 30th Int. Conf. on Infrared and Millimeter Waves and 13th Int. Conf. On Terahertz Electronics", Williamsburg, USA, 2005, pp. 299-300.

9 Jianbo Jin, Bernard Piosczyk, Manfred Thumm, Tomasz Rzesnicki, and Shichang Zhang
Investigation of a mirror system for a high power coaxial-cavity gyrotron
Proc. 6th International Vacuum Electronics Conference IVEC 2005, Noordwijk, Netherland, April 20-22, 2005, WPP-246, pp. 275-278.

10 Jianbo Jin, Bernard Piosczyk, George Michel, Manfred Thumm, Oliver Drumm, Tomasz Rzesnicki, and Shichang Zhang
The Design of a Quasi-Optical Mode Converter for a Coaxial-Cavity Gyrotron
Joint 29th Int. Conf. on IRMMW & 12th Int. Conf. on Terahertz Elect., Karlsruhe, Germany, pp. 669-670, 2004.

11 Jianbo Jin, Shichang Zhang, Xiaoping Linag and Chunrong Qiu
Proposal of a coaxial-cavity gyrotron with tapered guide magnetic field
27th International Conference on infrared and millimeter waves, pp. 187-188
September 22-26, 2002, San Diego, CA USA.

12 Jianbo Jin, Shichang Zhang, Xiaoping Linag and Chunrong Qiu
Parameter Optimum in a Free-electron Laser
27th International Conference on infrared and millimeter waves, pp. 287-288
September 22-26, 2002, San Diego, CA USA.

13 Tomasz Rzesnicki, Jianbo Jin, Bernard Piosczyk, Manfred Thumm, George Michel, and D. Wagner
170 GHz, 2MW, coaxial cavity gyrotron – design and experimental verification of the RF output system-.
Proc. 6th International Vacuum Electronics Conference IVEC 2005, Noordwijk, Netherland, April 20-22, 2005, WPP-246, pp. 303-306.

Acknowledgements

I wish to extend my deepest thanks to my advisor, Professor Manfred Thumm for giving me the opportunity to be part of his research group. I feel privileged to have been his student and to have had the chance to learn from his expertise in the field of gyrotron, as well as to interact with his personality. His guidance, encouragement, and patience have made this thesis possible.

I would also like to express my appreciation to my advisor Prof. Shichang Zhang, who is also my master's degree advisor, for his support, encouragement and contribution in my education.

I am grateful for the friendship and technical advices from Dr. Bernhard Piosczyk.

Furthermore, I would like to thank Dr. Günter Dammertz, Dipl. Tomasz Rzesnicki, Dr. Stefan Illy and Dipl. Oliver Prinz for helping me out from time to time.

This work, supported by the European Communities under the contract of Association between EURATOM and Forschungszentrum Karlsruhe, was carried out within the framework of the European Fusion Devolopment Agreement. The views and opinions expressed herein do not necessarily reflect those of the European Commission.